SCHOOL OF BUSINESS AND SOCIAL SCIENCES
AARHUS UNIVERSITY

Millimeter Wave Channel Modeling and its Implications in 5G Cellular Design

PhD dissertation

Sheeba Kumari M

Aarhus BSS
Aarhus University
Department of Business Development and Technology
2021

PhD supervisor:	Prof. Ramjee Prasad CTIF Global Capsule Dept. of Business Development & Technology Aarhus University
PhD co-supervisor:	Dr. Navin Kumar Amrita School of Engineering Bangalore Amrita Vishwa Vidyapeetham India

ENGLISH ABSTRACT

The emerging fifth generation (5G) new radio (NR) provides a global standard that delivers high capabilities to 5G wireless networks. It enables increased support for multiple use cases by operating in diverse frequency ranges. This includes sub-6GHz frequency bands to allow long term evolution (LTE) compatibility and millimeter wave (mmWave) bands to provide enhanced capabilities. Driven by the high bandwidth availability as well as the higher antenna gains achievable through directional beamforming, mmWave technology has evolved as a promising technique for 5G. Directional transmission in mmWaves is key to mitigating their limitations of higher path loss, blockage, and many other frequency-dependent losses. However, it also causes substantial multipath suppression as the paths that fall outside the antenna beam area are filtered out. The spatial filtering of directional antennas and higher attenuation at mmWaves both create a sparse multipath structure in directional mmWave channels as opposed to the rich scattering environments in sub-6GHz omnidirectional channels. These unique propagation characteristics of directional mmWave channels necessitate the need to develop new accurate channel models. The design of realistic channel models that can characterize mmWave features is vital in 5G mmWave research to budget the links, perform system architecture trade-offs, and provide true assessments of novel technological solutions.

In this work, we deterministically model a directional mmWave urban micro (UMi) street canyon (SC) outdoor channel using a low complexity custom ray tracing model, called millimeter wave directional deterministic channel model (MiDDCM). The model integrates a highly directional horn antenna geometry in 3D plane and exploits this antenna directionality for reducing ray tracing complexity. The effects of frequency-dependent specific attenuation and foliage losses are also incorporated to enhance the model accuracy. The proposed model is used to examine the implications of mmWave directional channel modeling in various realistic scenarios, such as the line of sight (LOS)/non-LOS (NLOS) transmissions along with antenna beam alignment/misalignment, by evaluating their path loss variations. The effect of antenna diversity in combating deep fades has also been analysed. The channel model is additionally used to assess the impact of intersecting crossroads in narrow

directional mmWave links. Further, we propose statistical modeling of directional channels by performing a mathematical curve fitting over the MiDDCM data set to develop a closed-form expression. A correction factor dependent on the deployment parameters is also proposed in this expression to minimize the fitting error in a directional statistical channel model. Furthermore, a metaheuristic learning algorithm called particle swarm optimization (PSO) is applied to optimize the SC deployment parameters for optimal directional channel path loss. The proposed optimization model efficiently manages the channel specifications and environment geometry in outdoor SC directional channels.

DANSK ABSTRAKT

Den nye femte generation (5G) nye radio (NR) giver en global standard det leverer høje kapaciteter til 5G trådløse netværk. Det muliggør øget understøttelse af flere use cases ved at operere i forskellige frekvensområder. Dette omfatter under 6-GHz frekvensbåndfor at tillade langsigtet evolution (LTE) skompatibilitet og millimeterbølge (mmWave) bånd at give forbedrede funktioner. Drevet af den høje båndbredde tilgængelighed såvel som den højere antenne gevinster opnåelige gennem retningsbestemt stråleformning, mmWave teknologi har udviklet sig som en lovende teknik til 5G. Retningsbestemt transmission i mmWaves er nøglen at formildende deres begrænsninger af højere banetab, blokering og mange andre frekvensafhængige tab. Men, det forårsager også betydelig multipath undertrykkelse som de stier, der falder uden for det antennen stråle område er filtreret ud. Den rumlige filtrering af retningsbestemte antenner og højere dæmpning ved mmWaves begge skaber en sparsom multipath-struktur i retningsbestemte mmWave-kanaler i modsætning til de rige spredningsmiljøer i sub-6 GHz omnidirectional kanaler. Disse unikke formeringsegenskaber af retningsbestemte mmWave-kanaler kræver at der udvikles nye nøjagtige kanalmodeller. Udformningen af realistiske kanalmodeller, der kan karakterisere mmWave-funktionerne, er afgørende i 5G mmWave-forskningen for at budgettere linkene, udføre systemarkitektursbyforbyder og give sande vurderinger af nye teknologiske løsninger.

I dette arbejde, vi deterministically model en retningsbestemt mmWave urban mikro (UMi) street canyon (SC) udendørs kanal ved hjælp af en lav kompleksitet brugerdefinerede ray tracing model, kaldet millimeter bølge retningsbestemt deterministiske kanal model (MiDDCM). Modellen integrerer en meget retningsbestemt horn antenne geometri i 3D-plan og udnytter denne antenne retningsbestemthed for at reducere ray tracing kompleksitet. Virkningerne af frekvensafhængig specifik dæmpning og tab af blade er også indarbejdet for at forbedre modellens nøjagtighed. Den foreslåede model anvendes at undersøge virkningen af mmWave retningsbestemt kanal modellering i forskellige realistiske scenarier, såsom synslinjen (LOS) / ikke-LOS (NLOS) transmissioner sammen med antenne stråle justering / forkert justering, ved at evaluere deres vej tab variationer.

Virkningen af antenne mangfoldighed i bekæmpelsen af dybe fades er også blevet analyseret. Kanalmodellen bruges desuden til at vurdere virkningen af korsvej i smalle retningsbestemte mmWave-kanals. Desuden, vi foreslår statistisk modellering af retningsbestemte kanaler ved at udføre en matematisk kurve fitting over MiDDCM-datasættet for at udvikle et lukket-form udtryk. En korrektionsfaktor at afhænger af det implementeringsparametre er også foreslås i dette udtryk for at minimere tilfittingfejlen i en retningsbestemt statistisk kanalmodel. Desuden, anvendes en metaheuristisk læringsalgoritme kaldet partikelsværmoptimering (PSO) for at optimere SC-implementeringsparametrene for optimalt retningsbestemt kanal stitab. Den foreslåede optimeringsmodel styrer effektivt kanalspecifikationerne og miljøgeometrien i udendørs SC-retningskanaler.

PUBLICATIONS

The PhD project has led to the following publications.

- **Journal Publications**

1. **Sheeba Kumari M.**, N. Kumar, R. Prasad, "Path Loss Model for nonuniform Variance in Directional mmWave Outdoor Channel," IEEE Transactions on Wireless Communications, 2021 (submitted).

2. **Sheeba Kumari M.**, N. Kumar, R. Prasad, "Optimization of Street Canyon Outdoor Channel Deployment Geometry for mmWave 5G Communication," AEÜ - International Journal of Electronics and Communications, Vol 125, Oct 2020, doi: 10.1016/j.aeue.2020.153368.

3. **Sheeba Kumari M.**, N. Kumar, "Channel Model for Simultaneous Backhaul and Access for mmWave 5G Outdoor Street Canyon Channel," Springer Wireless Networks, The Journal of Mobile Communication, Computation and Information, July 2020, doi: 10.1007/s11276-020-02421-0.

- **Book Chapters**

1. **Sheeba Kumari M.**, S. A. Rao, N. Kumar, "Outdoor Millimeter-Wave Channel Modeling for Uniform Coverage Without Beam Steering," Ubiquitous Communications and Network Computing. UBICNET 2017. Lecture Notes of the Institute for Computer Sciences, Social Informatics and Telecommunications Engineering, vol 218. Springer, 2017, doi: 10.1007/978-3-319-73423-1_21.

- **Conference Publications**

1. **Sheeba Kumari M.**, N. Kumar, R. Prasad, "Simplified Approach for Directional Multipath Component Modeling for mmWaves using Ray Tracing," Wireless World Research Forum 45 (WWRF45) Hyperconnectivity: Beyond 5G, Opportunities & Challenges, Malaysia, Jan 2021 (presented).

2. **Sheeba Kumari M.**, N. Kumar, R. Prasad, "Performance of mmWave Ray Tracing Outdoor Channel Model Exploiting Antenna Directionality, " 2020 IEEE 5G World Forum (5GWF), Bangalore, India, pp. 607-612, 2020, doi: 10.1109/5GWF49715.2020.9221090.

3. R. Makkar, V. Kotha, **M. Sheeba Kumari**, D. Rawal, V. K. Chakka and N. Kumar, "Performance of Downlink SISO NR System using MMSE-IRC Receiver," 2020 IEEE 3rd 5G World Forum (5GWF), Bangalore, India, 2020, pp. 619-624, doi: 10.1109/5GWF49715.2020.9221267.

4. **Sheeba Kumari M**., S. A. Rao, N. Kumar, "Deterministic Modeling for mmWave Outdoor Street Canyon Channel," 2019 IEEE PhD Colloquium on Ethically Driven Innovation and Technology (PhD EDITS), Bangalore, India, August 2019, doi: 10.1109/PhDEDITS47523.2019.8986945.

5. **Sheeba Kumari M**., S. A. Rao, N. Kumar, "Modeling and Link Budget Estimation of Directional mmWave Outdoor Environment for 5G," 2019 European Conference on Networks and Communications (EuCNC), Valencia, Spain, pp.106-111, June 2019, doi: 10.1109/EuCNC.2019.8802001.

6. **Sheeba Kumari M**., S. A. Rao, N. Kumar, "Characterization of mmWave Link for Outdoor Communications in 5G Networks," IEEE International Conference on Advances in Computing, Communications and Informatics (ICACCI), Kochi, India, pp. 44-49, Sept. 2015, doi: 10.1109/ICACCI.2015.7275582.

ACKNOWLEDGEMENTS

My greatest appreciation goes to Dr. Navin Kumar for being a great advisor and giving continued support and extremely relevant suggestions during my research work. I would like to gratefully acknowledge his invaluable and patient guidance toward my doctoral study and drafting this thesis. Without his time and support, be it academically or towards personal and professional development, it would have not been possible to accomplish this work. I would like to sincerely thank my supervisor Late Dr. Sudarshan A Rao for his advice and sharp insights into our problems which significantly helped me with my research work. My sincere gratitude to Professor Ramjee Prasad for his understanding, expert assistance, and feedback. It has been an honour working with him. Thank you professors for making this research journey extremely memorable and valuable. Without each of your advice and guidance, it would have not been possible to accomplish this work.

I am also incredibly grateful to Dr. Vinosh Babu James, Dr. Sendil Devar, Dr. Divyang Rawal, and the entire 5GIF team for allowing me to work on the collaborative project on 3GPP channel model development. It was a great learning experience to participate in 5G India Forum (5GIF) independent evaluation group (IEG) and contribute towards of the evaluation of compliance of 3GPP 5G NR with the IMT 2020 requirements.

I feel fortunate to have great friends and associates to work with, the discussions with whom gave lots of useful new ideas. My special thanks to my husband for his unconditional encouragement, as always, and my daughters for their understanding and constant support. I would like to express my deep appreciation for them, and I could not have finished my PhD work without their help. Thank you for all of their understanding and unconditional assistance.

TABLE OF CONTENTS

LIST OF FIGURES

LIST OF TABLES

LIST OF ABBREVIATIONS

1G	First Generation
2D	Two Dimensional
3D	Three Dimensional
3GPP	Third Generation Partnership Project
4G	Fourth Generation
5G	Fifth Generation
5GTF	5G Technology Forum
ABG	Alpha-Beta-Gamma
AI	Artificial Intelligence
AoA	Angle of Arrival
AoD	Angle of Departure
AP	Access Point
AR	Augmented Reality
BS	Base Station
C-BTS	Compact Base Transceiver Station
CDL	Clustered Delay Line
CI	Close-in Reference Distance
CP	Cyclic Prefix
C-RAN	Cloud-based Radio Access Network
CSI	Channel State Information
D2D	Device-to-Device
DoA	Direction of Arrival
DS	Delay Spread
eMBB	Enhanced Mobile Broadband
FBMC	Filterbank Multicarrier

FCC	Federal Communication Commission
FD-MIMO	Full Dimension MIMO
FNBW	First Null Beam Width
FQAM	Frequency and Quadrature Amplitude Modulation
FR	Frequency Range
FSPL	Free Space Path Loss
FWA	Fixed Wireless Access
GFDM	Generalized Frequency Division Multiplexing
GSCM	Geometry-Based Stochastic Channel Models
HPBW	Half Power Beam Width
IMT	International Mobile Telecommunications
InH	Indoor Hotspot
IoT	Internet of Things
ITU-R	International Telecommunications Union-Radio
KPI	Key Performance Index
LOS	Line of Sight
LTE	Long Term Evolution
LTE-A	Long Term Evolution-Advanced
M2M	Machine-to-Machine
METIS	Mobile and wireless communications Enablers for the Twenty-twenty Information Society
MiDDCM	Millimeter Wave Directional Deterministic Channel Model
MIMO	Multiple Input Multiple Output
MiWEBA	Millimeter-Wave Evolution for Backhaul and Access
MLE	Maximum Likelihood Estimate
mmMAGIC	Millimeter-Wave Based Mobile Radio Access Network for 5G Integrated Communications

MMSE	Minimum Mean Square Error
mMTC	Massive Machine-Type Communications
mmWave	Millimeter Wave
MPC	Multipath Component
NFV	Network Function Virtualization
NLOS	Non-Line of Sight
NOMA	Non-Orthogonal Multiple Access
NR	New Radio
NSA	Non-Standalone
O2I	Outdoor-to-Indoor
OCI	Other-Cell Interference
OFDM	Orthogonal Frequency Division Multiplexing
OLOS	Obstructed Line of Sight
PAPR	Peak-to-Average-Power Ratio
PLE	Path Loss Exponent
PSO	Particle Swarm Optimization
QPSK	Quadrature Phase Shift Keying
QuaDRiGa	Quasi Deterministic Radio Channel Generator
RAN	Radio Access Network
RMa	Rural Macro
RMS	Root Mean Square
RMSE	Root Mean Square Error
RX	Receiver
SA	Standalone
SC	Street Canyon
SDN	Software-Defined Networking
SINR	Signal-to-Interference-plus-Noise Ratio

SISO	Single Input Single Output
SL	Spatial Lobe
SNR	Signal to Noise Ratio
TC	Time Cluster
TDL	Tapped Delay Line
TX	Transmitter
UAV	Unmanned Aerial Vehicle
UE	User Equipment
UFMC	Universal Filtered Multicarrier
UHD	Ultra-High Definition
UMa	Urban Macro
UMi	Urban Micro
URLLC	Ultra-Reliable Low Latency Communication
VR	Virtual Reality
WINNER	World Initiative for New Radio

SYMBOLS

c	crossroad number
c_1 and c_2	personal and social acceleration coefficients of PSO
C	maximum number of crossroads on any street side
d	2D separation distance
d_{3D}	3D separation distance
d_c	critical distance
d_g	path length of ground reflection
d_{hc}	horizontal critical distance
d_{io}	path length of odd-numbered wall reflection
d_{ie}	path length of even-numbered wall reflection
d_{LOS}	path length of direct LOS
d_{max}	maximum separation distance
d_o	reference distance of CI model
d_{r_w}	distance from RX to near reflecting wall
d_s	street width
d_{sep}	vertical separation distance between array elements
d_{t_w}	distance from TX to far reflecting wall
d_{vc}	vertical critical distance
d_w	smallest distance either from TX to near wall or from
D_f	foliage depth
E	edge of the crossroad
E_b/N_0	bit-energy/noise

$EIRP$	effective isotropic radiated power
f	mmWave frequency
F	noise figure
F_d^{det}	deterministic directional fading gain
F_d^{stat}	statistical fading gain
$g(t)$	global best of the swarm particle of PSO
G_0	boresight gain
G_t	TX antenna gain
G_r	RX antenna gain
$G(\phi,\theta)$	directional antenna gain
$G_g(\phi,\theta)$	antenna gain product of ground reflection
$G_i(\phi,\theta)$	antenna gain product of ith wall reflection
$G_{LOS}(\phi,\theta)$	antenna gain product of LOS
h	channel impulse response
h^r	channel impulse response relative to LOS
$h^r{}_{mn}$	CIR between nth transmit and mth receive antenna
h_d	height correction
h_r	RX antenna height
h_{r1}	RX antenna height in a backhaul link
h_{r2}	RX antenna height in an access link
h_t	TX antenna height
H_g	CIR component for ground reflection
H_i	CIR component for ith wall reflection
H_{LOS}	CIR component for LOS

$HPBW_A$	azimuth half power beamwidth
$HPBW_E$	elevation half power beamwidth
K_a	coefficient of exponential absorption
L_{abs}	specific attenuation due to oxygen absorption
L_{fol}	foliage loss
L_{Margin}	link margin
M	maximum number of wall reflections
$MAPL$	maximum allowable path loss
n	order of wall reflected paths
n^{CI}	path loss exponent of the CI model
n^{stat}	path loss exponent of the directional statistical model
$nPop$	swarm particle population
N	maximum wall reflection order
P_e	un-coded bit error probability
$P_i(t)$	local best position of the i^{th} swarm particle of PSO
PL	path loss of MiDDCM
PL_{d_0}	FSPL at d_0
${PL_d}^{\mathrm{ABG}}$	path loss of ABG model
${PL_d}^{\mathrm{CI}}$	path loss of CI model
${PL_d}^{\mathrm{det}}$	directional deterministic path loss
${PL_d}^{\mathrm{stat}}$	directional statistical path loss
P_r	received power of MiDDCM
P_r^{CI}	received power of the CI model
P_r^{det}	deterministic received power

$P_{r,min}$	RX sensitivity
P_t	transmitting power
r_1 and r_2	uniform random variables in [0,1]
R_b	desired data rate
V	velocity of swarm particle
W	wall side
x_l_{cW}	lower bound of the reduced faded region
x_u_{cW}	upper bound of the reduced faded region
X	position of swarm particle
$X_{\sigma_{\mathrm{CI}}}$	fading factor of the CI model
$X_{\sigma_{\mathrm{ABG}}}$	fading factor of ABG model
ϕ	azimuth angle
ϕ_g	azimuth angle of ground reflected ray
ϕ_i	azimuth angle of the ith wall reflected ray
ϕ_{LOS}	azimuth angle of LOS
ϕ_{HPBW}	azimuth half power beamwidth
θ	elevation angle
θ_g	elevation angle of ground reflected ray
θ_{LOS}	elevation angle of LOS
θ_{HPBW}	elevation half power beamwidth
λ	wavelength
Ψ_i	angle of incidence of wall reflection
Γ_g	ground reflection coefficient

Γ_i	net wall reflection coefficient
Γ_{par}	parallel reflection coefficient
Γ_{perp}	perpendicular reflection coefficient
ε'	relative permittivity
ε_r	complex permittivity
μ'	relative permeability
σ	conductivity
$\Delta\phi$	antenna tilted in the azimuth plane
$\Delta\theta$	antenna tilted in the elevation plane
α	offset of path loss fitting curve of ABG model
α_i	relative amplitude of the i^{th} reflection
α_r	wall reflection angle
β	path loss slope of ABG model
β_i	relative phase of i^{th} reflection
β_g	relative phase of ground reflection
$\gamma_g(m,n)$	additional phase difference due to ground reflected path from n^{th} transmit to m^{th} receive antenna
σ_{ABG}	standard deviation of ABG model
σ_{CI}	standard deviation of the CI model
μ_{stat}	mean of the deterministic path loss distribution
σ_{stat}	std deviation of the deterministic path loss
σ_{mod}	corrected non-uniform std deviation
$\mathcal{C}_\sigma$	correction factor
ω	inertia weight

CHAPTER 1. INTRODUCTION

1.1 OVERALL SCENARIO

The fifth generation (5G) of mobile communication systems is expected to meet diverse requirements arising from varied application possibilities outside the traditional wireless broadband category [1], [2]. From a broader perspective, 5G mobile networks will offer higher data rates to support powerful smartphones with high bandwidth video streaming applications. It will provide improved latency and reliability for challenging services like autonomous cars, aerial vehicles, and virtual/augmented reality (VR/AR). Furthermore, to fully support services in terms of machine-to-machine (M2M) communications, 5G is also required to provide scalable, flexible, and robust connectivity. The existing fourth-generation (4G) long term evolution (LTE) technology [3], though evolved with advanced networking and signal processing capabilities, is inept to address these varied service demands as it relies on the heavily crunched low-frequency spectrum [4]. 5G-enabled technologies and networks open new research space and offer incredible potential to address several key challenges of traditional 4G systems, like the spectrum shortage crisis and high energy consumption [5]. Industry and academia worldwide are indeed working together to accelerate 5G deployment through extensive research and early network trials.

Unlike the former generations, 5G aims to provide a unified system that can be designed and optimized for different usage scenarios. Also, there is an inherent adherence to backward compatibility which allows 4G LTE and 5G technologies to coexist [6]. The international mobile telecommunications (IMT) 2020 envisioned by the radio communications sector of the international telecommunications union (ITU-R) will serve as a unified platform for the 5G system development, providing an explicit description of 5G objectives [7]. It also specifies a wide variety of use case scenarios for 5G in three broad categories, namely; enhanced mobile broadband (eMBB), ultra-reliable and low latency communications (URLLC), and massive machine-type communications (mMTC), along with their minimum technical performance requirements in actual deployments [8]. Several disruptive technologies will drive 5G to meet these requirements with prominence on ultra-densification of networks for smaller cells, millimeter waves (mmWaves) for increased bandwidths, and massive multiple input multiple output (MIMO) for improved spectral efficiencies, thereby creating a substantial change in the architectural and component design of 5G systems [9]. The wideband mmWave spectrum in the range of 30-300GHz will be essential to address the monthly global mobile traffic demand of 30.6B Gigabytes in 2020, which may even increase to 131B Gigabytes by 2024 [10]. Almost 25 percent of the world's mobile traffic is forecast to be fixed wireless access (FWA) that will feature new radio (NR) in the mmWave spectrum to provide gigabit internet speeds to homes, apartments, and businesses. As stated in [11], the applicability of mmWaves in eMBB, URLLC, and mMTC use cases is indeed immense. Some of the early research studies had demonstrated the feasibility of mmWaves specifically, the lower frequency ranges, for broadband outdoor mobile communication networks [12]–[15]. In addition to the availability of wide contiguous bandwidth, the mmWave spectrum provides other benefits such as short wavelength allowing to integrate larger antenna arrays in smaller areas, short transmission range supporting network densification and small cell concept, and so on [13]. As the wideband mmWave spectrum inherently offers higher data rates, multi-antenna technology can be exploited for mmWaves to support spatial diversity (for enhanced signal quality) and/or to provide narrow beamforming gains (for improved coverage).

Despite these advantages, enabling mmWave communications in 5G poses significant challenges- most importantly, the higher signal attenuation due to free space loss, atmospheric absorption, rain, foliage, human blockage, and building penetration [16], which collectively leads to poor channel quality, intermittent connectivity, and reduced coverage. The impact of penetration loss can be minimized using a cellular architecture that separates the indoor and outdoor transmission scenarios [5]. Literature also reflects that introducing highly directional antennas with narrow radiating beams essentially compensates the higher attenuation and offers an improved link budget than would omnidirectional antennas [17], [18]. Hence, it is imperative to reconsider the traditional statistical channel models with omnidirectional formulations to explore directional mmWave channels and to examine the impact of directionality on system modeling and link budgeting. Moreover, beamforming and steering technologies will be used in mmWave systems to enhance the link quality and coverage distance, which makes beam management an active research area for directional mmWaves [19]–[21]. This mandates the need to identify the exact beam steering direction in real-time to evaluate the best power performance. Therefore, further studies about the antenna directionality and the impact of beam steering in mmWave channels are needed to assess the alignment of transmitting and receiving beams. The ray tracing-based beam tracking demonstrates improved effectiveness in mmWave channels with abrupt channel changes. As the ray tracer inherently tracks the stronger paths, their departure angles could be easily stored and utilized to rearrange the beams [22]. Recent literature reflects mmWave channel characterization and modeling of various propagation scenarios such as outdoor open square [23], in-room [24], [25], outdoor street canyon [22], [26]–[29], aviation field [30], high-speed train [31], by exploring and exploiting antenna directionality. To date, several channel modeling approaches with varying accuracy, complexity, stability, and scenario specificity are employed in mmWave outdoor channel study, yet, most of them modify the sub-6GHz channel models by modifying their key parameters conforming to measurements. In general, the channel modeling strategies for mmWaves should capture the unique characteristics of heavily attenuated high frequency mmWave channels such as higher penetration loss, reduced number of multipaths, reduced impact of small-scale fading, and a clear distinction between the line of sight (LOS) and non-LOS (NLOS) propagations. However, most of the existing channel models are inadequate in capturing all these essential features of mmWaves [32], [33] which can lead to the incorrectly estimated performance of novel signal processing algorithms, transmission techniques, and other enabling technologies.

As apparent, highly directional antennas employed in mmWave links will provide substantial suppression of the multipaths that fall outside the antenna beam area [32]. This leads to a sparse multipath channel structure in directional mmWaves as opposed to the rich scattering environments in omnidirectional sub-6GHz channels [34]. Hence, the directional channel between two mmWave nodes is defined by strong specular paths. This necessitates the need to accurately model both azimuth and elevation angles of the contributing multipath components in a three dimensional (3D) plane, unlike the two dimensional (2D) antenna models adopted in various channel models for analytical tractability [35]. Typically, the mmWave channel models will need to apply and adapt to the spatial dynamics of the channel introduced by the deployment of high gain directional antennas [36]. In this perspective, deterministic ray tracing exhibits supremacy over statistical channel models in characterizing the mmWave channels in terms of multipath components to provide a highly accurate model. Moreover, the statistical channel models are inherently limited to scenarios specified in the underlying measurements. This also implies that a comprehensive characterization requires detailed empirical analysis or measurements [25]. As we drift to the higher frequency, broader bandwidth mmWave spectrum; the geometry-based stochastic channel models such as WINNER II might be inadequate to provide an accurate channel characterization as they model different deployment scenarios by identical approaches, but with varying channel parameters [23].

In summary, 5G mmWave communications will necessitate the redesign of the complete cellular framework opening up tremendous research opportunities in channel characterization and modeling, directional transmission, beamforming and steering, beam training and tracking, and many more.

1.2 AIMS AND OBJECTIVES

The main objective of the proposed research work is to provide a comprehensive characterization of mmWave directional links in an urban micro (UMi) street canyon (SC) outdoor scenario by estimating received power and path loss variations in several realistic scenarios. For example, LOS or NLOS, antenna beam aligned or unaligned, and road canyon with or without crossroads. In the outdoor channel modeling, UMi SC, unlike the open square scenario, generates the maximum number of strong reflected multipath components, thereby allowing evaluating the worst-case outdoor path loss performance. The study is extended for the diversity scheme of a 2 x 2 MIMO channel. The defined research goal is realized through the following sub-objectives:

- Investigate different PHY layer design challenges of emerging 5G communication systems with an emphasis on adopting millimeter wave transmission for small cell design.
- Examine the impact of unique propagation features of mmWaves and exploit them in characterizing the mmWave propagation channel.

- Analytically derive the channel model for small cell UMi SC outdoor deployment scenarios to provide a realistic approximation of mmWave propagation for single input single output (SISO) and MIMO transmissions. The path loss performance for various propagation conditions and environments will be analysed to draw useful insights.

- Validate the simulated channel models through a comparative analysis of the accomplished results with standard channel models.

- Study the implications of directional channel characterization on the overall performance of mmWave directional deterministic channels.

- Perform statistical analysis on the directional deterministic channel characteristics.

- Devise a method to optimize the street canyon deployment for optimal performance.

1.3 METHODOLOGY

In this thesis work, the deterministic ray tracing technique is employed to derive a custom ray tracing model of low complexity to characterize the performance of mmWave UMi outdoor SC links with highly directional propagation characteristics. The ray tracing complexity is reduced by exploiting mmWave channel sparsity arising from higher attenuation, the insignificance of diffraction, and link directionality. A generalized channel model that determines the number of specular reflections as a function of specific environment geometry and antenna characteristics is devised and validated using MATLAB. The approach will be more realistic and reliable compared to models that arbitrarily choose the number of contributing paths as a fixed value or based on an input specification. The deterministic model will be used to derive various performance metrics of the mmWave directional deterministic outdoor channel and also applied to assess different transmission scenarios that cannot be examined by traditional statistical models. A statistical approximation of the deterministic model is realized using a regression fit to directional deterministic path loss data to develop a convenient closed-form expression. The low complexity deterministic model is also integrated with a metaheuristic learning algorithm to efficiently administer the environment geometry of mmWave UMi SC directional outdoor channel. The model is meticulously analysed to assess its scope compared to the present work to exhibit the efficacy of the proposed design.

1.4 KEY CONTRIBUTIONS

The significant contributions of the thesis in mmWave channel modeling and its implications in 5G cellular design are summarised as follows:

- Investigation of unique propagation characteristics of mmWaves for the UMi SC outdoor scenario.

- Modeling of mmWave directional deterministic outdoor SC channel
    - The 3D directional properties of mmWave links in both elevation and azimuthal planes are examined by using a highly directional horn antenna design to integrate the effect of antenna directionality in channel modeling.
    - The unique properties of frequency-dependent oxygen absorption and foliage are modelled by including standard techniques.
    - A novel millimeter wave directional deterministic channel model (MiDDCM) based on custom ray tracing is developed for mmWave UMi SC outdoor channels with high gain antenna systems. The analytical framework exploits antenna directionality to reduce the complexity of ray tracing computations leading to a generalized design that dynamically determines the number of contributing multipaths from the choice of antenna beam area.
    - Two different link types, namely, the backhaul/fronthaul and the access are studied to examine the implications of mmWave directional channel modeling in various realistic scenarios, such as LOS/NLOS transmissions with antenna beam alignment/misalignment based on path loss variations.
    - The directional channel is characterized for varying input specifications, like, mmWave frequency, antenna polarization, and beamwidth, transmitter (TX)/receiver (RX) location and height, and deployment parameters.

  - The proposed MiDDCM for directional SISO channels is extended into 2 x 2 MIMO channels following the two ray channel modeling technique to examine the influence of antenna separations on channel performance.
  - The SISO MiDDCM is also extended to characterize a realistic SC layout with crossroads of arbitrary widths and to investigate the impact of street grids on mmWave fading characteristics.

- Statistical learning of mmWave directional channel characteristics and models
  - Here, statistical modeling of directional channels is proposed by performing a mathematical curve fitting over the directional deterministic LOS path loss data set to develop a closed-form expression identical to that of the power-law path loss model. A correction factor is hence proposed to produce a non-uniform variance for the fading factor in a directional link to minimize the fitting error.
  - A metaheuristic learning algorithm called particle swarm optimization (PSO) is applied for the optimal placement of SC deployment parameters that can yield minimum channel path loss. The implementation helps to efficiently manage the channel specifications and environment geometry in outdoor directional channels. The proposal stems from the insight that even small variations in deployment parameters cause considerable path loss fluctuations owing to the short wavelength of mmWaves.

1.5 THESIS ORGANISATION

The rest of this thesis is organized as follows.

Chapter 2 summarizes the state-of-the-art of significant technological developments in 5G communication systems with specific attention to the applicability of wideband high frequency mmWaves in meeting essential performance requirements foreseen in the 5G roadmap. The fundamental propagation features of mmWaves are briefly discussed to understand and appreciate the need for novel channel models. The popular methods used in the development of mmWave channel models and existing standard mmWave channel models are described. This chapter also presents a comprehensive review of PSO and its applications to the field of 5G communication theory and networks.

Chapter 3 provides the analysis and design of the original and proposed low complexity directional channel modeling based on deterministic ray tracing for the UMi SC outdoor mmWave channels. In this, antenna directionality is exploited to reduce ray tracing complexity. This chapter first examines channel sparsity due to the spatial filtering of directional antennas and presents the detailed mathematical formulation for the MiDDCM. The model is assessed and extended to investigate beam steering effects on the performance of LOS and NLOS directional channels by assuming both continuous and discontinuous reflecting sidewalls in road canyon. Analytical insight into the spatial diversity in sparse multipath channel structures in mmWave outdoor directional channels is provided.

Chapter 4 further develops the deterministic model to perform statistical analysis on the path loss data set to propose an easily computable closed-form expression with fewer input parameters. It also introduces a novel correction factor to provide necessary corrections to the traditional power-law path loss model to address channel directionality. The chapter also proposes a method to combine metaheuristic learning and mmWave channel modeling to efficiently plan the deployment parameters for optimal path loss performance.

Chapter 5 summarizes the significant results relating to the proposed study on mmWave directional channel characterization, providing a detailed description and discussion. The relevance and significance of the findings are explored with specific attention to their important implications.

Chapter 6 concludes the work in this thesis with a summary of significant contributions and potential future research directions in mmWave channel modeling for characterizing directional outdoor SC links.

CHAPTER 2. STATE OF THE ART

2.1 INTRODUCTION

5G standardization activities are actively initiated in ITU-R, and 3rd generation partnership project (3GPP) and, many milestones are being achieved to mobilize mmWaves for 5G [37]. Yet, multiple challenges in the characterization of mmWave links and the design aspects of mmWave communication systems remain elusive [33]. Even though mmWaves can achieve most of the performance requirements envisioned by 5G, transmission at mmWave frequencies is limited to short-range due to their high attenuation [38], [39]. Extensive research is directed to assess mmWaves for 5G mobile broadband by employing directional high gain antennas which offer a significant extension of the transmission range than would be possible with omnidirectional antennas. Accordingly, new models that account for the three-dimensional spatial characteristics of propagation are required to characterize mmWave channels which are fundamentally different from the existing sub-6GHz channels. This chapter provides the background information of mmWave channel characterization and modeling for 5G communication systems which forms the reference for the research problem addressed in this thesis.

2.2 5G WIRELESS TECHNOLOGY

Cellular systems have evolved over the years from narrowband networks of around 10Kbps to broadband networks of 100Mbps and have consistently followed the prediction that a new generation will be introduced every ten years [8], [40]. It has evolved from first-generation (1G) to 4G and is currently being investigated as a 5G system. The legacy LTE and LTE advanced (LTE-A) based 4G standard with its several release versions has been offering downlink data rates of 300Mbps and uplink data rates of 75Mbps which can be adequately enhanced to 1Gbps in the downlink through techniques like carrier aggregation, interference mitigation mechanisms as well as spatial multiplexing at the base station (BS) and/or the user equipment (UE) [3]. However, 4G has matured to a state where only incremental improvements and a limited spectrum can be expected. The adoption of smart devices with capabilities that require higher data rates and bandwidth usage has influenced the growth of global

IMT traffic demand which will continue to grow in the range of 10-100 times in the next ten years [7]. With the IMT-Advanced systems being deployed in the world, the next generation of mobile technology should evolve with superior performance to provide different services like ultra-high-definition (UHD) 3D video, augmented and virtual realities, Internet of Things (IoT), and unmanned aerial vehicles (UAV) [40]. In specific, the network must support the growing demand for higher data rates, combat the spectrum crisis scenario, service a myriad of wireless mobile devices and, most importantly, maintain a much low energy consumption [5].

The concept of 5G was coined before the year 2010, with considerable research development taking place in various directions since 2012 [4], [5], [37], [40]–[42]. As stated in [6], 5G will not be yet another mobile generation to improve data rate, coverage and capacity; instead it will open a new arena of cellular communication with the promotion of wideband higher frequency spectrum, virtualization of network infrastructure, integration of various types of devices and formation of unconventional mobile standards, to name a few. The ITU established IMT-2020 in 2015 to define the overall vision, process, and roadmap for the development of 5G mobile

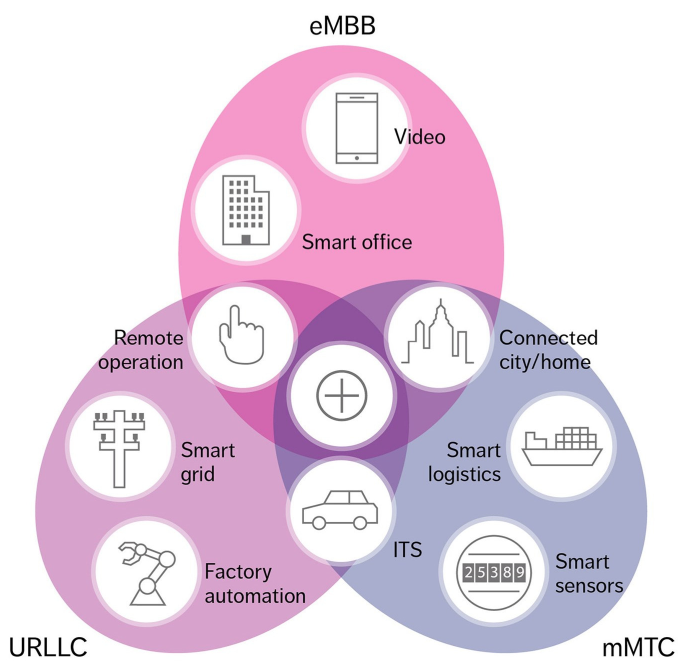

Figure 2.1 5G use cases and associated applications.

communication systems. In partnership with governmental bodies and the mobile industry worldwide, ITU is working towards the realization of IMT-2020. Accordingly, 5G is envisaged to support various services broadly categorized as eMBB, URLLC, and mMTC, as illustrated in Figure 2.1 [43]. The eMBB usage scenario is very much similar to existing mobile broadband, but with extended capabilities of higher data rate, seamless coverage, improved traffic capacity, and higher mobility. The URLLC services include emerging critical applications with stringent requirements for reliability and latency. Under the mMTC category, 5G accommodates applications that demand high connection density, scalability, and use devices having low cost and long battery life. The current deployments are fundamentally driven by FWA and eMBB services which utilize a slightly higher bandwidth of the available spectrum in 4G LTE. In fact, 5G technology development includes a combination of the existing 4G and an emerging NR technology [44]. After 3GPP released the 5G NR specifications for non-standalone (NSA) architecture in 2017, several industry researchers, vendors, and service providers are working stringently towards rolling out 5G NSA deployments [33].

To realize the unique vision [45] and use cases, ITU specifies well-defined

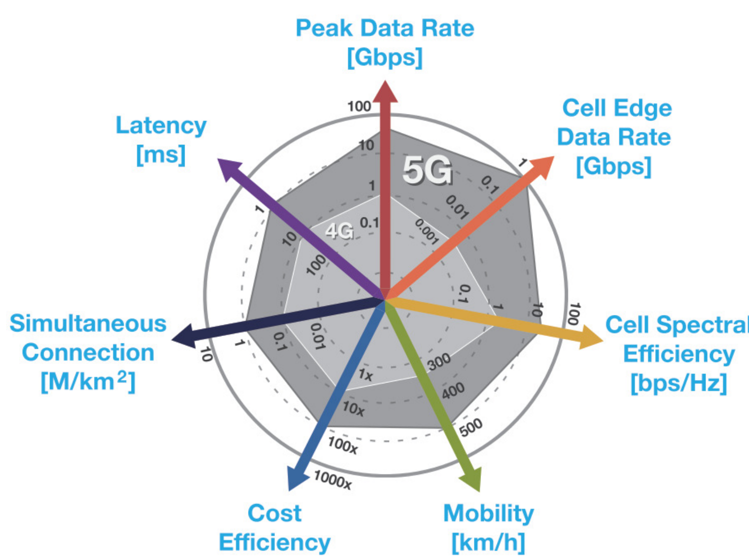

Figure 2.2 5G key requirements.

performance requirements for 5G [7]. Based on this, Samsung proposed seven key performance indices (KPIs), illustrated in Figure 2.2 [11]. Accordingly, 5G should achieve a targeted spectral efficiency of hundreds of giga-bits-per-second for eMBB services. At the same time, it should meet the requirement of low power, low data rate, and sporadic traffic needs of mMTC. Furthermore, it should address the stringent requirements of high reliability and low latency for URLLC. The potential technology candidates that require attention in the upcoming 5G and their challenges in delivering these design requirements are discussed in [5].

To meet the 5G vision and to achieve the performance requirements in different key dimensions, smart and efficient technologies are emerging into research fields [1], [2], [8], [9], [11], [42]. A theoretical consolidation of five disruptive technologies for 5G that could lead to a design change at both architectural and component levels is reported in [8] with a minimal assessment made on the individual suggestions themselves. In [9], authors summarize the emerging technologies in 5G research and development illustrating their key challenges. It also provides the significance of 3 key enabling technologies, namely: network densification, mmWaves, and massive MIMO in delivering the promised data rate for 5G eMBB services. The former two techniques can additionally improve the energy and the cost efficiency of 5G networks. In addition to the revolutionary technologies like mmWave and massive MIMO, 5G cellular network design will be directed towards device-centric architectures, a major contradiction with the existing BS based cellular architecture [9]. We now highlight major technological developments that can benefit 5G applications:

- **Millimeter waves**: Unlike the fragmented spectrum available in the sub-6GHz regime, the large contiguous spectrum of approximately 200GHz enhances the acceptance of mmWave technology in 5G systems. The mmWave band utilizes this large available channel bandwidth to realize higher data rates, higher capacity, and improved connectivity compared to low-frequency microwave bands. Even before entirely comprehending mmWave technologies, high frequency mmWaves were previously used in fixed, LOS applications such as satellite communications, radar systems, and wireless backhauls. However, the applicability of mmWaves in mobile access networks dominated by high user mobility and large signal blockage requires careful assessment. Deploying 5G networks that operate in the mmWave bands offer enormous challenges and opportunities with a significant focus on mitigating their adverse propagation conditions, among others [13]. This includes the high free space attenuation and the large channel fluctuations caused by atmospheric absorption, foliage, and signal blockages. The use of highly directional beam steering and adaptive beamforming solutions are suggested to overcome these losses [18][46]. Hence, mmWaves will use MIMO to exploit beamforming gains in order to enhance the SNR and the range of transmission links.

- **Massive MIMO:** Though MIMO was popularly employed in 4G, massive MIMO that deploys tens to hundreds of antennas at the BS will be a promising technique for 5G to achieve significantly higher throughput and capacity [32][47], [48]. The mmWaves with low carrier wavelengths are extremely favourable to allow the integration of several antenna elements into the same physical dimension. By placing antenna elements in a 2D-grid, it is possible to realize an efficient antenna array panel called full-dimension MIMO (FD-MIMO). This 3D MIMO architecture extends the array from the only horizontal plane to both horizontal and vertical planes, thus enhancing the spatial resolution and improving the signal to noise ratio (SNR). Design and development of a massive MIMO antenna array poses several architectural challenges. Primarily, the BS will have to be equipped with a large number of low-power amplifiers feeding the large number of tiny antenna elements. Moreover, the issues of scalability, mutual coupling and antenna correlations need to be sorted out. Also, to circumvent the limitations of precoding, massive MIMO will mostly use hybrid precoding to realize beamforming so as to reduce hardware constraints and power consumption [49].

- **Network densification:** As networks evolve to 5G, network densification through small cells will play a major role in enhancing system capacity and achieving better coverage. The 5G dense networks can gain from the benefits offered by proximal transmissions and high spatial reuse of available resources [50]. In fact, the high-density deployments of small cells in a heterogeneous network configuration will offload the user plane traffic while the existing macrocells can continue to carry the control plane traffic [51]. Recent advances in distributed and self-configuring network technologies will indeed ease the deployment. Implementing small cells (such as micro, pico, or a femtocell based on the cell radius) also provides human-safe transmissions as the small cell BSs, known as compact BSs (C-BTS), transmit relatively low power signals to reduce the interference. The C-BTSs are typically lightweight, easy to maintain BSs positioned at a low height of 5-15m covering small cell sizes of 100-200m radius. While these BSs can be made and mounted at reduced costs, cost-effective backhauling them using fiber or mmWave is a major research challenge. In this context, wireless backhauling using non-orthogonal multiple access (NOMA) based solutions have been investigated [52]. Furthermore, the large cell density and the irregular deployments will increase other-cell interference (OCI) besides increasing the number of handovers for mobile UEs [8]. Even though 4G progressively used network densification, it is easily achievable in mmWave-based 5G that inherently benefits from a limited range due to higher path loss.

- **Device-to-device communications**: Unlike traditional mobile generations, 5G supports device-to-device (D2D) communication which uses direct communication between devices to offload data from the core network. Basically, a UE can communicate with another UE over D2D links without the core intervention, thereby reducing end-to-end latency in URLLC and mMTC applications of 5G. Moreover, the proximity of devices allows considerable power saving within the network. D2D communications also provide improved link reliability, spectral efficiency, and capacity. To fully exploit this technology, it is required to understand the underlying challenges [51]. In a D2D system, multiple D2D devices that communicate with each other share the same resources with an existing cellular UE to maximize spectral efficiency provided the interference between these devices is acceptable. Accordingly, efficient interference management algorithms should be developed to control interference between D2D and cellular users. Besides, in D2D with mmWave transmission, highly directional beamforming will reduce the interference to nearby co-channel links. Other challenges include resource allocation, power control for devices, and above all, privacy and security of communication.

- **Advanced network**: To fulfil the diverse requirements of latency, improved data rate, and increased simultaneous connections, 5G should accommodate new technologies at the network architecture level. In that respect, a major event is a shift from the traditional radio access network (RAN) to the cloud-based RAN (C-RAN) [6]. In general, RAN used two network architectures, either a single cell site architecture wherein the digital baseband unit and the radio unit are co-located, or a distributed BS architecture wherein the radio unit is separated from the digital unit and is placed nearer to the BS antenna. C-RAN follows the decoupled architecture of distributed BS wherein multiple digital baseband units separated from the radio unit are moved to a centralized cloud to support access from anywhere and any platform. The design of fronthaul communication between the pool of baseband units and the radio units is a major research challenge in C-RAN. C-RAN redefines the endpoints and the time frame for which network services are provisioned which requires the network architecture to be more scalable and flexible. This can be accomplished using two programmable design technologies: network function virtualization (NFV) and software-defined networking (SDN) [11]. NFV aims to separate the network functions from the dedicated hardware infrastructure to a virtual instance. This way, NFV will virtualize the core network and centralize the baseband processing within RAN. SDN is an intelligent architectural framework for creating programmable networks. It decouples the control and data planes, logically centralizes the network intelligence and state, and also abstracts the underlying network infrastructure from the application. Both SDN and NFV enable the orchestration and control of the technological resources in RAN. They help to realize the concept of network slicing which creates and partitions network services. This enables the operators to provide optimum support for these services. However, dealing with different network slices that provide services with differing requirements in terms of latency, reliability, capacity, and functionality would be a major challenge. In addition, immense research is required in obtaining guaranteed QoS, efficient resource utilization, and proper isolation between slices.

- **Waveform design**: Transition to 5G involves a major change in signaling and multiple access formats [53]. While orthogonal frequency division multiplexing (OFDM) was adopted for 4G to realize the need for increasing signal bandwidths, some of its disadvantages like high peak-to-average-power ratio (PAPR), strict requirements of orthogonality, and longer cyclic prefixes (CP) could be more pronounced in 5G systems. Moreover, the need for OFDM in mmWave based 5G networks with huge channel bandwidths is questionable. Hence, alternate multicarrier techniques such as generalized frequency division multiplexing (GFDM), filterbank multicarrier (FBMC), and universal filtered multicarrier (UFMC), or even single carrier techniques are being investigated [41]. Also, variants of OFDM like filtered OFDM, frequency packed OFDM, and tunable OFDM are suggested to reduce the above-mentioned disadvantages of OFDM [6], [11]. Besides, active interference design strategies are desired to improve the cell-edge performance of 5G networks, and a new modulation scheme called frequency and quadrature amplitude modulation (FQAM) is being examined in this regard.

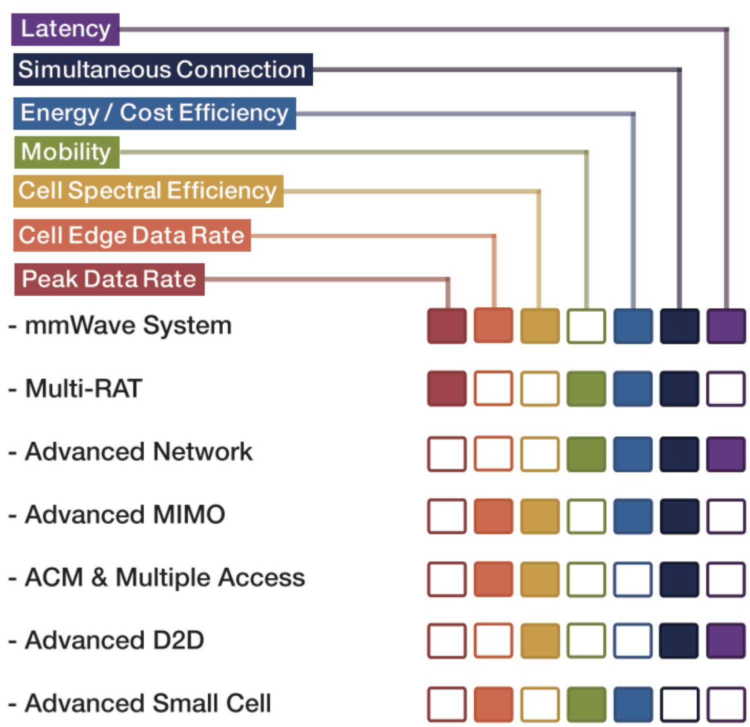

Figure 2.3 5G key enabling technologies and KPIs.

Table 2.1 Comparison of LTE and NR

Features	LTE	NR
Operating frequency	Sub-6 GHz	Sub-6 GHz and mmWave band
Carrier bandwidth	Up to 20 MHz	Up to 100 MHz for sub-6 GHz Up to 1 GHz for mmWave band
Channel coding	Turbo codes, Convolutional codes	Polar codes, LDPC codes
Subcarrier spacing	15 kHz	15 kHz, 30 kHz, 60 kHz, 120 kHz, 240 kHz
Carrier aggregation	Up to 32	Up to 16
Analog beamforming	Not supported	Supported
Digital beamforming	Up to 8 layers	Up to 12 layers

A mapping between the key enabling technologies and the proposed KPIs is depicted in Figure 2.3 [11]. It is tough to devise a unique technology that fulfils all the projected performance indices. However, all the KPIs need not be concurrently satisfied in all the 5G use cases. For example, streaming high definition video may require very high data rates but can relax on latency and reliability. But a driverless car clearly needs a reliable network with an end-to-end roundtrip latency of sub-1ms. Meanwhile, applications like virtual and augmented reality and tactile internet would necessitate both low latency as well as high bandwidth. Hence, 5G adopts appropriate enabling technologies to suit the desired category of use cases/usage scenarios. These technologies [42] have been intensively evaluated and validated through efficient testbeds [54] to guarantee successful deployments. 5G trials are also being directed [55]–[57] to verify and solve several innovative features like air interface, D2D communication, NFV in core and radio networks, edge computing, network slicing, security, and the like, to support different vertical sectors, such as mobility, health care, energy, automobile, automation, and logistics [1].

5G development gained momentum as Verizon formed the 5G technology forum (5GTF) in collaboration with industry leaders like Ericsson, Qualcomm, Samsung, and Intel accelerating the 3GPP NR release in 2017 [58]. The new 5G NR is a highly capable unified air interface that supports various services, spectrum, and deployments, and it offers several significant advantages when compared to 4G LTE [37]. Table 2.1 provides a brief comparison of LTE and NR, highlighting the main features. Aimed at achieving the 5G vision, NR operates at two distinct frequency ranges (FR) designated as FR1 specifying the sub-6GHz spectrum and FR2 for the high frequency mmWave spectrum above 24.25GHz, unleashing an extensive bandwidth that can solve the spectrum scarcity problem in FR1 bands. As observed, major telecom players have already made their initial treads towards 5G NSA deployment on the existing LTE infrastructure using FR1. For instance, Qualcomm and Nokia completed their interoperability test in 2018, and Ericsson, Huawei, and Vodafone launched the 5G networks in 2019. However, the implementation of standalone (SA) networks that support FR2 mmWave bands will be required to fully achieve the 5G envisioned features and performance requirements.

The deployment of 5G using the mmWave spectrum is likely to be revolutionary. Figure 2.3 clearly illustrates that mmWave technology is a key enabler that fulfils most of the 5G KPIs. Another advantage of mmWaves is that it readily complements many other enabling technologies. For instance, the short wavelengths of mmWaves support the massive MIMO concept. The short wavelengths also make it feasible to generate highly focussed beams to minimize the interference in 5G small cells and D2D links. Moreover, their high propagation losses and short transmission ranges are favourable for the network densification paradigm. In this view, we examine mmWave technology in detail in the next section.

2.3 MILLIMETER WAVE TECHNOLOGY FOR 5G

The first iteration of 5G NR that proposed the high frequency mmWaves as frequency bands for FR2 was introduced in 3GPP Release 15 [59]. The mmWave bands suggested for NR FR2 will provide an increase in the speed and capacity through increased spectrum bandwidth. As illustrated in Figure 2.4, the mmWave spectrum that spans the frequency range of 30 - 300GHz offers an order of magnitude higher bandwidths than the sub-6GHz bands, alleviating the spectrum crunch at lower

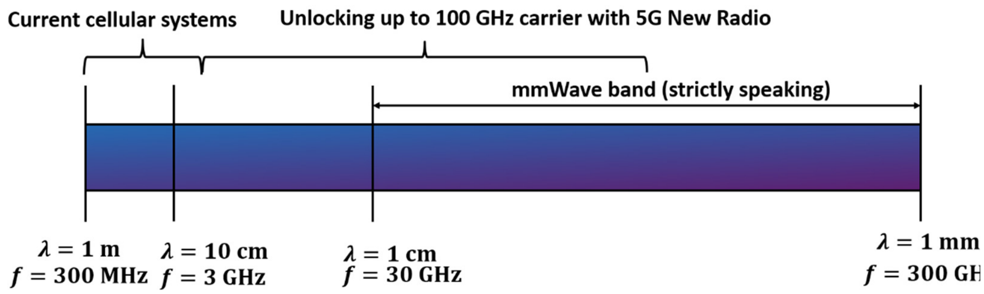

Figure 2.4 Operational frequency ranges of existing sub-6 GHz and future mmWave communication systems.

frequencies [60]. Even though mmWave communication systems were used in the past in fixed, LOS applications, their applicability in NLOS probable mobile access networks is a new frontier [15]. As the high frequency mmWaves travel along localized paths, there was a fear that its propagation is less favourable in cellular communication systems dominated by mobility and blockage. In this perspective, several studies have investigated the feasibility of mmWaves for future broadband networks [12]–[14], [16], [46], [61]. In earlier mmWave studies [62]–[65], significant focus was given to the unlicensed 60GHz band which alone offered 5-9GHz of overall bandwidth as opposed to the 90MHz and 500MHz bandwidths in the 2.4GHz and 5GHz bands, respectively. However, with the newly introduced 5G NR air interface, other bands in the mmWave spectrum are being investigated and explored to achieve the envisioned performance requirements [66]–[68]. Interestingly, mmWave communication systems can accomplish the 5G goals of multi-gigabits-per-second peak data rate, lower latency, together with enhanced user experience, connection density, and capacity through minimal engineering efforts [11].

The potential of mmWaves in realizing wireless links operating at optical speeds was earlier suggested in [69] wherein the authors proposed a cost-effective massive MIMO architecture that could establish highly directive links of speed up to 40Gbps even in adverse weather conditions. Though the model was not directly meant for 5G and was restricted to E-band frequencies (71-95GHz, excluding the unlicensed 60GHz band), it highlighted the significance of mmWaves unified with massive MIMO. However, the study assumed LOS conditions without the analysis of multipath components. The initial research on mmWave based 5G reported in [13] performed measurement campaigns at 28GHz and 38GHz frequency bands to analyse their path loss, building penetration, reflection characteristics, and other statistical parameters. The study asserted that mmWaves would work well for 5G outdoor cellular communications. Also, the work in [70] characterized the 38GHz band by using vertically polarized steerable rectangular horn antennas and revealed exciting novel findings: (i) transmission within a cell radii of 200m observed nearly no outage irrespective of the height of the antenna, (ii) the NLOS link exhibited almost 50dB higher path loss than a LOS/OLOS (obstructed LOS) link, (iii) increasing BS heights can increase the coverage, and most importantly, (iv) transmission is successful in mmWaves even for lower BS heights due to multiple reflections from the reflecting bodies in the environment. From the literature, it is found that realistic deployments of mmWave cellular systems may often rely less on methods to improve data rate and more on different techniques to reduce overhead. This establishes the need to explore alternate modulation techniques [71], [72]. As the available mmWave bandwidth is quite broad, the reliance of mmWave systems on traditional techniques like OFDM and higher order modulation which improve the transmission data rate is uncertain. Instead, a simple single carrier modulation with suitable spatial multiplexing may suffice the targeted performance specification [72], [73]. Furthermore, most of the mmWave studies considered simple quadrature phase shift keying (QPSK) as the reference modulation technique [74]–[76], requiring a lower receiver E_b/N_0 for a given error rate even in the absence of complex channel coding. Studies conducted for mmWaves also indicated that mmWave cellular systems would be power-limited, unlike the interference-limited microwave systems [33]. Several research opportunities of mmWaves are described in the context of 5G, particularly in heterogeneous networks and multi-antenna transceiver technologies [15]. As reported in [77], [78], the potential capabilities of mmWaves have also inspired their use in UAV assisted future 5G networks which use UAV as a promising solution to enhance both capacity and coverage.

Besides the wide bandwidths that directly translate to higher data rates and increased capacity, the mmWaves offer several other advantages. It is known from Friis' equation that the omnidirectional path loss increases with the square of the frequency. However, the shorter wavelength of mmWave signals allows comparably higher antenna gain for the same antenna aperture. Hence, by keeping the physical antenna size fixed, it is possible to transmit high frequency mmWaves with reduced path loss creating highly directional links with beamforming gains so as extend the cell coverage. The short wavelength of the band also allows integrating a multitude of antenna elements in a small form factor of even 1-2cm^2 through advancements in CMOS RF [46]. Hence, mmWaves can effectively exploit novel spatial processing techniques like massive MIMO and beamforming. The massive MIMO concept will be differently used in mmWave and sub-6GHz bands due to their unique propagation behaviours and hardware characteristics, as illustrated in Table 2.2 [79]. The short transmission range of mmWaves increasingly benefit from as well as contribute to the network densification which is progressively used even with sub-6GHz mobile communication systems [6], [9]. As mmWaves can be directionally transmitted at relatively lower power, transmissions will be limited to the desired cell itself permitting cell shrinking with ease. Although the significance of mmWaves is promising, the viability of mmWave mobile communications is determined by their adverse propagation conditions.

Table 2.2 Multi-antenna technology in sub-6 GHz and mmWave frequencies

Features	Sub-6 GHz	mmWave
Deployment scenario	Macrocells with high user mobility	Small cells with low user mobility
Simultaneous users per cell	Tens of users	One or a few users
Usage of multi-antenna technology	Spatial multiplexing of users by virtue of array gain and spatial separation to improve spectral efficiency	Beamforming to a single user to improve link budget and thereby coverage
Channel characteristics	Rich multipath	Sparse multipath
Channel bandwidth	Small	Large
Spectral efficiency	High due to spatial multiplexing	Low due to few users, larger path loss and noise power
Transceiver implementation	Fully digital	Hybrid analog-digital

2.3.1 PROPAGATION CHALLENGES OF mmWAVES

The challenges of using mmWaves as an alternative solution to the existing sub-6GHz spectrum are enormous, with a significant focus on mitigating these unfavourable propagation conditions[15], [16], [46]. The major challenge in deploying mmWaves in outdoor mobile communications is the higher free space path loss with distance. The free space path loss (FSPL) refers to the LOS path loss between two isotropic radiators in free space and its value at distance d due to carrier frequency f is given by $(4\pi d/\lambda)^2$. As stated earlier, employing directional antennas will help to more than compensate these high losses. Another significant challenge in mmWaves is its vulnerability to shadowing which can lead to an increased signal outage and an intermittent channel quality. Considering the mm-long wavelengths of mmWaves, objects as small as few tens of centimetres can create shadowing effect creating a signal attenuation as high as 40-80dB. Even the human body attenuation attributes to few tens of dB. However, shadowing effects, including human shadowing can be reduced by using electronically steerable antennas. It is also reported that the absorption of mmWave signals by atmospheric oxygen and water vapour make the signal strength drop off rapidly with distance compared to the low frequency microwave bands. Several study have characterized the atmospheric and molecular absorption [80], [81], and the rain attenuation [82], [83] characteristics of mmWaves. The wave is heavily attenuated at 60GHz with the oxygen absorption coefficient reaching a peak value of 16dB/km, and at 164-200GHz with the water vapour absorption causing a peak attenuation of 20-30dB/km. Interestingly, these highly attenuated waves can be used to implement small cell structures with minimal interference mitigation mechanisms. A further impairment in mmWave propagation is the foliage induced attenuation that cannot be neglected while characterizing mmWave channels. ITU recommends an experimental relationship to deduce this attenuation for foliage depths below 400m [32], [33].

In general, the NLOS propagation mechanism of radio waves attributes to reflection, diffraction, and scattering which enables signal transmission even in the absence of a direct LOS path. These mechanisms are quite different for mmWaves compared to sub-6GHz because of the extremely short wavelength of mmWaves. Literature reports mmWave measurement campaigns conducted to explore the NLOS propagation mechanisms at different mmWave frequencies [14], [84]. As inferred, the short wavelength typically causes the diffracted path to incur significant attenuation producing higher shadowing effects. Moreover, urban outdoor communications with heavily attenuated buildings and low height antennas are less prone to diffraction and diffused scattering mechanisms which elevate the significance of signal reflections. Most importantly, the quasi-optical nature of mmWaves enhances the rough surface scattering effects making the reflected paths more specular-like. That is, specular reflections that obey the reflection law will be the dominant propagation mechanism [22]. Hence, mmWave outdoor transmission power is mainly propagated through the direct LOS path and a few specular reflected paths [66]. This implies that the channel multipath of mmWave outdoor links is sparse as compared to the rich scattering multipath structure of sub-6GHz channels. Hence, mmWave channels should be carefully characterized using accurate and realistic channel models and are extensively being designed and developed in recent years [32], [33], [36].

2.3.2 SIGNIFICANCE OF ANTENNA DIRECTIONALITY IN mmWAVES

As evident, 5G with mmWaves will incorporate greater gain directional antennas to compensate for the additional path loss of mmWave channels. In fact, highly directional narrow beam transmission with advanced beamforming and beam steering techniques will be exploited by mmWave systems to create high-quality links with extended range and high SNR [17], [18], [24]. In [73], the channel statistics of mmWaves were evaluated using an isotropic antenna and then compared against the phased array beamforming case so as to study the need and effect of beamforming in various deployment scenarios. Beamforming techniques are largely discussed in recent literature [73], [85], [86]. Unlike traditional cellular systems where beamforming is implemented at the baseband level, mmWave system architecture would desire beamforming at the passband and the analog domain. Accordingly, hybrid beamforming is being proposed for mmWaves to overcome the need for having a dedicated RF chain for each antenna element in baseband beamforming, and also to handle the channel sparsity arising from the directional transmission.

By and large, the relative positions of the UE and the BS continuously vary over time in a mobile broadband network. In a beam steering aided directional communication system, the beam directions of the TX and/or the RX antenna will be dynamically aligned for maximum signal reception. It assumes that the RX's beam is always steered to TX with the help of instantaneous location information and beam reference signal [87]. The directional transmission with beam steering offers several benefits. Primarily, it supports the spatial reuse of the channel. That is, by steering spatially separate beams in different unique directions, a single BS can serve multiple users in one cell. Moreover, targeting the narrow beams directly to the UE could increase the network capacity. It also reduces interference to neighbouring cells thereby improving the spectral efficiency. However, a significant implementation challenge will be to test the beam steering capabilities of BSs and UEs that also requires examining the channel characteristics by dynamically steering the directional antenna beams towards the strongest energy. This will be extremely challenging in small cell mmWave networks having a large handoff probability.

Incorporating directionality in mmWave transmission invokes unique propagation characteristics for mmWave channels. Clearly, it reduces the angular spread of multipath components (MPCs), causing very few multipaths to aggregate at the receiver, unlike the rich scattering sub-6GHz signals generated in an omnidirectional scenario. In specific, the directional antenna radiation pattern filters out all the higher order reflections that fall outside the narrow beam area, further reducing the resolvable specular reflections of the channel [32]. The resulting directional channels are spatially sparse and often simpler than the omnidirectional channels with multipaths arriving from every direction. Therefore modeling the mmWave directional propagation requires redesigning the standard omnidirectional models due to their inadequacy in modeling the spatial filtering effects of directional antennas [32].

2.3.3 CHANNEL MODELS FOR mmWAVES

Channel modeling refers to determining how the physical propagation channel impacts the transmitted signals. It helps to realize specific channel properties that show high variance in frequency, space, and time. The development of accurate channel models for mmWaves is vital to design efficient devices as well as to define useful and realistic test cases. The design and performance evaluation of efficient channel state feedback algorithms, beamforming/tracking algorithms, link adaptation schemes, and novel signaling protocols for mmWaves also depends on the precision of the channel model even more than at sub-6GHz frequencies. Unlike the low-frequency channel models, mmWave channel models should cater to a variety of channel modeling requirements. This includes accommodating a wide frequency range, large channel bandwidth, an extensive range of directional antenna arrays, and high mobility while offering a moderate computation complexity. The model should additionally ensure good temporal/spatial/frequency consistency [35]. These unique requirements of mmWave characterization have resulted in diverse channel modeling techniques discussed in quite a few survey papers [32], [33], [36], [88], and recent research papers [[89]–[94]]. Each of these models could realize specific key challenges of mmWave requirements, yet they are inadequate in characterizing all aspects of mmWaves [32]. The existing models attempt to cover some of the deployment scenarios such as urban macro (UMa), rural macro (RMa), and indoor hotspot (InH) besides UMi. In addition to these typical scenarios, 3GPP Release 14 identifies D2D, open-roofed stadium, close-roofed Gym, and urban SC backhaul with small cell BSs placed on the lamp posts as other key scenarios of interest for mmWave channel modeling [68].

2.3.3.1 mmWAVE CHANNEL MODELING METHODOLOGIES

A channel model typically provides a mathematical representation of the multipath components arising from various propagation mechanisms and is an essential part of physical layer simulations. Wireless channel models are broadly classified into two main groups, i.e., physical models and analytical models. Physical channel models characterize an environment by describing the wave propagation between the TX and RX antennas. In contrast, analytical channel models represent the channel between the TX and RX mathematically without accounting for wave propagation. As physical models provide accurate modeling of radio propagation, they are commonly used to characterize the stringent propagation requirements of mmWave channels and are discussed further in this chapter. Among the physical channel models, ray tracing based deterministic channel models and geometry-based stochastic channel models (GSCM) have attracted much attention. Note that the choice of channel model depends on the accuracy, generality, and simplicity, among other factors.

- **Stochastic Channel Modeling**: The GSCMs define the stochastic distribution of scatterers based on geometric information. It describes the channel attributes in terms of their statistical moments derived from mmWave measurements taken in specific scenarios. By increasing the channel attributes used in characterizing the channel, model accuracy can be improved. Hence, the stochastic models generally rely on using expensive channel sounders. The stochastic channel modeling typically derives a propagation path loss model and a fading model. The path loss model first identifies a scenario to be LOS or NLOS and appropriately applies different equations for deriving the large scale path loss. Furthermore, spatial channel models based on measurements or analytical formulations are used for characterizing the effect of fading [95]. Statistical channel models usually are simple models with low computation complexity and execution time.

- **Deterministic Channel Modeling:** The deterministic channel models are best suited for characterizing real environments. This site-specific channel model also comprises two sub-models, i.e., an environment model and a wave propagation model. The environment model defines the position and deployment geometry of the channel. It also specifies the material composition of the objects and obstacles in the channel. The wave propagation model is typically characterized by Maxwell's equations. An analytical solution of these equations is practically difficult due to the high computation time. However, the quasi-optical nature of high frequency mmWave considerably simplifies the description of wave propagation. Due to this, iterated approaches such as ray tracing based geometric optical models with substantially reduced complexity and computing time can be used to characterize mmWaves. Deterministic ray tracing models can also be used to perform real-time prediction of the channel's directional characteristics reducing the need for time-consuming exhaustive search techniques [22].

Literature states that the ray tracing technique addresses most of the propagation challenges and is useful in accurately characterizing mmWave channels for specific scenarios [22], [24], [28], [31], [90], [93], [96]. As reported in [97], deterministic models provide reduced generality in terms of scenario selection. However, the main advantage with deterministic modeling is that the channel is realistically defined in terms of MPCs which are functions of signal power, TX/RX location, arrival/departure angles, and the material properties of reflecting/scattering surfaces. Moreover, the MPCs are generated following the scenario geometry and are consistent with the mobility model of the communicating nodes [90].

2.3.3.2 mmWAVE CHANNEL MODELING EFFORTS

While existing literature reports several channel modeling efforts for mmWaves, this section briefs some of the popular and highly cited mmWave outdoor channel models.

- **QuaDRiGa Model** [98]: Quasi Deterministic Radio Channel Generator (QuaDRiGa) channel model is a 3D GSCM supported by data from measurement campaigns at 28-, 43-, 60-, and 82GHz. It is an extension of the WINNER channel model which was initially designed for sub-6GHz and later modified for mmWave channel characterization.

- **METIS Model** [45]: The Mobile and wireless communications Enablers for the Twenty-twenty Information Society (METIS) channel model characterizes mmWave frequencies up to 60GHz and uses the alpha-beta-gamma (ABG) model for large scale analysis. It uses existing modeling strategies to realize the specific requirements of mmWaves such as high bandwidth and 3D polarization modeling. The model essentially provides three different methodologies: (i) a map-based ray tracing model that supports the 3D geometrical description of the environment (ii) a stochastic model which is an extension of the WINNER II model based on GSCM, and (iii) a hybrid model as a combination of deterministic and stochastic modeling approaches.

- **NYUSIM Model** [94]: NYUSIM developed by New York University (NYU) applied the close-in (CI) reference distance models to derive the large scale characteristics of mmWaves at 28-, 38-, 60-, and 73GHz. The model parameters for each mmWave frequency were discreetly determined from channel measurements. The choice of the CI model is due to its ease of applicability, model stability, and fewer model parameters. NYUSIM primarily uses the concepts of time cluster (TC) and spatial lobe (SL) to characterize multipath components in omnidirectional CIRs. A significant advantage of NYUSIM stated by the authors is the reduced number of TCs and

SLs as compared to the unrealistically large cluster numbers in the 3GPP channel model.

- **mmMAGIC Model** [99]: Millimeter-Wave Based Mobile Radio Access Network for 5G Integrated Communications (mmMAGIC) is a research project sponsored by the European Union intended to provide extensive radio channel measurements in the 6-100GHz range. Large scale path loss analysis follows the standard ABG model with unique parameter values. The mmMAGIC model is also a statistical channel model (GSCM) derived from measurements and is well suited for link-level and system-level simulations. The proposed 3D modeling framework uses QuaDRiGa as a reference and provides enhancements in terms of blockage modeling, spatial consistency, and outdoor-to-indoor (O2I) modeling.

- **MiWEBA Model** [23]**:** Millimeter-Wave Evolution for Backhaul and Access (MiWEBA) channel model chose the deterministic approach to accurately support spatial consistency which would not be possible with statistical formulations. MiWEBA model is a quasi-deterministic channel model that uses the ABG model for large scale path loss prediction. The model used measurements performed at 60GHz across a 5-50m propagation range using omnidirectional antennas to derive both access and backhaul channel parameters. To provide an accurate channel description, the model uses a geometry-based deterministic method to evaluate the strongest reflections called D-rays and uses a statistical channel modeling approach to derive random weaker paths called R-rays.

- **3GPP Model** [68]: The 3GPP channel model specified in TR 38.901 proposed the clustered delay line (CDL) and tapped delay line (TDL) modeling strategies for link-level simulation. The model evaluates large scale path loss for the LOS scenario by using a dual slope CI breakpoint model. In contrast, the NLOS scenario is modelled using the ABG model with an additional term to accommodate the UE height dependency. A 3D TX-RX separation distance is applied accounting for the differences in the BS and UE heights, which corrects the misalignment between TX and RX in the vertical plane alone. In fact, the applicability of dual slope models in mmWave UMi small cell modeling is questionable as their breakpoint distances generally exceed the UMi cell radius of 150-200m, even with the smallest BS and UE heights [36]. Moreover, the realization of small-scale fading in the 3GPP model is based on the 3D statistical spatial approach earlier proposed by 3GPP and is computationally very demanding.

2.3.3.3 mmWAVE CHANNEL MODELING RESEARCH GAPS

In this section, we identify the research gaps in mmWave channel modeling with specific attention to channel directionality, a vital channel modeling component in mmWaves. The large signal attenuation and the high antenna directivity of mmWave directional channels can result in channel sparsity in the angular domain (i.e., low angular spread) as well as in the delay domain (i.e., low Doppler spread). This suggests that the mmWave directional channels with fewer contributing multipaths are often simpler than the omnidirectional channels. Hence, mmWave development would require unique channel model designs that can capture signal directionality and the related channel sparsity. Most importantly, these models should essentially characterize the spatial dynamics of the channel.

As inferred from literature, standard bodies generally develop omnidirectional path loss models by considering unity gain antennas to provide generality as well as to preserve the traditional sub-6GHz modeling methodologies [64], [68], [94]. For instance, the models could be either distinctly omnidirectional as in the case of the 3GPP model [68], or developed from omnidirectional measurements like the MiWEBA model [64] or occasionally converged to omnidirectional model formulations as suggested in the NYUSIM model [94]. It is found that NYUSIM and MiWEBA models use unique methods to create directional channel formulations. However, authors in [36] have highlighted the inadequacy of omnidirectional path loss models in performing the directional channel analysis unless the antenna patterns and accurate spatial/temporal multipath channel statistics are known or effectively modelled. In general, directional channel models cannot be developed by merely adding directional antenna gains into the omnidirectional channel model since fewer paths participate in the directional transmission due to spatial filtering of directional antennas [94]. It is inferred that this approach could overestimate the channel performance parameters such as coverage and interference. In this respect, a directional beam-combining CI (BC-CI) model using just about three parameters was proposed in [27] for NLOS mmWave propagation. However, the model characterizes only specific frequencies (28, 60, and 73GHz) and antenna heights. Also, it requires the number of beams used for combining, as a user-specified input parameter.

Existing statistical channel models are indeed computationally simpler with fewer input parameters; however, they do not provide consistency of model parameters between changing specifications. While performing mmWave study, it is quite challenging to extract the exact model parameters best fitting a required set of input specifications by using CI and FI models. Especially, as their model parameters such as path loss exponents and fading factors are derived from measurements for definite deployments, frequencies, and environments (LOS/NLOS). This also implies a lack of measurement values and model parameters at "non-popular" frequency bands. Moreover, the stochastic and analytical models usually characterize mmWave channels based on stochastic variables derived from measurements, hence, they are inaccurate in describing specific scenarios. Furthermore, they fail to account for the temporal-spatial consistency of LOS and the unique evolution of channel multipaths in mmWave channels. As reported in [36], the channel models based on GSCM will produce large variations in the estimated model parameters and capacity analysis due to their diverse assumptions on parameters such as the number of strong paths, LOS distance, cluster size, number of sub-rays, and the like.

While statistical models are widely used to predict mmWave propagation effects, they reach their limits in highly directional channels [25]. Due to the usage of directional antennas in mmWaves and the need to analyse their impact on channel statistics [8], [85], it is suggested that the channel model design should support directional antenna settings in both horizontal and vertical planes. In particular, the model should define the effective antenna gains, instead of boresight gains, so as to model the effect of non-uniform magnification of MPCs. Therefore, a need arises to develop a channel model design for characterizing both azimuth and elevation directions of propagation in a 3D plane. Intuitively, deterministic models based on ray tracing are well suited to predict the directional characteristics of mmWave channels. Deterministic models present supremacy over statistical and empirical models as they can be easily employed in the analysis of beamforming and beam steering. The beamforming strategies generally conduct an extensive search over a discrete set of beams and assess their signal-to-interference-plus-noise ratio (SINR) to define the best combination of steering vectors for transmission. The possibility of narrow beams can extensively slow down this search technique in the mmWave case. However, if the channel's directional characteristics can be described in real-time by using low complexity ray tracers, they can be used as a tool to assist beamforming. Accordingly, authors in [22] have used ray tracing simulators to assess the radial, single and multi-beamforming strategies for mmWaves and have validated them against directional channel measurements for indoors. Furthermore, a well validated ray tracing tool can characterize any new channel scenario even in the absence of expensive measurement set up strictly matching the needed.

The environment dependency of mmWaves leads to the preference of site-specific deterministic modeling. Their benefits of accuracy and site-specificity are often overpowered by computational complexity and time-intensive implementations. Fortunately, the computational complexity of the deterministic model (and in turn, system-level, and link-level models) can be reduced by reducing the number of contributing multipaths. To this end, authors in [90] propose to reduce the total number of multipaths by following a two-fold discarding strategy, i.e., (i) discarding the number of waves that undergoes multiple bounces from scattering surfaces as the absorption on these surfaces degrades the overall received power, (ii) rejecting the weakest path by providing a minimum threshold for its path gain as compared to the gain of the strongest path. As is known, directional transmission in mmWaves implies a reduced number of channel multipath components and thereby a sparse channel structure which can be exploited as a strategy to reduce the participating paths in ray tracing simulations allowing an appropriate accuracy-complexity trade-off.

In mmWave statistical channel study, considerable research is driven towards correcting closed-form expressions to accommodate mmWave specific propagation characteristics. For instance, [100] proves the significance of incorporating a blockage dependent correction factor in the popular simplified received power model while modeling mmWave networks with directional beamforming and blockage effects. Authors in [26], [27], [101] provide corrections to path loss slope so as to adapt the models to the larger path loss of mmWaves. The mmWave study also reflects correction of the shadow fading factor, X_σ, of the path loss equation. Consequently, [102] reported a hybrid probabilistic path loss model as an alternative to traditional path loss modeling over distance and proposed a distance dependent shadowing factor to characterize the large scale shadowing. However, the proposed model uses omnidirectional propagation. Moreover, it should compute a complex weighing function that states the LOS probability curve for every TX-RX pair to compute the corrected X_σ value. The correction of the shadow fading factor to accommodate antenna directionality in mmWave channel modeling has not been reported in the available literature.

A significant impact of having a short wavelength is that even small spatial variations, in terms of a few centimetres, in the channel substantially increase the changes in mmWave path loss. To this end, antenna diversity using MIMO is generally exploited to ensure stable transmissions [28], [76], [103]. The small wavelength of mmWaves combined with antenna directionality also makes the outdoor channel path loss largely dependent on the deployment parameters of the scenario. Hence, the usage of correct values for them is vital to achieving optimal channel performance [104]. One of the recent research directions in literature is the applicability of artificial intelligence (AI) machine learning in mmWave 5G networks [105]–[109]. Authors in [108] used a 2D ray tracing to determine the UE position and applied machine learning-based fingerprinting to increase the accuracy of positioning. Machine learning approach can be employed in mmWave based 5G networks to minimize the number of BSs and to optimize their placements [109].

In summary, 5G mmWave communications will necessitate the redesign of the complete cellular framework opening up tremendous research opportunities in channel characterization and modeling, directional transmission, beamforming and steering, beam training and tracking, and many more. With the emergence of direction transmission assisted by beamforming and steering techniques, understanding the role of antenna directionality in channel spatial filtering and determining its impact on outdoor SC deployments require further exploration.

2.4 CHAPTER SUMMARY

In general, 5G research deals with the algorithms and implementations of modulation and coding schemes, new spatial signal processing technologies, new spectrum opportunities, channel modeling, 5G proof of concept systems, and other system-level enabling technologies. We have briefly reviewed different aspects of the 5G system design and development. Further, we discussed the propagation challenges of mmWave channels arising from high signal attenuation and channel fluctuations arising from mmWave specific adverse losses such as absorption, penetration, and foliage losses. The need to develop channel models that can reflect the unique features of mmWaves is established and the related studies have been briefed. The significance of antenna directionality and its implications on mmWave channel modeling has been discussed. At the end of this chapter, we provide the open research issues related to the mmWave directional channel modeling and highlight the possibility of exploring channel directionality to offer realistic and reduced complexity channel modeling approaches.

CHAPTER 3. ANALYSIS AND DESIGN-I: SIMPLIFIED DIRECTIONAL DETERMINISTIC CHANNEL MODELING

3.1 INTRODUCTION

In this chapter, we develop a detailed mathematical formulation of the mmWave outdoor propagation model MiDDCM which can serve as a reference for their implementation and further development. The proposed MiDDCM efficiently models the sparse multipath structure of directional mmWave channels. Additionally, it evaluates various transmission scenarios that cannot be modelled by traditional statistical channel models. Accordingly, the model is applied for multiple realistic scenarios such as backhaul/access links, LOS/NLOS transmissions, beam aligned/unaligned propagations, and road canyon deployment with/without crossroads. The chapter also examines a scheme to extend the MiDDCM for a directional SISO channel to model a 2 x 2 MIMO channel by following the two ray technique to investigate the influence of antenna separations on channel performance. However, we start with the mmWave propagation characteristic to build up the theory.

3.2 mmWAVE PROPAGATION CHARACTERISTICS

In this section, we explain some of the significant characteristics of mmWave directional outdoor channels and their influence on our channel modeling methodology.

3.2.1 LINK DIRECTIONALITY AND DIRECTIONAL ANTENNA MODEL

Here, we first provide a brief insight into the link directionality in mmWaves, the associated channel sparsity, and their implications followed by a highly directional horn antenna design used in our channel model.

The high propagation loss of mmWaves motivates a design change from omnidirectional antennas to spatially focussed, high-gain antennas to generate comparable system performance. Hence, both TX and RX will use narrow directional beams that are well aligned for maximum signal reception. There are several implications of antenna directionality on mmWave channels and their characterization. Most importantly, these directional antennas will act as spatial filters that filter out the multipath energy from directions outside the antenna beam area. Hence, unlike the rich scattering low-frequency omnidirectional transmissions, beamforming-aided directional communication would aggregate only a limited number of MPCs of those that fall within the beam-ranges of transmitting and receiving directional antennas [32]. The number of contributing channel multipaths further reduces due to the triviality of diffraction and diffused scattering effects in mmWave urban outdoors comprising low-height antennas and severely attenuated buildings. Thus, the channel typically consists of a direct LOS path and low-dense multipaths. This implies that the mmWave outdoor directional channel is spatially sparse with sufficiently strong reflected paths causing significant fades in the received power. The sparsity can also cause substantial variations in the channel characteristics even with small changes in the propagation geometry, thereby compromising the link robustness. Hence, a detailed description of the site-specific directional mmWave channel is required.

The channel sparsity also implies that the mmWave directional channel is more straightforward to model than an omnidirectional sub-6GHz channel. Since, for omnidirectional rich scattering environments, deterministic ray tracing simulation is quite complex due to the intricacy in calculating numerous participating paths arriving from all directions. The omnidirectional ray tracing models traditionally used simple two ray models [64], [99] for assessing the ground reflected ray and the direct LOS ray to reduce this modeling complexity with a trade-off in the accuracy. However, the sparse multipath structure of the mmWave directional channel inherently allows the ray tracing technique to acquire all specular reflections with acceptable complexity. Hence, it is imperative to understand and model antenna directionality while deriving directional channel models for SC outdoor deployments. In this work, we modelled antenna directionality by using a simplified, highly directional horn antenna design. Fundamentally, the goal is to understand directionality effects and diversity in sparse multipath channels. Also, it is reported in [26], [32], [96] that the mmWave channel sounding experiments often use horn antennas as a plausible directional antenna configuration at both TX and RX sides. On the other hand, a more realistic antenna array having a smaller gain for each element can also be used to achieve the desired directional antenna gains. Note that, MiDDCM supports the inclusion of custom antenna radiation patterns.

The directional radiation pattern of the suggested horn antenna design comprises of the main lobe with an azimuth half power beamwidth of $HPBW_A$ and an elevation half power beamwidth of $HPBW_E$. The single side lobes are 14dB attenuated as compared to the main lobe peak amplitude. For the given azimuth and elevation HPBWs, the directional horn antenna gain at any azimuth angle (ϕ) and elevation angle (θ), relative to the antenna boresight, can be approximated by [110]:

$$G(\phi, \theta) = G_0\,[\mathrm{sinc}^2(\mathrm{a}.\sin(\phi))\cos^2(\phi)].[\mathrm{sinc}^2(\mathrm{b}.\sin(\theta))\cos^2(\theta)] \qquad (3.1)$$

where G_0 is the boresight gain of the chosen horn antenna (at $\phi = \theta = 0$) evaluated as a function of its azimuth and elevation HPBWs as,

$$G_0 = 7.5\,(\,67/HPBW_A\,).(\,56/HPBW_E\,) \qquad (3.2)$$

The constants a and b are functions of $HPBW_A$ and $HPBW_E$ of the horn antenna, evaluated by solving (3.3) and (3.4), respectively, i.e.,

$$\mathrm{sinc}^2\left(\mathrm{a}.\sin\left(\frac{HPBW_A}{2}\right)\right)\cos^2\left(\frac{HPBW_A}{2}\right) = \frac{1}{2} \qquad (3.3)$$

$$\mathrm{sinc}^2\left(\mathrm{b}.\sin\left(\frac{HPBW_E}{2}\right)\right)\cos^2\left(\frac{HPBW_E}{2}\right) = \frac{1}{2} \qquad (3.4)$$

For instance, if $HPBW_A = 15°$ and $HPBW_E = 13°$, one of the design choices, then a = 3.35 and b = 3.88 with boresight gain G_0 = 21.6dBi. Equation 3.1 used in the system model helps to avoid analytical solving of complex double integration.

Figure 3.1 shows the sample normalized antenna radiation pattern of the horn antenna design used in the channel model simulations. This reference antenna model is the basis for evaluating the strength of each MPC at their respective angles of

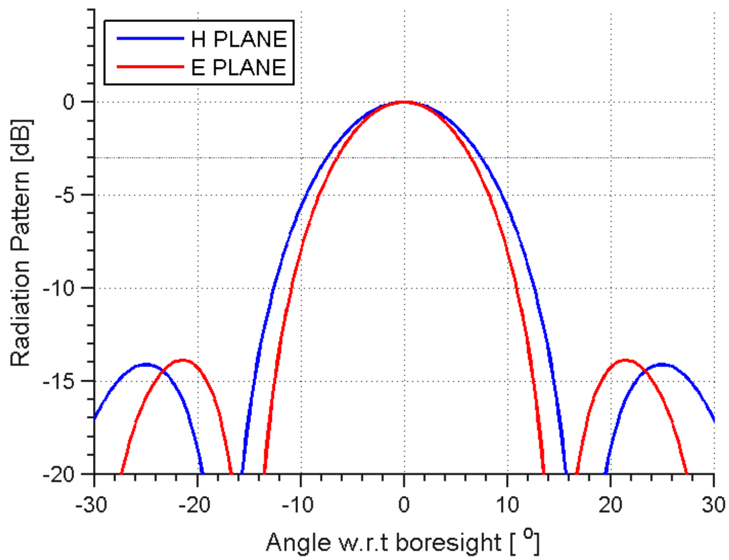

Figure 3.1 Normalized power pattern for a horn antenna, $HPBW_A = 15°$ and $HPBW_E = 13°$.

arrival/departure that is assessed in Section 3.3. Note that in our simulation, 0° implies the horizontal and vertical orientation of the beam along the reference axis.

3.2.2 OXYGEN ABSORPTION MODEL

The mmWave bands suffer higher attenuation over distance due to molecular resonances of oxygen in the air, which causes specific frequency bands to undergo signal absorption in the atmosphere. The signal attenuation from atmospheric oxygen is a function of the carrier frequency. For example, 60GHz signals experience an additional attenuation of about 16dB/km. It is essential to evaluate the oxygen absorption loss while estimating the received signal strength to have a realistic estimation of mmWave propagation characteristics. Most commonly, channel studies include the attenuation values either in the link budget estimation [32] or in the path loss slope calculation [26], [27], [101]. However, this work includes the oxygen absorption model in the channel model itself, intending to generate accurate predictions across the mmWave spectrum. As reported in the literature, two models are popularly used to model the oxygen absorption properties of mmWaves. That is, the approximate model proposed by ITU-R [80] and the empirical model developed by Hans J. Liebe [81]. The former technique uses simple algorithms that carry out

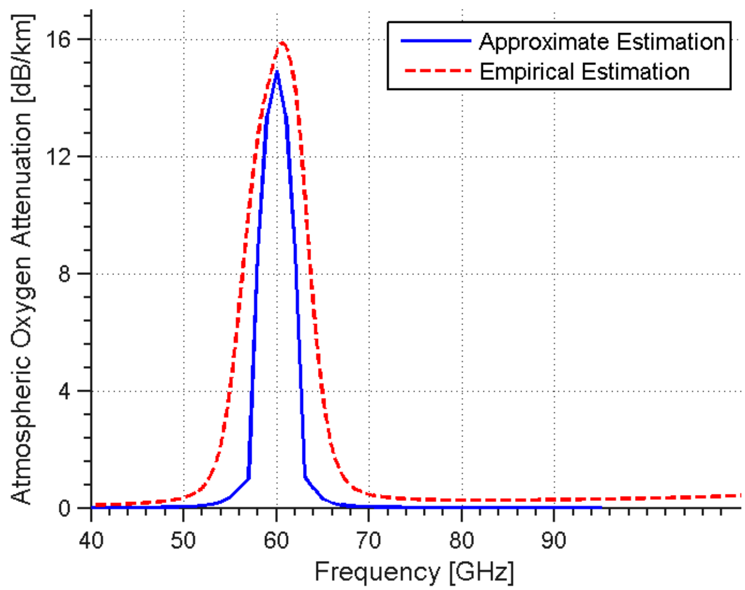

Figure 3.2 Specific attenuation simulated using Leibe's Model and Approximation Model.

curve-fitting to the line-by-line calculation of the specific attenuation. However, the method usually trades-off accuracy for simplicity. On the other hand, Leibe's model provides accurate attenuation values. But it is quite complicated and requires empirical parameters obtained from laboratory experiments to estimate the attenuation factor.

In Figure 3.2, we compare the attenuation values simulated for mmWave E-band frequencies using the two abovementioned methodologies. As illustrated, the variation in the attenuation values, predicted by the two models, is upper bound at 0.3dB/km for frequencies in the higher E-band. Even at 60GHz, where the specific attenuation peaks, we observed a maximum variation of 0.62dB/km. Due to the nominal differences observed in the simulation, we choose to integrate the simpler approximate estimation method in our channel model for generating absorption losses across the mmWave spectrum.

3.2.3 LINK BUDGET ESTIMATION

In the study of mmWave communications, it is essential to analyse the link budget to establish a mmWave link successfully. In this part of the thesis, we present the basic technique of estimating the link budget that depends mainly on the transmitting power, directional antenna gains of TX and RX, SNR, and the desired throughput of the link. Accordingly, the link is budgeted by cautiously designing the TX power P_t, TX and RX antenna gains at boresight G_t and G_r, and the RX sensitivity $P_{r,min}$ to achieve the desired data rate R_b for a link, given the thermal noise at the receiver and the receiver noise figure F. For a specified constellation and un-coded bit error probability P_e, the minimum bit-energy/noise E_b/N_0 can be easily calculated [111]. Given this, the link budget can be evaluated for any unknown parameter, with all the other parameters fixed as required/specified, by using (3.5) and (3.6).

$$P_{r,min}\,[\text{dBm}] = \frac{E_b}{N_0}\,[\text{dB}] + R_b\,[\text{dB}] - 174\,[\text{dBm}] + F\,[\text{dB}] \tag{3.5}$$

$$P_{r,min}\,[\text{dBm}] = \text{ EIRP}\,[\text{dB}] + G_r\,[\text{dBi}] - \text{MAPL}\,[\text{dB}] - L_{Margin}\,[\text{dB}] \tag{3.6}$$

where EIRP is the effective isotropic radiated power. The maximum allowable path loss (MAPL) for free space in a mmWave link is the sum of FSPL and the mmWave specific losses, like the atmospheric absorption loss and foliage loss. For example, by assuming a maximum separation distance, $d = d_{max}$, the FSPL = $20\log_{10}(4\pi d_{max}/\lambda)$ and the signal attenuation due to oxygen absorption = $10\log_{10} e^{K_a \cdot d_{max}}$. Here, λ is the wavelength of operating frequency. The coefficient of exponential absorption, K_a, is obtained from the oxygen absorption model. For instance, K_a is considered as $0.0016\log_e 10$ for 60GHz signals attenuated at 16dB/km. L_{Margin} indicates the link margin in dB that provides for an additional attenuation due to channel fading. By suitably selecting the parameters P_t and G_t, we can limit the resulting EIRP within the recommended federal communication commission (FCC) limit of 40dBm. Note that the value is raised to 82dBm only for the 60GHz outdoor links with high gain antennas [112].

3.3 MILLIMETER WAVE DIRECTIONAL DETERMINISTIC CHANNEL MODEL (MIDDCM)

MiDDCM is a low complexity deterministic channel model based on custom ray tracing used in the characterization of a typical mmWave directional UMi SC environment, as illustrated in Figure 3.3. As stated, the complexity reduction is achieved by exploiting antenna directionality and mmWave attenuation that allows us

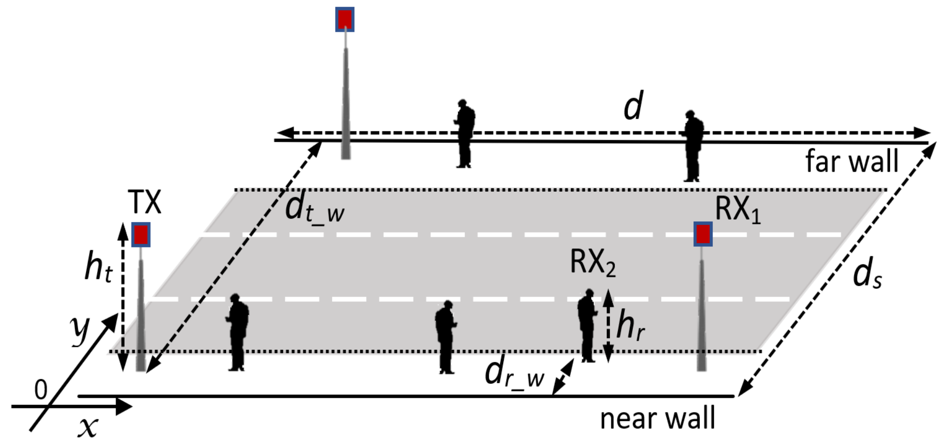

Figure 3.3 A typical UMi street canyon environment deploying gNodeBs on the lamp posts.

to model only specular reflections that fall inside the antenna beam area and to discard the paths with higher angles of arrival/departure. Hence, MiDDCM is a generalized framework, wherein the choice of directional antenna HPBWs in both azimuth and elevation plane determines the maximum order of wall reflections for every channel instance. This approach is more realistic and reliable compared to the current modeling approaches where the number of reflected paths participating in the evaluation of received signal strength is either fixed [23], [62], [99], or explicitly specified as an input parameter [27]. The model also provides improved accuracy compared to the simplified approach of using a two-ray propagation model pursued by various ray tracing simulators.

3.3.1 ENVIRONMENT GEOMETRY OF OUTDOOR UMI SC

In this work, we consider a typical 3D UMi SC outdoor environment geometry with tall buildings on both sides of the road canyon. We assume that the nodes which function as mmWave base stations (BSs)/access points (APs) are positioned on top of the lamp posts at an anchored distance from the sidewalls of the buildings, lower than their rooftops, or on the building sidewalls themselves. These nodes can be mounted either on the same side of the street or opposite side. The assumption of mmWave nodes placed lower than the rooftops promotes wall reflections. These wall reflections together with the ground reflection from the road ensure signal reception even in NLOS or obstructed LOS transmission condition. The implementation of high-gain

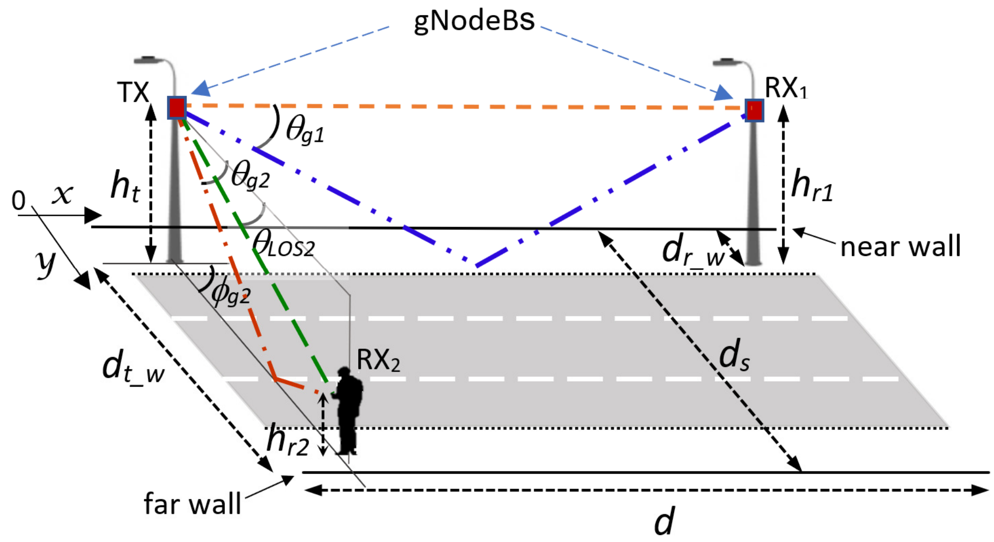

Figure 3.4 The mmWave UMi SC scenario illustrating direct LOS and ground reflected paths for backhaul and access links.

narrow beam antennas at both transmitter and receiver typically creates a sparse multipath channel wherein a maximum of third-order wall reflections generally contribute towards the received signal. Note that *order* refers to the number of times the ray gets reflected from the wall surface before the reception. Clearly, higher order reflections create paths with a larger angle of arrivals (AoAs) and angle of departures (AoDs) which may fall outside the directional antenna beam. Such paths are considered invalid and are not aggregated at the receiver.

The typical UMi SC geometry in Figure 3.3 is simplified and shown in Figure 3.4 to clearly illustrate a single backhaul link (between two BSs/gNodeBs) and an access link (between a gNodeB and UE). It represents the 3D front view of the specific geometry in the x-y-z plane depicting the direct LOS path and the ground reflected path between TX and RX. Also, (i) the transmitting node is placed at an antenna height of h_t; (ii) h_{r1} is the height of receiving node in the backhaul link, while, h_{r2} shows the receiver height for the access case; (iii) street width is denoted by d_s; (iv) d_{t_w} is the distance from TX location to the far reflecting wall; (v) d_{r_w} is the distance between RX and the near reflecting wall; (vi) d defines the 2D separation distance between TX and RX, *i.e.*, the straight line distance along the x-direction (with y-coordinate = 0, disregarding the displacement along the y-axis). For convenience, we

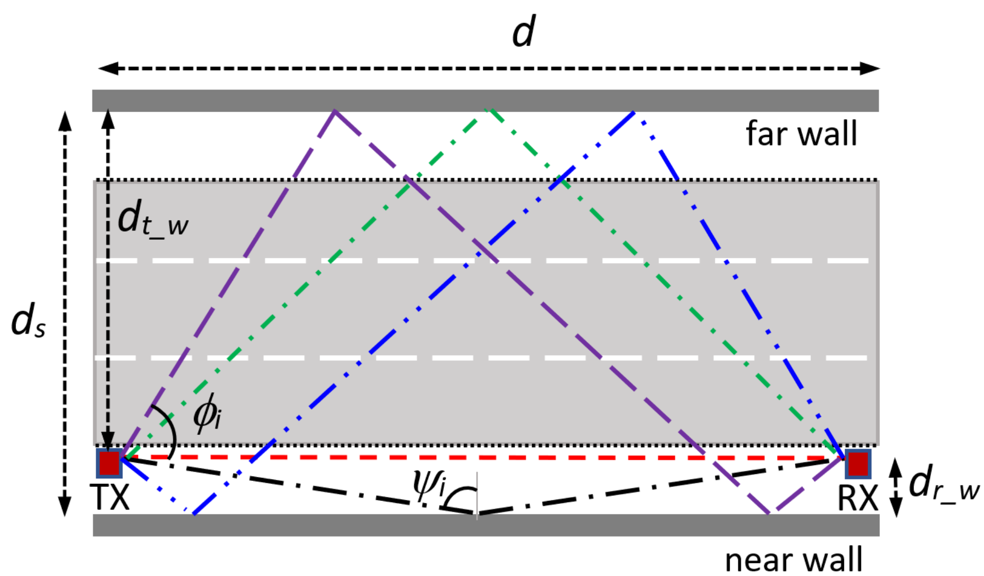

Figure 3.5 2D top-down view of mmWave directional UMi SC scenario showing first and second order wall reflections for "System I".

use the generalized notation of RX and h_r in the rest of the thesis to denote RX1 and h_{r1} of backhaul links; and RX2 and h_{r2} of access links. However, we consider the receiver antenna heights for h_{r1} and h_{r2}, as appropriate.

In general, (θ_{LOS}, ϕ_{LOS}) denotes the elevation and azimuth angles of the direct LOS path and (θ_g, ϕ_g) the ground reflected path. The azimuth and elevation angle notations used in Figure 3.5 are explained below. As shown, the direct LOS and ground reflected paths for both backhaul and access links are illustrated in two different planes. Accordingly, for the backhaul link (if h_t = h_{r1} (typically)), we consider the LOS elevation angle $\theta_{LOS} = 0$ and $\theta_g = \theta_{g1}$. The elevation angles for the access link are denoted as $\theta_{LOS} = \theta_{LOS2}$ and $\theta_g = \theta_{g2}$. For the backhaul link, the azimuth angle $\phi = 0$ (for both LOS and ground reflected rays) if the TX and RX positions are aligned along the length of the street, as shown in the illustration. The azimuth angle ϕ for both LOS and ground reflections in the access link is the horizontal angle between the backhaul and access planes, denoted as ϕ_{g2}. Note that ϕ for LOS is always the same as ϕ_{g2}.

In the model description, we first consider a traditional SC layout with reflecting buildings contiguously placed on either side of the road. We refer to the model design for this layout as "System I". Tightly packed buildings generate maximum wall reflections demonstrating a worst-case reflected scenario which creates high channel variations and significant fades. The top-down view of the canonical environment geometry of "System I" is shown in Figure 3.5, illustrating the LOS path and wall reflected paths for a given backhaul link. Here, ϕ_i represents the azimuth angle of the i^{th} wall reflection. The illustration shows four wall reflections, two each of 1st and 2nd order reflections for a typical scenario with narrow antenna beamwidths and small cell ranges. The specified channel can be accurately characterized using a six ray model that considers five specular reflections, i.e., four wall reflections and one ground reflection together with the direct LOS path. Unlike an indoor scenario with roofs/ceilings, the UMi SC channel yields a single ground reflected path.

3.3.2 ANGLE OF ARRIVAL/ DEPARTURE CALCULATION

The omnidirectional channel models generally consider the antenna effects by determining the LOS antenna gain and then allocating this gain to all multipath components to provide equal magnification. The approach merely implies that all MPCs arrive and depart with the same azimuth and elevation AoAs and AoDs. However, this approach is inadequate to model the directional channels wherein higher order specular paths having larger AoAs/AoDs fail to contribute to the net received signal. Moreover, the beam steering and beamforming approach employed in mmWave directional channels mandate that every MPC be magnified by the exact antenna gain related to its AoA and AoD. Hence, to facilitate the non-uniform magnification of MPCs, a full 3D directional channel model needs to first evaluate the azimuth and elevation angles of individual MPCs and then relate these angles to the TX/RX directional antenna radiation patterns [85].

The azimuth and elevation angles of individual MPCs required to obtain their corresponding directional antenna gain $G(\phi,\theta)$ is derived from the environment geometry discussed in the previous section.

The azimuth (ϕ) and elevation (θ) angles for the direct LOS path and the ground reflected path are obtained from the geometry (refer to Figure 3.4) as,

$$\phi_{LOS,g} = \tan^{-1}\left[\left(d_s - d_{t\_w} - d_{r\_w}\right)/d\right] \tag{3.7}$$

$$\theta_{LOS,g} = \tan^{-1}[(h_t \mp h_r)/d_{3D}] \tag{3.8}$$

While calculating θ, "–" and "+" relate to θ_{LOS} and θ_g, respectively. Also, $d_{3D} = \sqrt{d^2 + (d_s - d_{t\_w} - d_{r\_w})^2}$ denotes the corrected 3D separation distance between the transmitting and receiving nodes which accounts for their unaligned, arbitrary placements in the x-y plane. The azimuth (ϕ) and elevation (θ) angles for wall reflections are obtained by amending [113] for the desired geometry (refer Figure 3.5) and are given by,

$$\phi_{io} = \pm\tan^{-1}\left[(nd_s \mp d_{t\_w} \pm d_{r\_w})/d\right] \tag{3.9}$$

$$\theta_{io} = \frac{\pi}{2} - \tan^{-1}\left[\sqrt{d^2 + (nd_s \mp d_{t\_w} \pm d_{r\_w})^2}/h_d\right] \tag{3.10}$$

$$\phi_{ie} = \pm\tan^{-1}\left[\left((n \mp 1)d_s \pm d_{t\_w} \pm d_{r\_w}\right)/d\right] \tag{3.11}$$

$$\theta_{ie} = \frac{\pi}{2} - \tan^{-1}\left[\sqrt{d^2 + \left((n \mp 1)d_s \pm d_{t\_w} \pm d_{r\_w}\right)^2}/h_d\right] \tag{3.12}$$

where *n* represents the *order* of wall reflections. ϕ_{io} and θ_{io} denote the odd-ordered reflection angles corresponding to odd values of *n* and ϕ_{ie} and θ_{ie} are the even-ordered reflection angles corresponding to even values of *n*. For each *n*, the model evaluates two wall reflected paths, i.e., a reflection from the near wall and one from the far wall, analytically deduced by selecting the lower (upper) signs together. As an example, when *n* = 1 (odd value), the model uses 3.9 and 3.10 to create two discreet (ϕ_{io}, θ_{io}) angles corresponding to the first order near as well as far wall reflections. The order *n* can take as many values as, *n* = 1, 2, .., *N*, where *N* represents the maximum wall reflection order evaluated by the model by determining the number of wall reflected paths that fall within the antenna beam area. Hence, if the model captures up to third order wall reflections owing to their individual θ and ϕ falling within the 3D beam area of the directional antenna, then *N* = 3, with *n* =1 and 3 describing the odd order wall reflection parameters and *n* = 2 describing the even order. h_d is the height correction required in the access links to support different TX and RX antenna heights, given as $h_t - h_r$. Note that the "–" and "+" signs are selected by choosing upper (lower) signs together to obtain near (far) wall reflections for each order n.

3.3.3 REFLECTION PATH CALCULATION

In this work, we use the conventional methods of images to find the path length of all valid reflected paths reaching the receiver. The analytical approach is accurate and faster than the ray launching technique in modeling mmWave directional channels since the channel sparsity facilitates to calculate only a few images and their related MPC paths based on the antenna's beam area. We express the 3D path lengths for different signal paths as,

$$d_{LOS,g} = \sqrt{{d_{3D}}^2 + (h_t \mp h_r)^2} \tag{3.13}$$

$$d_{io} = \sqrt{d^2 + \left(nd_s \mp d_{t\_w} \pm d_{r\_w}\right)^2 + {h_d}^2} \tag{3.14}$$

$$d_{ie} = \sqrt{d^2 + \left((n \mp 1)d_s \pm d_{t\_w} \pm d_{r\_w}\right)^2 + {h_d}^2} \tag{3.15}$$

where d_{LOS} and d_g are the path lengths of the direct LOS ray and the ground reflected ray evaluated using the upper and lower signs, respectively. d_{io} and d_{ie} are the path lengths for odd and even-numbered wall reflections, respectively. The "–" and "+" signs are selected by choosing upper (lower) signs together, as explained earlier.

3.3.4 REFLECTION COEFFICIENTS

By assuming relatively smooth and infinite reflecting surfaces, we consider the Fresnel reflection coefficients to relate the incident and reflected rays. The parallel reflection coefficient is used when the E-field of the incident ray is parallel to the plane of incidence. At the same time, the perpendicular reflection coefficient is used when the E-field is perpendicular to the plane of incidence. The Fresnel equations used in our model for two polarization cases of the wall reflections are given as,

$$\Gamma_{par} = \frac{\mu'\varepsilon_r \cos\Psi_i - \sqrt{\mu'\varepsilon_r - \sin^2\Psi_i}}{\mu'\varepsilon_r \cos\Psi_i + \sqrt{\mu'\varepsilon_r - \sin^2\Psi_i}} \tag{3.16}$$

Table 3.1 Specifications of the material properties

Materials	Relative permittivity Real (ε')	Conductivity (σ)
Concrete	6.495	1.43
Aerated Concrete	2.26	0.339
Wood	1.5	0.3
Brick	3.95	0.244
Stone	6.72	0.112
Plasterboard	3.08	0.185
Glass	4.7	0.518

$$\Gamma_{perp} = \frac{\cos\Psi_i - \sqrt{\mu'\varepsilon_r - \sin^2\Psi_i}}{\cos\Psi_i + \sqrt{\mu'\varepsilon_r - \sin^2\Psi_i}} \tag{3.17}$$

As depicted in the layout geometry, Ψ_i is the angle of incidence. Equations 3.16 and 3.17 are applied for wall and ground reflections in line with the antenna polarization assumed in the simulation. For the wall reflections, Ψ_i is derived from the azimuth angle ϕ_i and for ground reflections, it is a function of elevation departure angle θ_g (θ_{g1} for backhaul link and θ_{g2} for access link). Considering the reflecting material to have a relative permeability of μ', a relative permittivity of ε' and a conductivity of σ, the complex permittivity of the material, ε_r, is expressed as $\varepsilon_r = \varepsilon' - j\frac{\sigma}{2\pi f\varepsilon_0}$. Here, f denotes the mmWave transmission frequency and $\varepsilon_0 = 8.854 \times 10^{-12}$Farad/m. By assuming wood for building sidewalls, we obtain $\varepsilon' = 1.5$ and $\sigma = 0.3$ at 60GHz yielding the imaginary component of relative permittivity $\left(\frac{\sigma}{2\pi f\varepsilon_0}\right)$ as 0.09. The concrete roads can be modelled using $\varepsilon' = 6.495$ and $\sigma = 1.43$ producing the imaginary component as 0.4284 at 60GHz. The simulation can be modified for glass walls with $\varepsilon' = 4.7$ and $\sigma = 0.518$. Alternatively, the material characteristics for any mmWave frequency range can be derived from Table 3.1 or the data specified in [68].

3.3.5 GENERATION OF CHANNEL IMPULSE RESPONSE

As indicated in Section 3.2, employing directional transmission in mmWaves augments the need to provide realistic modeling of all specular reflected paths contributing to the received signal strength. When deriving a precise directional channel model, it is preferred to model the resolvable specular reflections as a function of the position and deployment parameters of the channel. As noted, in MiDDCM, unlike statistical models, we use the geometrical image technique to compute path lengths as well as the azimuth/elevation angles in the 3D plane as a function of d, d_s, d_{t_w}, d_{r_w}, h_t, and h_r. Moreover, the path lengths and their antenna gains $G(\phi, \theta)$ for the backhaul and the access scenarios are computed only for *valid* paths with azimuth and elevation angles of arrival/departure falling within the antenna beam area. While the paths with ± AoA/AoD ≥ HPBW/2 are considerably attenuated compared to the LOS path, they may sparingly contribute to the received signal. Accordingly, we consider the beamwidth of the first null (FNBW) to assess the beam coverage. The deliberation is also pessimistic from the diversity point of view. The analysis used is hence of the form, ± AoA/AoD ≤ FNBW/2. Therefore, a path is aggregated at the receiver if it satisfies the following condition: $|\phi_{LOS,g,i}| \leq HPBW_A$ and $|\theta_{LOS,g,i}| \leq HPBW_E$.

Using the computed parameters, we now characterize the mmWave direction dependent deterministic channel. By making the narrowband assumption as in the case of OFDM transmission, the received signal bandwidth will be smaller than the channel coherence bandwidth allowing us to focus on the variations of the channel due to spatial geometry. Accordingly, the channel impulse response (CIR) of the proposed multi-ray channel model for a narrowband channel is:

$$h(f, d, \phi, \theta) = \sqrt{G_{LOS}(\phi, \theta)}\, H_{Los} + \sqrt{G_g(\phi, \theta)}\, H_g + \sum_{i=1}^{M} \sqrt{G_i(\phi, \theta)}\, H_i \quad (3.18)$$

where $G_{LOS}(\phi, \theta)$, $G_g(\phi, \theta)$ and $G_i(\phi, \theta)$ are the antenna gain products $G_t(\phi, \theta).G_r(\phi, \theta)$ of the direct LOS, ground reflection, and the i^{th} wall reflections, respectively. The antenna gain of each path is evaluated at its corresponding θ and ϕ as explained earlier. Here, M is the maximum number of resolvable specular wall reflections in the simulated channel model dynamically determined from the choice of input parameters d_s, d_{t_w}, d_{r_w}, h_t, h_r, and 3D antenna HPBWs which satisfies the condition on θ, and ϕ, as mentioned earlier. M is related to N, the maximum wall reflection order, as $M = 2N$ since each reflection order corresponds to one of the near and far wall reflections.

For example, if $M = 4$ (as illustrated in Figure 3.5), the MiDDCM is a six ray channel model that accounts for the LOS, the ground reflection, and four wall reflections (2 each of first and second order wall reflections, attributing to $N = 2$). Alternatively, if the model captures up to third order wall reflections, then $N = 3$ and M is determined as six, suggesting an eight ray model.

The channel impulse response (CIR) components, H_{LOS}, H_g, and H_i, are given by,

$$H_{LOS} = \left[\frac{\lambda}{4\pi d_{LOS}} e^{(-K_a d_{LOS}/2)}\right] e^{\left(-j\frac{2\pi}{\lambda} d_{LOS}\right)} \tag{3.19a}$$

$$H_g = \left[\Gamma_g \frac{\lambda}{4\pi d_g} e^{(-K_a d_g/2)}\right] e^{\left(-j\frac{2\pi}{\lambda} d_g\right)} \tag{3.19b}$$

$$H_i = \left[\Gamma_i \frac{\lambda}{4\pi d_i} e^{(-K_a d_i/2)}\right] e^{\left(-j\frac{2\pi}{\lambda} d_i\right)} \tag{3.19c}$$

where $2\pi/\lambda$ is the wavenumber. Here, each signal path is compensated for an additional oxygen absorption loss by applying K_a, the coefficient for exponential absorption. As the reflected paths suffer higher atmospheric attenuation than the LOS path due to their longer path lengths, the approach offers a stable model parametrization for all mmWave frequencies. Γ_g denotes the ground reflection coefficient, and Γ_i denotes the net wall reflection coefficient. MiDDCM models both horizontal and vertical antenna polarization, where Γ_g equals Γ_{par}, and Γ_i equals Γ_{perp} for vertical polarization and vice versa for horizontal polarization.

3.3.6 BEAM STEERING FOR LINK QUALITY IMPROVEMENT

In mmWave channels with short wavelength carrier signals, even spatial variations on the order of a few centimetres contribute to significant path loss variations. Fortunately, beam steering aided directional communication helps to improve the signal strength of mmWave serving links as compared to interfering links. This optimizes the mmWave link budget and improves link performance. Beam steering strategy can be efficiently exploited to steer directional radiation patterns by orienting the main lobe towards the strongest path rather than towards the boresight direction. The steering keeps the transmit power focused on the desired direction. In this work, by assuming that the LOS path is the strongest energy path, which is true in most cases, beam steering assumes that the main lobe is steered towards the radial direction (i.e., the direct path between TX and RX) irrespective of the transmission scenario. (i.e., even in NLOS simulation case with obstructed LOS component).

From the deployment geometry, the backhaul link is modelled such that orienting the transmit and receive antenna radiation patterns along LOS also implies that they are steered in the boresight direction. The geometry hence assures optimal channel performance as the highest energy LOS path is always magnified by the peak boresight gain. To enhance the received signal strength in the access links with differently aligned BS and UE antennas, the antenna radiation patterns should be tilted in both azimuth and elevation planes by an estimated correction angle $\Delta\phi$ and $\Delta\theta$, respectively. The antenna tilt angles in azimuth and elevation directions which allows for beam alignment through beam steering can be analytically deduced from the model geometry as,

$$\Delta\phi = \tan^{-1}\left[\left(d_s - d_{t\_w} - d_{r\_w}\right)/d\right] \tag{3.20}$$

$$\Delta\theta = \tan^{-1}[(h_t - h_r)/d_{3D}] \tag{3.21}$$

Note that, MiDDCM dynamically corrects the arrival and departure angles of every participating path with the estimated tilt angles. As apparent, steering the main lobe in the radial direction just requires the knowledge of the SC deployment parameters, including the TX/RX position/orientation. The approach is more straightforward as it eliminates the need for channel state sensing required to identify the beam steering direction in real-time (sensing is needed when the beam must be steered towards the

Figure 3.6 Proposed small cell layout geometry devoid of beam steering for uniform coverage.

strongest path among multiple specular reflections). However, radial beamforming is inapt for optimal performances in NLOS scenarios wherein it is desirable to steer the main lobe in the direction of the strongest NLOS reflected path with the overall model simplicity traded off.

3.3.6.1 A NEW DIRECTIONAL MMWAVE SC GEOMETRY WITHOUT BEAM STEERING

The beamforming and steering techniques in mmWave communications enhance the channel performance in terms of coverage extension and deep fade elimination. However, the practical implementation of beamforming involves obtaining comprehensive channel state information (CSI). Moreover, a key technical challenge in dynamically steering the beam is to develop protocols that help BSs and UEs to locate and track each other. It also requires efficient signal processing algorithms to estimate the spatial signatures, such as azimuth and elevation directions of arrival (DoA) of the signal. As known, the codebook-based beam tracking and ray tracing-based beam tracking require considerable signal computations which will increase the overall implementation complexity.

In the suggested mmWave UMi deployment geometry, we observe that the tilt angle variations are trivial in small cells with an approximate cell range of 200m and with APs/BSs mounted at low heights. Accordingly, we propose a simplified SC antenna

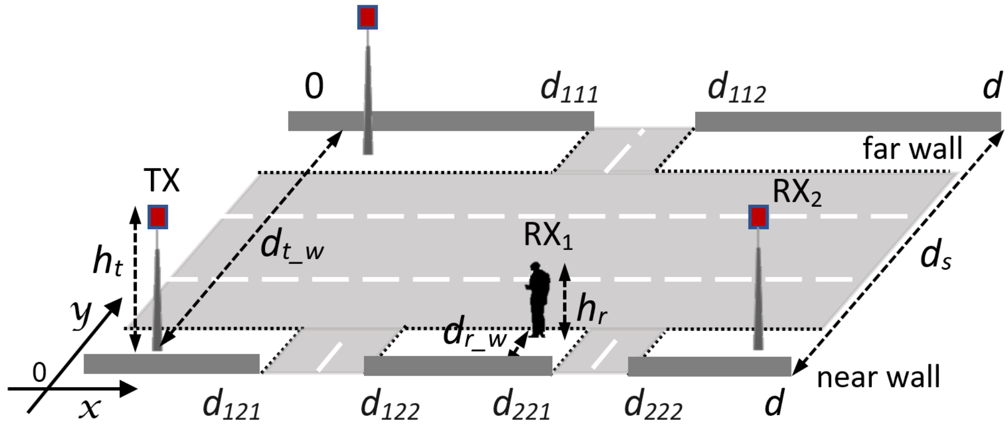

Figure 3.7 A general UMi SC layout of the street grid with crossroad gaps.

geometry as depicted in Figure 3.6. Here, an antenna configuration with two differently oriented antenna elements is placed on the lamppost to provide uniform coverage. As shown, the antenna radiation pattern which is oriented horizontally along the boresight serves the backhaul link and the UEs far from the transmitter, say, near to the cell edge. For a small cell SC layout, a tilt in the radiation pattern is required primarily in the serving area close to BS, where all the multipaths fall outside the receiver antenna beam area. Hence, besides an antenna beam oriented along the horizontal direction, it is sufficient to have a single additional beam tilted by an angle of [5°-15°] range relative to boresight in order to provide a uniform signal strength to the UE located anywhere in the SC layout. This part of the work is similar to our former study [114].

3.3.7 MODELING OF STREET GRIDS WITH CROSSROADS

In Section 3.3.1, we illustrated the SC geometry with continuous reflecting sidewalls on both sides of the canyon referred to as "System I". However, a realistic SC layout typically consists of crossroad gaps creating discontinuities in the reflecting buildings, creating distinct fading profiles. In this section, we model a typical street-grid with any number of crossroads and propose a simple analytical formulation that models the propagation regions with reduced signal fades [115]. To this end, we consider a real SC layout with an arbitrary choice of crossroad placements hereafter referred to as "System II", as shown in Figure 3.7. Note that all other deployment parameters are identical to the earlier consideration. However, the presence of gaps/crossroads reduces the number of participating paths. Most importantly, all the wall reflections

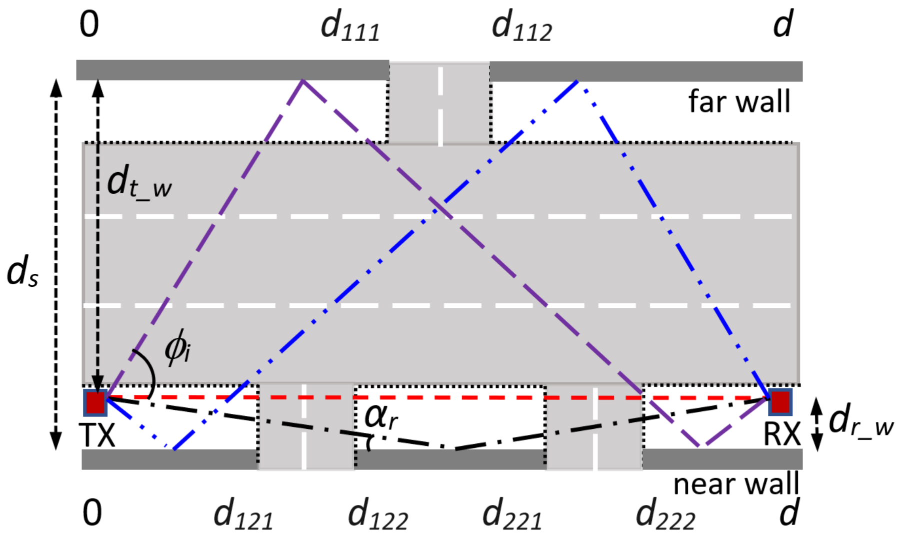

Figure 3.8 2D top-down view of mmWave directional UMi SC scenario showing first and second order wall reflections for "System II".

that are aggregated at the receiver while modeling "System I" will not necessarily contribute to the CIR of "System II" deployment (refer, Figure 3.8), thereby reducing the signal fades.

In "System II" deployment, a wall reflected ray would only contribute to the received power if its point of reflection is a wall and not the crossroad itself. Hence, in addition to satisfying the ϕ and θ requirement as in "System I", MiDDCM for "System II" aggregates a wall reflected ray at the receiver only if its reflection angle, α_r, does not belong to the set of all α_rs for c = 1,2,…C, where c is the crossroads' number, and C is the maximum number of crossroads on one side of the street [113].

$$\alpha_r\colon \alpha_{cW2} < \alpha_r < \alpha_{cW1} \tag{3.22}$$

where

$$\alpha_{cWE} = \tan^{-1}\left[\frac{\left(\left(n-(2-W)\right)d_s-(-1)^W d_{t\_w}\right)}{\left(\sqrt{{d_{cTE}}^2+{h_d}^2}\right)}\right] \tag{3.23}$$

In the given deployment layout with crossroads, the crossroads' number c considers 1 and 2 in the near wall case with two crossroads and 1 in the far wall case with a single crossroad. Here, W denotes the wall side (considered as 1 for the far wall and 2 for the near wall) and $T = W^{(W-1)}$ for odd n and $W^{(W-2)} + [2-W]$ for even n. E represents the edge of the crossroad, assumed as 1 for the near edge, and 2 for the far edge.

We next propose a simple analytical formulation, which distinctly models the propagation regions in a UMi SC layout that are impacted by the sidewall discontinuities. This region with reduced signal fades is modelled for two different cases of beam steering.

Case 1- "System II" with elevation beam steering alone: In this case, we consider the antenna beam tilted in the elevation plane primarily to correct the variations in TX-RX orientation due to antenna height variations. We analytically model the lower and upper bound of the reduced faded region $\{x\_l_{cW}, x\_u_{cW}\}$ along the x-axis as a function of; (i) TX - RX location in the layout, and; (ii) location (bound) of crossroads along the street, where $\{x\_l_{cW}, x\_u_{cW}\} \in \{0, d\}$:

$$\begin{aligned}&\{x\_l_{cW}, x\_u_{cW}\}\\&= \left[\left(d_{r\_w} + (d_s - d_{t\_w})\right)/(d_s - d_{t\_w})\right] * \{d_{cW1}, d_{cW2}\}\end{aligned} \tag{3.24}$$

Case 2- "System II" with both elevation and azimuth beam steering: In this case, we consider the antenna beam tilted in the elevation and azimuth planes to correct the variations in TX-RX orientation due to antenna height variations and due to RX placed unaligned with the TX. Accordingly, the analytical expression for the lower and upper bound of the reduced faded region $\{x\_l_{cW}, x\_u_{cW}\}$ is redefined as:

$$\{x\_l_{cW}, x\_u_{cW}\} = \left[d_{r\_w}/\left((d_s - d_{t\_w})/2\right)\right] * \{d_{cW1}, d_{cW2}\} \tag{3.25}$$

where d_{cW1} and d_{cW2} represent the distance of c^{th} crossroad on the W^{th} wall side at the first and second edges, respectively.

Finally, we provide the algorithm of the proposed MiDDCM developed to model backhaul and access channel impulse response for various realistic scenarios such as LOS/NLOS transmissions, beam aligned/unaligned propagations, and road canyon deployment with/without crossroads.

Algorithm 1: UMi SC low complexity mmWave directional channel modelling

Initialize Channel Model
    (i) Set *Scenario*: UMi SC deployment parameters, TX/ RX separation distance, Frequency, Antenna specifications.
    (ii) Set *Environment_criteria1: LOS / NLOS*,
        _criteria2: *Beam steering / no Beam steering*,
        _criteria3: *System I / System II*.
Compute $(\phi, \theta)_{LOS,g,i}$ for all specular paths using methods of images.
Compute K_a the coefficient of exponential absorption specific to mmWave carrier frequency.
if *Environment_criteria1* == *LOS* **then**
    if *Environment_criteria2* == *Beam steering* **then**
        Correct (ϕ, θ) to steer main lobe towards the radial direction in access links and/or unaligned TX-RX placements.
    end if
end if
while $|\phi_{LOS,g,i}| \leq HPBW_A$ **and** $|\theta_{LOS,g,i}| \leq HPBW_E$
    if *Environment_criteria1* == *LOS* **then**
        Generate direct LOS path by computing d_{Los}, $G_{LOS}(\phi, \theta)$.
    end if
    Generate ground reflection by computing Γ_g, d_g, $G_g(\phi, \theta)$.
    if *Environment_criteria3* == *System I* **then**
        Generate all M wall-wall reflections by computing Γ_i, d_i, $G_i(\phi, \theta)$.
    else if *Environment_criteria3* == *System II* **then**
        Generate wall-wall reflections by computing Γ_i, d_i, $G_i(\phi, \theta)$ only if their reflection angles, $\alpha_r \notin \{\forall \alpha_r : \alpha_{cW2} < \alpha_r < \alpha_{cW1}\}$ for c = 1,2,…C, where C is the maximum number of crossroads on one side of the street.
    end if
end while
Aggregate all signal paths to evaluate CIR $h(f, d, \phi, \theta)$.

As apparent, the channel impulse response for a narrowband mmWave directional link expressed in (3.18) and (3.19) can be rephrased as,

$$h(f, d, \phi, \theta) = \frac{\lambda}{4\pi}\left(\frac{\sqrt{G_{LOS}(\phi, \theta)}\, e^{-(K_a d_{LOS}/2)-\left(\frac{j2\pi d_{LOS}}{\lambda}\right)}}{d_{LOS}} + \frac{\Gamma_g\sqrt{G_g(\phi, \theta)}\, e^{-(K_a d_g/2)-\left(\frac{j2\pi d_g}{\lambda}\right)}}{d_g} + \sum_{i=1}^{M}\frac{\Gamma_i\sqrt{G_i(\phi, \theta)}\, e^{-(K_a d_i/2)-\left(\frac{j2\pi d_i}{\lambda}\right)}}{d_i}\right) \tag{3.26}$$

For ease of representation and further developments, we combine both ground and wall reflections as i multi-ray components (total of $M + 1$ multi-rays) and normalize the CIR relative to the ideal LOS link. Accordingly, the relative channel response as a function of f, d, ϕ, and θ (the representation is discarded in the subsequent discussion for convenience), is represented as,

$$h^r = 1 + \sum_{i=1}^{M+1} \alpha_i\, e^{-j\beta_i} \tag{3.27}$$

where α_i is the normalized amplitude of the i^{th} reflection, which can be either the ground reflection or any of the M wall reflections, given by:

$$\alpha_i = \Gamma_i\, \frac{d_{LOS}}{d_i}\sqrt{\frac{G_i(\phi, \theta)}{G_{LOS}(\phi, \theta)}}\, e^{-\left(\frac{K_a \Delta d_i}{2}\right)} \tag{3.28}$$

the relative phase β_i is $(2\pi/\lambda)\Delta d_i$, where $\Delta d_i = (d_i - d_{LOS})$. Note that d_i, $G_i(\phi, \theta)$ and Γ_i are appropriately considered for the ground reflected path. Accordingly, the received power is expressed as,

$$P_r(f, d, \phi, \theta) = P_t G_{LOS}(\phi, \theta)\left(\frac{\lambda}{4\pi d_{LOS}}\right)^2 e^{\frac{-K_a . d_{LOS}}{2}} . |h^r|^2 \tag{3.29}$$

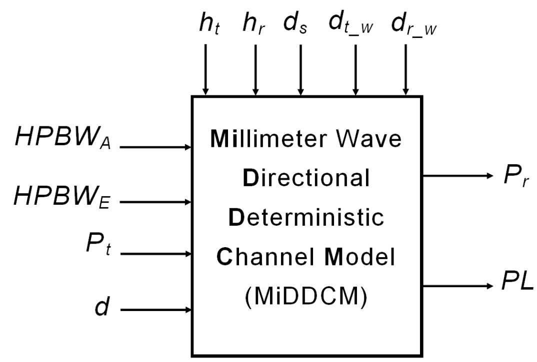

Figure 3.9 Proposed MiDDCM specifying the model inputs and outputs.

where $G_{LOS}(\phi, \theta) = G_t(\phi, \theta).G_r(\phi, \theta)$, is the product of the TX and RX antenna boresight gains for beam aligned/steered antenna radiation patterns. Clearly, P_r is a function of mmWave frequency, f, separation distance, d, and the 3D antenna geometries. The mmWave deterministic directional path loss expressed as a positive quantity and can be evaluated as:

$$PL(f, d, \phi, \theta) = 10 \log_{10}\left(\frac{P_t}{P_r(f, d, \phi, \theta)}\right) \tag{3.30}$$

We further model the effects of mmWave foliage by adding the foliage loss given by L_{fol} [dB] = $0.2f^{0.3}D_f^{0.6}$ to (3.30), where D_f is the foliage depth represented in meters [32]. To sum-up, MiDDCM estimates the SISO channel characteristics for varying input specifications, as illustrated in Figure 3.9.

3.4 SPATIAL DIVERSITY IN DIRECTIONAL LINKS

In this section, we explore spatial diversity using multiple antennas at the TX and RX side to provide link robustness in "System I", which is the worst-case reflecting scenario. We show in the result section that the sparse channel structure and the strong multipaths in the mmWave directional channel create significant fades and, most importantly, large fading variations even with small changes in the environment geometry. However, the short wavelength of the mmWave spectrum makes it easier to implement diversity in mmWave communications and effectively use it to improve the system performance parameters like coverage, capacity, and signal-to-interference noise ratio (SINR). Mainly, the channel model is analysed for the specific cases of 1 ×

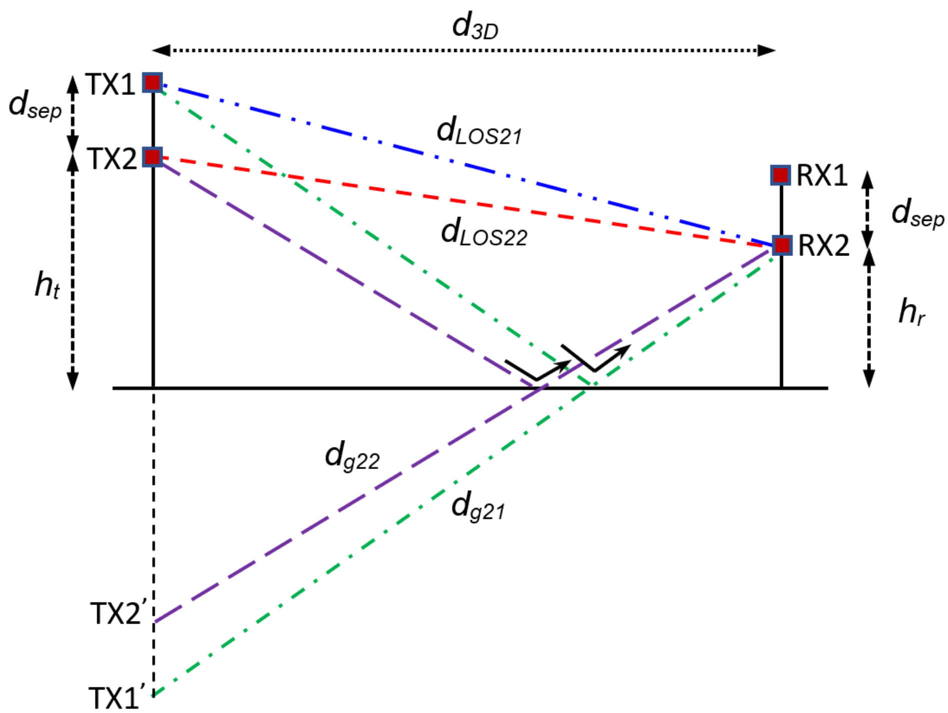

Figure 3.10 Deployment geometry with 2 × 2 MIMO illustrating transmit diversity with direct LOS paths and ground reflected rays.

2 single-input-multiple-output (SIMO) receive diversity, 2 × 1 multiple-input-single-output (MISO) transmit diversity, and 2 × 2 MIMO diversity.

The SISO channel impulse response denoted by (3.27) is now extended to model a simple MIMO link to explore vertical diversity. As we analyse vertical diversity by employing the vertically separated multi-antenna configuration, it is reasonable to approximate the generalized model by considering only the direct LOS path and the ground reflected path. Accordingly, (3.27) can be written as $h^r = 1 + \alpha_g\, e^{-j\beta_g}$. The multipaths between every TX and RX are aggregated by their respective directional antennas if and only if their angles fall within the directional antenna beam area, as stated in Section 3.3.

We illustrate in Figure 3.10 the propagation geometry of a 2 × 2 MIMO system with two TX antennas and two RX antennas each separated by a small vertical distance d_{sep}. The geometrical illustration explicitly shows the LOS and ground reflected paths in a 2 × 1 MISO system comprising TX1, TX2 and RX2, illustrating the formation of

h_{21}, and h_{22}. The propagating paths contributing to the channel response can be likewise deduced for the MIMO geometry.

The relative CIR between n^{th} transmit element and m^{th} receive element can be expressed as,

$$h^{r}{}_{mn} = 1 + \alpha_{gmn}\, e^{-j(\beta_{gmn})} \tag{3.31}$$

where β_{gmn} is the relative phase between n^{th} TX and m^{th} RX obtained as $(2\pi/\lambda)\Delta d_{gmn}$, where $\Delta d_{gmn} = \left(d_{gmn} - d_{LOSmn}\right)$. Also,

$$\alpha_{gmn} = \Gamma_g\, \frac{d_{LOSmn}}{d_{gmn}} \sqrt{\frac{G_{gmn}(\phi,\theta)}{G_{LOSmn}(\phi,\theta)}}\, e^{-\left(\frac{K_a \Delta d_{gmn}}{2}\right)} \tag{3.32}$$

From the geometry, various path lengths can be modelled as:

$$\begin{aligned}
d_{LOS11,g11} &= \sqrt{{d_{3D}}^2 + \left((h_t + d_{sep}) \mp (h_r + d_{sep})\right)^2} \\
d_{LOS12,g12} &= \sqrt{{d_{3D}}^2 + \left(h_t \mp (h_r + d_{sep})\right)^2} \\
d_{LOS21,g21} &= \sqrt{{d_{3D}}^2 + \left(h_t \mp h_r + d_{sep}\right)^2} \\
d_{LOS22,g22} &= \sqrt{{d_{3D}}^2 + (h_t \mp h_r)^2}
\end{aligned} \tag{3.33}$$

We now present a simplification procedure to reduce the ray tracing complexity in mmWave spatially diverse channels. As is known, the small wavelength in mmWaves allows a dense packing of antenna elements. Hence, the separation distance between individual elements will be considerably short. Because of the small wavelength, the separation d_{sep} will be in small millimeter range even if the antenna separation needs to be of the order of a few multiples of the wavelength. That is, $d_{sep} \ll d_{3D}$. Accordingly, the path length differences between LOS paths amongst various antenna pairs are extremely small and the phase differences between them are negligible. The ray tracing computations can be thereby reduced by disregarding the computations of individual LOS paths. Hence, only the phase difference due to ground reflected paths are considered in the channel impulse approximation. Hence without loss of generality, the relative channel impulse response between n^th transmit element and m^th receive element can be expressed as:

$$h^r{}_{mn} = 1 + \alpha_{gmn}\, e^{-j(\beta_g + \gamma_g(m,n))} \tag{3.34}$$

where β_g is the relative phase of the ground reflected path with respect to LOS for the TX1-RX1 pair and $\gamma_g(m,n)$ is the additional phase offset due to the path length difference between the ground reflected path from n to m relative to the ground reflected path from TX1 to RX1. It is defined as $(2\pi/\lambda)\left[d_{gmn} - d_{g11}\right]$ by setting $\gamma_g(1,1) = 0$.

Next, we provide an insight into the calculation of the normalized channel responses h_{11}, h_{12}, h_{21}, and h_{22}.

The channel gains in the MISO system illustrated in Figure 3.10 can be modelled as,

$$\begin{aligned} h_{22} &= 1 + \alpha_{g22}\, e^{-j(\beta_g + \gamma_g(2,2))} \\ h_{21} &= 1 + \alpha_{g21}\, e^{-j(\beta_g + \gamma_g(2,1))} \end{aligned} \tag{3.35}$$

Likewise, h_{11} and h_{12} can be defined.

Furthermore, under the assumption $(d_{sep} \ll h_t, h_r \ll d_{3D})$, the path difference between the ground reflected path of TX1-RX2 (or TX2-RX1) and the ground reflected path of TX1-RX1 can be approximated as $\left[(h_t + h_r)d_{sep}\right]/d_{3D}$. Similarly, the path difference between d_{g22} and d_{g11} can be approximated as $\left[2(h_t + h_r)d_{sep}\right]/d_{3D}$. We would like to highlight that the approximate path difference remains the same while considering RX2 as the receiving antenna. Furthermore, even for a SIMO system, it is possible to approximate the path length difference between the ground reflections for any two TX-RX combinations to the same expression by following the earlier stated assumption. Therefore, the phase difference between the two ground reflected paths could be generalized as:

$$\gamma_g = \left(\frac{2\pi}{\lambda}\right)\left(\frac{(h_t + h_r)d_{sep}}{d_{3D}}\right) \tag{3.36}$$

Most importantly, this phase difference should be adequate to implement spatial diversity that improves the received signal strength in a mmWave directive deterministic channel, thereby improving the reliability of the system. Specifically, we propose to implement spatial diversity in reception, transmission, or both ends using a 2 x 2 scheme with a maximum of 4 diversity paths and estimate the channel gain using various diversity schemes. The channel capacity will be evaluated and analysed for a variety of specifications and schemes.

3.5 CHAPTER SUMMARY

In this chapter, we have derived a detailed mathematical formulation of the proposed MiDDCM that characterizes UMi SC outdoor channels with continuous/discontinuous reflecting sidewalls, disregarding the computation of higher order wall reflections that fall outside the narrow beamwidth of the high gain directional antenna. The aggregated multipaths include a direct LOS (if not obstructed), a ground reflected path in addition to antenna directionality-dependent wall reflected paths. The model is also extended to analyse the vertical antenna diversity required to reduce the extent of fading and, most importantly, to stabilize the channel variations that arise from even slight changes in geometric parameters.

Although more complex multipath behaviour such as diffused scattering and diffraction could increase the NLOS path loss, this model/study provides an essential first step in understanding the mmWave transmission possibilities and performing numerous analyses on channel propagation characteristics that cannot be modelled through traditional statistical channel models.

CHAPTER 4. ANALYSIS AND DESIGN-II: STATISTICAL MODELING OF DIRECTIONAL CHANNELS AND DEPLOYMENT GEOMETRY OPTIMIZATION

4.1 INTRODUCTION

In the previous chapter, we have derived the low complexity MiDDCM based on ray tracing for different setups to investigate the implications of antenna directionality in mmWave outdoor channels for a UMi SC deployment environment. In this chapter, we further use the proposed MiDDCM "System I" design (worst-case reflection scenario) to analyse the directional channel path loss and to explore different aspects of statistical learning of mmWave directional channel characteristics and models. The investigation is novel to mmWave directional channel studies.

The rest of this chapter is organized as follows. Section 4.2 explains MiDDCM validation using standard statistical models reported in the existing literature. It also provides a statistical approach to parametrize the mmWave directional deterministic outdoor channel. Section 4.3 explores the optimization of SC deployment parameters in 5G mmWave backhaul and access channels using a metaheuristic PSO algorithm. Section 4.4 presents the chapter summary.

4.2 STATISTICAL MODELING OF DIRECTIONAL CHANNELS

The focus in this section is still the modeling of directional mmWave channels. The intention is to achieve two definite goals: (i) to compare the MiDDCM simulator with well-cited existing models to validate the model and identify its benefits, limitations, and usage scenarios. To this end, we provide a simplified step procedure to yield the direction-dependent large scale LOS and NLOS path loss values by trying to preserve the expression of popular statistical models, allowing for easier comparison. (ii) to derive a statistical formulation and adapt the channel parameters (PLE and fading factor) to characterize a directional mmWave channel. As we recall, the channel model development in the previous chapter emphasized the deterministic formulation yielding exact path loss values at every location as a function of deployment and 3D antenna geometries. However, several system designs do not require to compute accurate values of the instantaneous path loss; instead, a statistical distribution of the mmWave directional path loss could be the focus.

4.2.1 STANDARD POWER LAW PATH LOSS MODELS

Here, we analyse the channel modeling methodology employed in popular mmWave channel models. Generally, the channel models based on measurements are derived either from the CI model based on one parameter or from the three parameters based ABG model [27], [116]–[119], appropriately modified to meet the mmWave requirement. For example, the reference distance d_0 of CI models is fixed to 1 or 5m for mmWave systems with low height base stations and small cell sites, while the sub-6GHz systems employed 100m or 1km. This work uses the CI model to benchmark the proposed MiDDCM due to its physical basis and closeness to environmental propagation conditions, besides the ease of implementation. The path loss equation of the CI model at a 2D separation distance d is given by,

$$PL_d{}^{\mathrm{CI}}[\mathrm{dB}] = PL_{d_0}[\mathrm{dB}] + 10\, n^{\mathrm{CI}} \log_{10}\left(\frac{d}{d_0}\right) + X_{\sigma_{\mathrm{CI}}} \tag{4.1}$$

where $PL_{d_0}$is the path loss at a reference distance d_0 = 1m [26], [117], and n^{CI} is the path loss exponent (PLE), which holds different values for the LOS and NLOS transmission scenarios. The first two terms collectively constitute the FSPL at link distance, d. $X_{\sigma_{\mathrm{CI}}}$ is zero mean Gaussian random variable representing the fading factor that describes large scale signal fading about the mean path loss. The distribution of $X_{\sigma_{\mathrm{CI}}}$ is statistically random and yet consistent with the entire range of d, determined from the standard deviation $\sigma_{\mathrm{CI,dB}}$ such that $X_{\sigma_{\mathrm{CI}}} \sim \mathcal{N}\left(0, \sigma_{\mathrm{CI,dB}}{}^2\right)$. Most importantly, $X_{\sigma_{\mathrm{CI}}}$is a log-normal random variable of uniform variance. The CI model typically uses two different σ_{CI} values to establish the LOS and NLOS transmissions, thus increasing the number of model parameters that should be tracked/acquired for channel analysis.

The value of FSPL at d_0 can be either obtained from measurements or derived from the FSPL equation as:

$$PL_{d_0}[\mathrm{dB}] = 20 \log_{10}\left(\frac{4\pi d_0}{\lambda}\right) \tag{4.2}$$

This method of deterministically modeling the reference value is valid only for LOS scenarios and not for NLOS scenarios where the path between TX and RX antennas is partially/fully obstructed.

The three-parameter ABG model, on the other hand, predicts the distance dependent expected path loss of mmWaves by using a simple regression fitting to the measured data, specified as:

$$PL_d{}^{\mathrm{ABG}}[\mathrm{dB}] = \alpha[\mathrm{dB}] + 10\,\beta \log_{10}\left(\frac{d}{d_0}\right) + X_{\sigma_{\mathrm{ABG}}} \tag{4.3}$$

where α is the offset of the path loss fitting curve at d_0, β is the path loss slope as a function of distance d (if α is identical to the FSPL at d_0, then $\beta = n^{\mathrm{CI}}$) and σ_{ABG} is the standard deviation of the zero mean Gaussian random variable, $X_{\sigma_{\mathrm{ABG}}}$.

4.2.2 FORMULATION OF MIDDCM FROM STATISTICAL MODEL

In this section, we apply the proposed MiDDCM framework wherein the model expression is articulated by starting from the traditional statistical model expression to provide for easy comparison. This part of the study intends to validate the MiDDCM with standard models that use the CI or ABG path loss expressions for large scale modeling, paying specific attention to the limitations of these statistical formulations. The method explained below primarily considers the CI closed-form expression; however, a similar line of analysis can be followed for the ABG model.

By assuming d_o = 1m, the received power of the traditional statistical CI model, defined in (4.1), can be expressed as:

$$P_r{}^{\mathrm{CI}}(f, d) = P_t\left(\frac{\lambda}{4\pi}\right)^2 d^{-n^{\mathrm{CI}}}.F_d^{\mathrm{CI}} \tag{4.4}$$

where $F_d^{\mathrm{CI}} = 10^{\,X_{\sigma_{\mathrm{CI}}}/10}$ is the statistical fading gain which characterizes the large scale fading and is log normal. Note that, F_d^{CI} is generally computed for the omnidirectional and the directional propagations by choosing distinct values for σ_{CI}.

Obviously, the CI model does not reflect the frequency dependency of P_r beyond the first meter of propagation [36]. That is, even though (4.4) is a function of *f*, it does not specify any mmWave specific losses that are functions of both frequency and distance. While the absorption loss is a function of *d*, the CI model accounts for it only at *d* = 1m. Furthermore, there is no reference to other deployment parameters like the antenna heights or beamwidths in the model expression, even though they significantly define the characteristics of a mmWave directional sparse multipath channel. In summary, *n* and *σ* values in standard statistical models are deduced to best fit the antenna height, the beamwidth, and the carrier frequency specified in a well-defined channel setup.

On the contrary, deterministic ray tracing modeling used in MiDDCM characterizes the actual effect of the environment. The resulting deterministic direction-dependent received power as a function of 3D deployment parameters and antenna geometries, was developed in Section 3.3 (refer (3.29)). We now rephrase this equation to provide an expression equivalent to the statistical model expression in (4.4) by which the deterministic received power is represented as:

$$P_r{}^{\mathrm{det}}(f, d, \phi, \theta) = P_t G_t(\phi, \theta) G_r(\phi, \theta) \left(\frac{\lambda}{4\pi d_{LOS}}\right)^2 e^{\frac{-K_a . d_{LOS}}{2}} . F_d^{\mathrm{det}} \qquad (4.5)$$

where, $F_d^{\mathrm{det}} = |h^r|^2$ is the deterministic directional fading gain which is a function of antenna height and position. It characterizes the fading phenomenon due to all resolvable specular reflections falling within the directional antenna beam area. As it is not required to aggregate every possible ray arriving at the receiver (as in the case of an omnidirectional rich scattering environment), F_d^{det} can be easily and accurately computed using the MiDDCM framework and does not demand efficient commercial ray tracing simulators and powerful computing units. It may be noted that to compare the two models, either (4.4) should be multiplied with or (4.5) should be eliminated with the boresight gain, $G_{LOS}(\phi, \theta)$.

Accordingly, the deterministic directional path loss of MiDDCM is expressed as:

$$
\begin{aligned}
{PL_d}^{\mathrm{det}}[\mathrm{dB}] = FSPL\,(d_{LOS}, f) -\ G_t[\mathrm{dB}] - G_r[\mathrm{dB}] + L_{\mathrm{abs}}[\mathrm{dB}] \\
-\ F_d^{\mathrm{det}}[\mathrm{dB}]
\end{aligned}
\tag{4.6}
$$

where $FSPL\,(d_{LOS}, f)$ is the FSPL evaluated at d_{LOS}. $L_{\mathrm{abs}}[\mathrm{dB}] = 10\log_{10} e^{K_a \cdot d_{LOS}}$ is the specific attenuation due to oxygen absorption in mmWave frequencies.

4.2.3 CLOSED-FORM EXPRESSION FOR DIRECTIONAL PATH LOSS MODEL

The proposed MiDDCM realistically predicts the mmWave channel's directional characteristics and offers low complexity by exploiting the same. However, it should undoubtedly compute parameters such as path lengths, reflection coefficients, elevation, and azimuth directions of propagation and the related antenna gains for every reflected path in addition to the direct LOS parameters. This kind of detailed MPC analysis is not always required, particularly in channel analysis that involves studying path loss distributions and not their instantaneous values. In this perspective, we devise a statistical approach identical to the standard CI model to define the directional path loss distribution. The method uses a simple curve fitting over the deterministic path loss data set.

Before detailing the approach, we would like to highlight a significant feature of the MiDDCM framework that exploits antenna directionality in mmWave links. That is, the deterministic path loss over distance predicted by the model can be well categorized into two distinct regions: i) the path loss at near TX regions which is identical to the reference FSPL (as the narrow beam directional antennas act as spatial filters and filter out reflections with large arrival/departure angles) and; ii) the path loss in far TX regions that fluctuates relative to the reference FSPL with a non-uniform variance for the fading factor (as the reflected paths that fall within the directional antenna pattern at the receiver progressively combine with distance). However, statistical models based on power-law path loss equations, like CI and ABG, fail to capture these aspects.

The following steps are performed to deduce a statistical closed-form expression that can approximate the path loss distribution in directional channels: (i) firstly, modify the FSPL in the statistical closed-form expression to accommodate the antenna gains and, (ii) secondly, introduce a novel correction factor in the closed-form expression to convert the uniform variance of the fading factor to a non-uniform variance which is a function of separation distance, model geometry, and antenna beamwidth. To develop the statistical approximation of MiDDCM, we first rephrase (4.6) as (4.7) to match the statistical power-law path loss formulation as:

$$PL_d{}^{\text{stat}}[\text{dB}] = PL_{d_0}[\text{dB}] + 10\, n^{\text{stat}} \log_{10}\left(\frac{d}{d_0}\right) - G_t[\text{dB}] - G_r[\text{dB}] + X_{\sigma_{\text{stat}}} \tag{4.7}$$

4.2.3.1 MODIFICATION OF FSPL

To provide a rational statistical approximation of the directional deterministic model, we first match the FSPL of the statistical formulation with that evaluated by MiDDCM by including the boresight antenna gains as:

$$FSPL_{d_0}{}^{\text{stat}}[\text{dB}] = PL_{d_0}[\text{dB}] - G_t[\text{dB}] - G_r[\text{dB}] \tag{4.8}$$

Subsequently, we examine the variations in mmWave directional path loss about its mean value caused by the reflected MPCs to compute the path loss distribution of the MiDDCM. This distribution is further used to model $X_{\sigma_{\text{stat}}}$, while its statistical parameters are estimated using the maximum likelihood estimate (MLE) technique.

4.2.3.2 MODIFICATION OF STANDARD DEVIATION ACCOMMODATING DIRECTIONALITY

To statistically model directionality, the variance of the fading factor should satisfy the unique nature of path loss fluctuations relative to reference FSPL. Most importantly, it should capture the two unique regions of distinct propagation characteristics, i.e., the near TX region with FSPL characteristics and far TX region with non-uniform fading variance. In this context, we define the point of separation between the near and the far TX regions as *critical distance* d_c which is a function of antenna directivity and deployment parameters. The first reflected path starts contributing to the received signal strength at d_c beyond which each MPC progressively contributes to the received signal strength with increasing distance. The effect is a gradual increase in the variance. Hence, we suggest that $\sigma_{\text{dB}}\sigma_{\text{dB}}$, which is generally a constant for the entire transmission range, should be modified by a distance-dependent correction factor. The correction factor is analytically deduced as explained in this section.

To this end, we first deduce an expression for the critical distance d_c. As known, the first specular reflection that contributes to the received signal can arise from the ground reflection or from the first order wall reflections, whichever arrives first. The ground reflected path would fall within the antenna beam area if $\theta_g \leq \theta_{HPBW}$, where $\theta_g = \tan^{-1}[(h_t + h_r)/d_{3D}] \approx (h_t + h_r)/d_{3D}$, when the angle is in radians and is sufficiently small. That is,

$$\frac{h_t + h_r}{\sqrt{d^2 + \left(d_s - d_{t\_w} - d_{r\_w}\right)^2}} \leq \theta_{HPBW} \tag{4.9}$$

Similarly, the first order wall reflected path would fall within the antenna beam area, if $\phi_i \leq \phi_{HPBW}$, where $\phi_i = \tan^{-1}\left[\left(d_s \mp d_{t\_w} \pm d_{r\_w}\right)/d\right] \approx \left(d_s \mp d_{t\_w} \pm d_{r\_w}\right)/d$. That is,

$$\frac{\left(d_s \mp d_{t\_w} \pm d_{r\_w}\right)}{d} \leq \phi_{HPBW} \tag{4.10}$$

Accordingly, the minimum 2D distances at which the ground reflection (vertical reflection) and the wall reflection (horizontal reflection) participate in the directional signal reception are defined as the vertical critical distance d_{vc}, and the horizontal critical distance d_{hc}, given by,

$$d_{vc} = \sqrt{\left(\frac{h_t + h_r}{\theta_{HPBW}}\right)^2 - \left(d_s - d_{t\_w} - d_{r\_w}\right)^2} \tag{4.11}$$

$$d_{hc} = \frac{\min\left(d_s \mp d_{t\_w} \pm d_{r\_w}\right)}{\phi_{HPBW}} \tag{4.12}$$

It is clear from the geometry that if TX and RX are positioned on the same side of the street aligned with the x-axis, then $d_s = d_{t\_w} + d_{r\_w}$. Accordingly, d_{vc} and d_{hc} reduces to $((h_t + h_r)/\theta_{HPBW})$ and $(2d_w/\phi_{HPBW})$, respectively. Here, d_w is the smallest distance amongst the distance from TX to near reflecting wall and from RX to far reflecting wall.

The critical distance d_c which is the minimum TX/RX separation distance at which a reflected ray starts to participate in the directional signal reception is then,

$$d_c = \min\ (d_{vc}, d_{hc}) \tag{4.13}$$

For all link ranges greater than d_c, the path loss variations relative to reference FSPL is an increasing function of distance. The non-uniform variance of directional channel fading is modelled in this work as follows. From the path loss distribution of the MiDDCM, we first estimate the statistical parameters $(\mu_{\text{stat,dB}}, \sigma_{\text{stat,dB}})$ of path loss variations by using the MLE technique. The log-normal distribution is ideally suited for fitting the distribution of fading amplitude [120]. Next, we use a novel distance-dependent correction factor to convert the uniform standard deviation $\sigma_{\text{stat,dB}}$ to a non-uniform standard deviation. The introduced correction factor $\mathcal{C}_\sigma$ is a function of the *critical distance* d_c, the maximum allowable range d_{max} and the 2D link distance d, given by:

$$\mathcal{C}_\sigma = \begin{cases} 0, & if\ d < d_c \\ \dfrac{log\ (d - d_c)}{log\ (d_{max} - d_c)}, & if\ d_c < d < d_{max} \end{cases} \tag{4.14}$$

The corrected non-uniform standard deviation is hence developed from the estimated standard deviation as,

$$\sigma_{\text{mod,dB}} = \mathcal{C}_\sigma . \sigma_{\text{stat,dB}} \tag{4.15}$$

The statistical closed-form expression that characterizes directional path loss hence employs a distance dependent shadow fading factor $X_{\sigma_{\text{mod}}}$ such that $X_{\sigma_{\text{mod}}} \sim \mathcal{N}\left(\mu_{\text{stat,dB}}, {\sigma_{\text{mod,dB}}}^2\right)$.

The proposed statistical path loss model that approximates the deterministic directional mmWave path loss is then expressed as:

$${PL_{d,\text{mod}}}^{\text{stat}}[\text{dB}] = {FSPL_{d_0}}^{\text{stat}} + 10n^{\text{stat}} \log_{10}\left(\frac{d}{d_0}\right) + X_{\sigma_{\text{mod}}} \tag{4.16}$$

This simple closed-form expression can predict the path loss distributions identical to the path loss simulated by MiDDCM over all the frequencies and distances simultaneously. Most importantly, it excludes estimating the channel MPCs which involves calculating their the pathlengths $d_{g,i}$, reflection coefficients $\Gamma_{g,i}$, 3D angles $(\phi,\theta)_{g,i}$ and the physical direction dependent antenna gains, $G_{g,i}(\phi,\theta)$ for each reflected path during every instance of channel prediction. Moreover, the directional statistical path loss is predicted as a function of the 2D separation distance between the TX and RX in the UMi SC layout.

For 'O' simulated observations, the best fit minimum mean square error (MMSE) PLE, n^{stat}, that estimates the time-averaged MiDDCM path loss values with the smallest error is determined as,

$$n^{\mathrm{stat}} = \arg\min_{n_k} \sum_{k=1}^{O} \left({PL_d}^{\mathrm{det}}(k) - {PL_d}^{\mathrm{stat}}(k) \right)^2 \tag{4.17}$$

4.3 OPTIMIZATION OF SC DEPLOYMENT PARAMETERS

4.3.1 PROBLEM FORMULATION

In summary, we show that the directional path loss of a mmWave outdoor SC channel is a function of the operating frequency, antenna directionality, SC geometry parameters h_t, h_r, d, d_s, d_{t_w}, d_{r_w}, and also the transmission condition (LOS/NLOS) [121]. Even small variations in the positioning of TX and RX are observed to create significant fluctuations in the mmWave channel path loss due to the extremely short wavelength of mmWaves. As it is evident, mmWave propagation conditions are constrained by the environmental effects and mmWave transmission frequency by its availability. However, all other parameters related to the SC deployment geometry and the TX/RX position are free parameters and can be optimized. In this perspective, a population based stochastic technique called PSO is used for arbitrarily optimizing the choice of free parameters to minimize the generated path loss, which forms the objective function. While optimizing the free parameters, we assume the other parameters as constant within the recommended bound to reduce the complexity of PSO simulation.

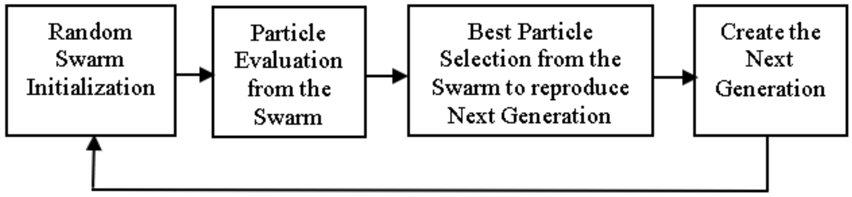

Figure 4.1 The general iterative process of PSO.

Accordingly, the optimization problem (P) is defined as,

P: *minimize* $\quad PL(f, d, \phi, \theta)$ (4.18)

s.t. 1. $1 \leq d \leq 50$m for LOS transmission (4.19)

2. $50 \leq d \leq 20$m for NLOS transmission (4.20)

3. $5 \leq d_s \leq 20$m (4.21)

4. $0 \leq d_{t\_w}, d_{r\_w} \leq d_s$ (4.22)

5. $5 \leq h_t \leq 17$m (4.23)

6. $1.5 \leq h_r \leq 20$m (4.24)

We realistically choose the bound of the parameters in (4.19) – (4.24) from the insights gained from the existing literature [28], [32], [35], [36], [122], [123]. The proposed solution is effective in the planning of SC deployment geometry of mmWave directional outdoor channels knowing that even small variations in antenna placement could considerably vary the propagation characteristics [104].

4.3.2 PARTICLE SWARM OPTIMIZATION

In this section, we briefly provide an insight into the population evolutionary algorithm called PSO. PSO is a multidimensional search algorithm based on heuristics, inspired by swarm intelligence. The system consists of a population of particles, called a swarm, interacting with each other and the environment. These particles are potential solutions to the optimization problem. To find the optimal solution, each particle finds the best position called the local best and the global best. The local best is a memory of its own best experience, and the global best is the common best experience found by any neighbour particle. Hence, the algorithm uses the best position (solution) encountered by a particle and/or its neighbour to determine the new position of the particle in the swarm. The position X and velocity V of the particles are given by [124]:

$$X_i(t+1) = X_i(t) + V_i(t+1) \tag{4.25}$$

where i is the particle index, and t is the time index that shows the iteration number of the algorithm. The velocity of particle i in time step $(t+1)$ is updated based on:

$$V_i(t+1) = \omega V_i(t) + c_1 r_1\big(P_i(t) - X_i(t)\big) + c_2 r_2\big(g(t) - X_i(t)\big) \tag{4.26}$$

where ω is the inertia weight used to control the speed of convergence, c_1 and c_2 are personal and social acceleration coefficients, r_1 and r_2 are uniform random variables in [0,1], $P_i(t)$ is the local best position of the i^{th} particle and $g(t)$ is the global best of the swarm. The general process of PSO can be well realized from the basic block diagram shown in Figure 4.1 [109].

4.3.3 PSO PROCEDURE FOR DEPLOYMENT GEOMETRY OPTIMIZATION

The optimization of SC deployment geometry using PSO to minimize the mmWave path loss is presented in Algorithm 2.

Algorithm 2: Particle Swarm Optimization based deployment parameter optimization

---

1 Initialize the swarm particle population, *nPop*, for as many particles as free parameters, *FP*, and maximum iterations to be run by the algorithm, *maxiter*.

For each particle P_{ij}, $i = 1,2, \ldots, FP$ and $j = 1, 2, \ldots, nPop$

(i) Set the position of each particle P_{ij} as $X_{ij}(0)$ uniformly distributed in $[LB, UB]_i$, where LB and UB are the lower and upper bounds of the i^{th} free parameter's range in Table 4.

(ii) Set the velocity of each particle P_{ij} as $V_{ij}(0) = 0$.

(iii) Set *pbest* for each particle P_{ij} to its initial position: $pbest_{ij}(0) = X_{ij}(0)$.

(iv) Set *gbest* to the minimal value of the swarm: $gbest_i$ = best particle in $X_{ij}(0)$ for which *cost_function* $[X_{ij}(0)]$ (i.e., path loss) is minimum.

(v) Set the range of velocity of the particles as $[-0.1*|UB - LB|, 0.1*|UB - LB|]$.

Assign PSO parameters.

(i) Inertia weight ω used to control the speed of convergence.

(ii) Personal and social acceleration coefficients c_1 and c_2.

(iii) Uniform random variables in [0,1] r_1 and r_2.

while $t \leq maxiter$

For each particle P_{ij}, $i = 1,2, \ldots, FP$ and $j = 1, 2, \ldots, nPop$

Update particle's velocity as,

$$V_{ij}(t+1) = \omega V_{ij}(t) + c_1 r_1 \left(pbest_{ij}(t) - X_{ij}(t)\right) + c_2 r_2 \left(gbest_i(t) - X_{ij}(t)\right)$$

Update particle's position as,

$$X_{ij}(t+1) = X_{ij}(t) + V_{ij}(t+1)$$

If X_{ij} extends beyond the ranges of P_{ij}, it is corrected by $[\mathrm{LB}, \mathrm{UB}]_i$.

if *cost_function* $[X_{ij}(t)] <$ *cost_function* $[pbest_{ij}(t)]$ **then**

Update the best-known position of particle P_{ij}: $pbest_{ij}(t) = X_{ij}(t)$.

if *cost_function* $[X_{ij}(t)] <$ *cost_function* $[gbest_i(t)]$ **then**

Update the swarm's best-known position: $gbest_i(t) = X_{ij}(t)$.

end if

end if

end while

Output $gbest_i(t)$ as the optimal free parameters that yield minimum channel path loss.

4.4 CHAPTER SUMMARY

In this chapter, the MiDDCM expression that provides direction dependent path loss values due to specular reflections has been carefully rephrased to preserve the channel formulations of the popular statistical models. This allows for easier comparison and validation.

A statistical closed-form expression identical to the power-law path loss model has been defined to parameterize the directional characteristics. To this end, a new distance-dependent correction factor is proposed to correct the uniform variance of multipath fading in power-law path loss models in order to predict the path loss distributions realistically and accurately in highly directional mmWave channels.

While the mmWave directional channel path loss can be substantially dependent on SC deployment parameters due to the link directionality and the short wavelength of mmWaves, it is essential to plan the deployment geometry with precise parameters to obtain optimal channel performance. To this end, a metaheuristic algorithm called PSO has been applied to determine the optimal deployment and position parameters of mmWave SC layout geometry to yield the best directional channel path loss.

CHAPTER 5. RESULTS AND DISCUSSION

5.1 INTRODUCTION

In this chapter, we provide the simulation results of the proposed low complexity mmWave channel model, MiDDCM, which characterizes direction-dependent transmission in specific scenarios and applications. The model is used to investigate mmWave channel characteristics in a typical deployment scenario of UMi outdoor SC employing directional transmission. The implication of directionality is analysed and exploited for several usage scenarios. The strength of the proposed channel model constitutes path loss predictions for various propagation scenarios, antenna specifications, TX/RX heights and positions, and deployment parameters.

The rest of this chapter is organized as follows. Section 5.2 presents MiDDCM implementation results at varying parameters and validation against measurement-based statistical formulation reported in the literature. The channel is analysed for an idealistic SC with continuous sidewalls and a realistic SC with crossroads. Section 5.3 presents the statistical approach to parametrize MiDDCM, and Section 5.4 provides significant results on SC deployment geometry optimization by using the PSO algorithm. Section 5.5 presents the chapter summary.

5.2 MMWAVE DIRECTIONAL DETERMINISTIC CHANNEL CHARACTERIZATION

This section evaluates the channel characterization capabilities of the proposed antenna angle-dependent deterministic ray tracing approach that invokes channel sparsity to characterize a highly directional mmWave outdoor channel. To understand the path loss distributions modelled by MiDDCM, this work identifies distinct propagation geometries (PGs) and propagation scenarios (PSs):

Propagation Geometry 1 (PG1): PG1 represents "System I" with lamppost-style deployment wherein we assume that the TX antenna is mounted on a lamppost along the street at an anchored distance of 4m from the near reflecting sidewalls, i.e., d_{t_w} = 16m for 20m street width. Hence, the 3D location of the TX antenna from the origin of the coordinate system is established as (0, 4, h_t).

Propagation Geometry 2 (PG2): This geometry also depicts "System I" with the TX antenna located on the reflecting building along the near sidewall of the street, i.e., d_{t_w} = 20m. Accordingly, the 3D location of the TX antenna is established as (0, 0, h_t).

Propagation Geometry 3 (PG3): PG3 illustrates "System II" deployment that assumes discontinuities in the reflecting sidewalls in the form of crossroads, unlike PG1 and PG2 settings with continuous sidewalls.

Propagation Scenario 1 (PS1): PS1 assumes LOS up to the maximum link range, i.e., d = 200m. Also, the TX and RX beams are aligned by providing suitable horizontal and vertical slant angles to ensure maximum signal strength. We even discard attenuation due to foliage in this strong LOS path scenario to evaluate the best-case channel performance.

Propagation Scenario 2 (PS2): PS2 depicts the worst-case propagation scenario of NLOS transmission with an obstructed LOS path and attenuated by the frequency-dependent foliage losses. Also, the model assumes no beam steering in this scenario leading to the worst-case propagation scenario.

Propagation Scenario 3 (PS3): Here, we again consider an NLOS channel with obstructed LOS and foliage attenuation, however, the antenna is assumed to be steered in the 3D plane towards the direction of the blocked LOS path. We intend to examine the impact of beam steering on NLOS signal transmission in this final scenario.

5.2.1 BACKHAUL AND ACCESS ANALYSIS FOR LOS / NLOS SISO CHANNELS

In this section, we simulate MiDDCM to examine the channel performance of a mmWave directional link for both backhaul and access SISO cases. To provide a useful comparison, we first set the simulation parameters of MiDDCM such as the frequency, antenna specifications, TX/RX heights, and the environment (LOS/NLOS) to a default representative value identical to the mmWave measurement studies provided in [26] (Refer Table 5.1). We choose the initial settings of the SC deployment parameters as d_s = 20m, d_{t_w} = 16m, d_{r_w} = 4m, and d_{max} = 200m, illustrating PG1, which is used by the simulator unless otherwise stated. As shown in Figure 3.3, setting deployment parameters as d_{t_w} = 16m, d_{r_w} = 4m with d_s = 20m

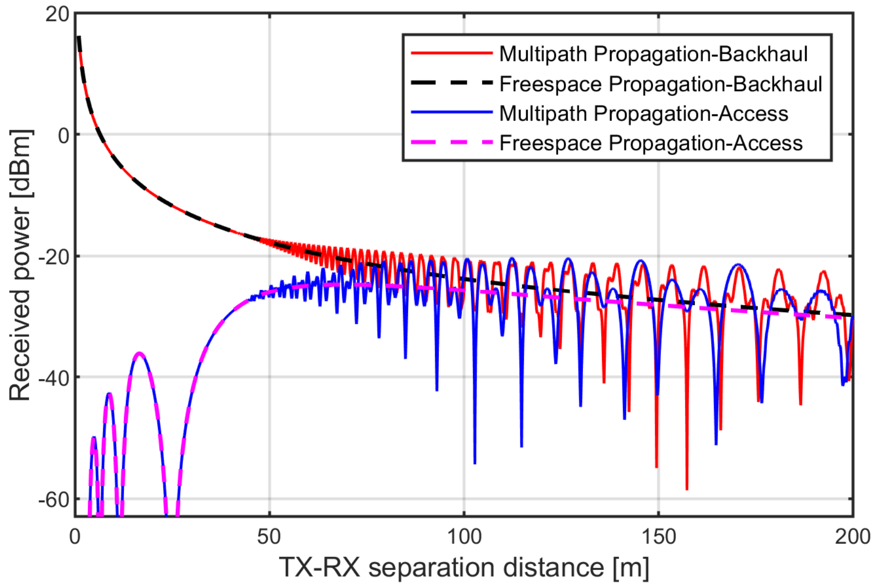

Figure 5.1 Received signal strength at 28 GHz simulated for the backhaul link and the access link without beam steering.

implies that both TX and RX are on the same street-side at 4m from the near reflecting wall. Here, we assume that the TX antenna is mounted on the lamppost at 7m from the ground. The RX antenna height is considered as 7m for the backhaul analysis and as 1.5m to analyse access channels. The simulation assumes vertically polarized antennas at the TX and RX sides.

Accordingly, the MiDDCM first evaluates the LOS received power for backhaul and access mmWave links at 28GHz in discrete steps of 2D separation distance for a maximum cell radius of 200m, as illustrated in Figure 5.1. Note that, in this analysis, the radiation patterns of TX and RX are aligned in the boresight (i.e., $\phi = \theta = 0$) with no beam steering in both elevation and azimuth planes. For this simulation settings, the directional channel is non-faded up to a separation distance of 41.5m for the selected antenna directionality of 23.7dBi realized using half power values of $HPBW_{A,E} = 10.9°$. That is, at $d \approx 2d_w/(HPBW_A)_{rad}$ as the TX and RX are positioned on the same side of the street aligned with the x-axis with $d_s = d_{t\_w} + d_{r\_w}$. Although the ground and the building side walls could create reflected paths, the channel within this region is purely LOS since the angles of arrival/departure of specular reflections are larger than the half power beamwidths of directional antennas

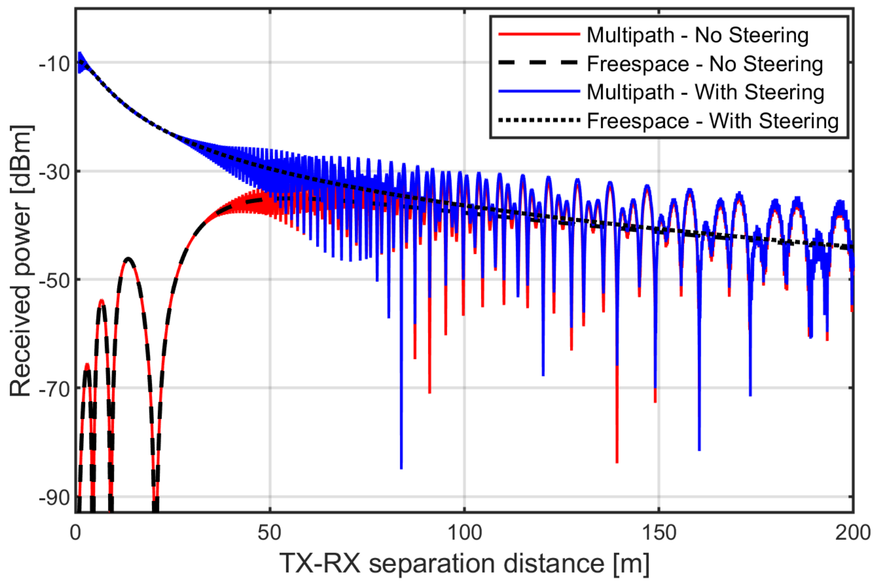

Figure 5.2 Received signal strength at 60GHz simulated using $HPBW_{A,E}$ = 15°, 13° for the access link comparing the effects of elevation beam steering.

in both azimuth and elevation planes. This separation distance at which specular reflection starts contributing as a propagation mechanism is indeed a function of deployment parameters like h_t, h_r, d_{max}, and d_s, in addition to the antenna HPBWs in elevation and azimuth planes. Accordingly, the reflected paths begin to contribute towards received power beyond 41.5m, causing multipath induced fading effects.

We observe that the signal fluctuations relative to their FS benchmark increase drastically for link distances larger than 100m due to higher order multipath reflections. For every simulation scenario, the model evaluates the maximum wall reflection order N from the choice of input specifications, as detailed in Section 3.3. The backhaul channel characterization at cell edge (d = 200m) shows three specular reflections constructively or destructively interfering with the direct LOS. i.e., a ground reflection and two first orders wall reflections. For a directional channel with an unobstructed LOS path, the links beyond 120m exhibit comparable characteristics for both backhaul and access links even in the absence of beam steering. However, the positions of deep fades were observed to have visible variations. For the backhaul link, the deepest fade of -58.7dBm occurred at 157m. However, the fade of -54.4dBm occurred at 103m in the access link.

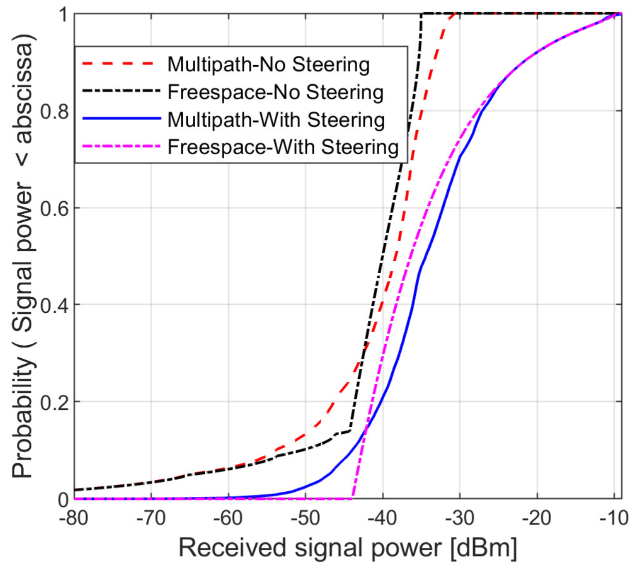

Figure 5.3 Probability of received signal strength analysed for the 60GHz access link with and without beam steering.

The analysis of access channels employing directional antennas displays extensive signal outages at small link ranges closer to the lampposts in the absence of beam steering. Moreover, UEs far away from the TX will rely on NLOS transmission. These obstructed LOS paths may experience a significant drop in the link quality if the antenna radiation patterns are not aligned. These observations suggest the need for beam steering enabled directional transmission in mmWave channels. Accordingly, the main lobes of TX and RX antennas shall be tilted in azimuth and elevation planes to align their radiation patterns for maximum signal strength.

5.2.2 PERFORMANCE ANALYSIS WITH BEAM STEERING

Beam steering in mmWave directional transmission improves the link performance by directing the transmitting beam towards the beam area of the receiving antenna. Moreover, it helps to eliminate the large path loss variations that a mmWave directional link experiences even with channel spatial variations on the order of a few centimetres. To investigate the impact of beam steering, we now consider 60GHz, the heavily attenuated band compared to several other mmWave frequency ranges. Also, we assume a slightly wider beam area to examine the effect of having a larger number of contributing multipaths with comparable strengths. Accordingly, the directional

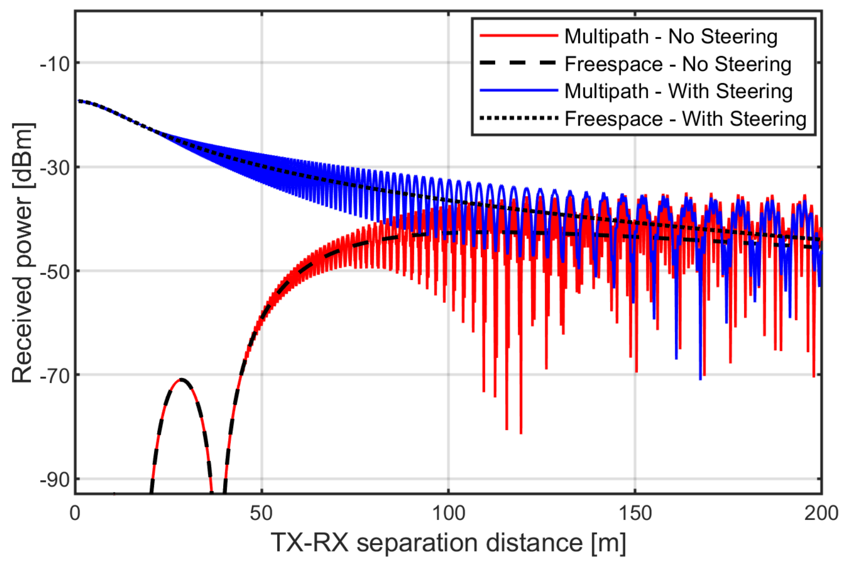

Figure 5.4 Received signal strength at 60GHz simulated using unaligned TX-RX positions comparing the combined effects of elevation and azimuth beam steering.

antenna HPBW is increased to $HPBW_A = 15^{\circ}$ and $HPBW_E = 13^{\circ}$. Figure 5.2 depicts the received signal variations considering no beam steering and elevation beam steering that corrects the antenna height differences. Figure 5.3 illustrates the cumulative distribution function (CDF) of the LOS received power upon varying the link range from 1-200m. As observed, the received signal when beam steering is not enabled exhibits large signal fluctuations below 35m. The CDF plot clearly illustrates that elevation beam steering improves signal reception in access channels.

To further examine the impact of beam steering in the 3D plane and to appreciate the capabilities of MiDDCM, we extend the beam steering analysis of access channels by assuming an RX placement unaligned with the TX in the horizontal plane with and without beam steering. In particular, we assumed d_{t_w} = 16m, d_{r_w} = 16m, which implies that RX is placed on the other side of the street from where the TX is located. The new deployment parameters (i.e., unaligned TX-RX placement) help to appreciate antenna tilting in the azimuthal plane in addition to elevation beam steering. Accordingly, in Figure 5.4, we compare the received power obtained by orienting the antenna radiation patterns in boresight (no steering) to that obtained by dynamically providing suitable azimuthal and elevation antenna tilt. As shown, the simulation setting produces larger signal variations for the entire range of d and is

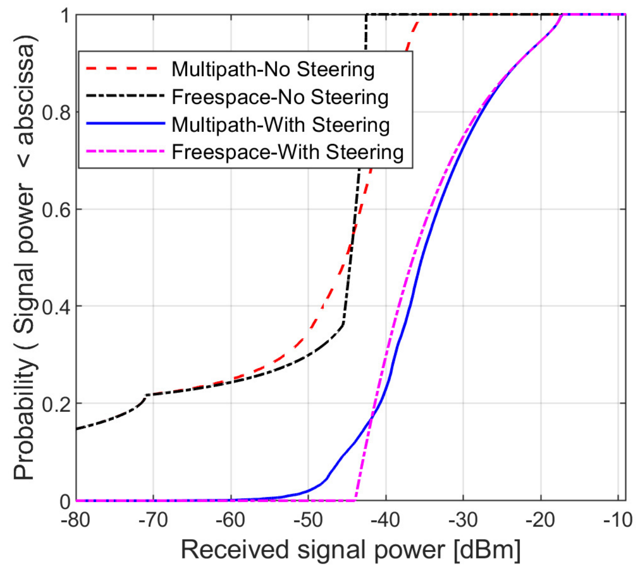

Figure 5.5 CDF of received power of the 60GHz access link without beam steering and with azimuth and elevation beam steering.

clearly illustrated in the CDF plot in Figure 5.5. The received power without beam steering exhibits significant attenuation having a signal level lower than -80dBm almost 15% of the time. However, by providing 3D beam correction, we can ensure at least -42dBm nearly 85% of the time.

5.2.3 VALIDATION AGAINST STANDARD CHANNEL MODELS

After implementing the MiDDCM framework in MATLAB, we validate the model against the measurement-based statistical CI model. Channel validation is an essential step in channel modeling and to this end, we compare the simulated path loss of MiDDCM with those predicted by the CI model in Table 5.1. Note that the path loss at two separation distances; one to depict the LOS range and the other for NLOS are provided. While evaluating the LOS path loss using MiDDCM, targeted transmission through beam steering was assumed (PS1). Also, the effects of foliage losses were neglected owing to the shorter distance. However, for the NLOS case, we analyse the worst-case scenario without beam steering and increased attenuation due to foliage (PS2).

We use the MATLAB implementation of the path loss expression specified in [26] by considering the model parameters reported for specific frequencies and deployment scenarios to yield the CI path loss. The CI path loss values are very close to the mmWave measurement values. As stated in the literature, we considered PLE = 1.9dB and shadow fading factor = 1.1dB for the CI LOS scenario and PLE = 4.5dB, and

Table 5.1 Comparison of MiDDCM path loss with measurement-based CI predictions.

mmWave Link Budget	*Freq* [GHz]	P_t [dBm]	$HPBW_{A,E}$ [°]	Gain [dBi]	Link Type	h_t / h_r [m]	Env	*d* [m]	*PL* [dB]
Measurement [26]	28	30.1	10.9	24.5	Access	7 / 1.5	LOS	50	94.2
							NLOS	200	170.3
	73	14.6	7	27	Access	17 / 2	LOS	50	108.2
							NLOS	200	170
This Work	28	30.1	10.9	23.7	Backhaul	7 / 7	LOS	50	95
							NLOS	200	125.9
					Access	7 / 1.5	LOS	50	96.5
							NLOS	200	123.4
	73	14.6	7	27.6	Backhaul	7 / 7	LOS	50	103.3
							NLOS	200	140.3
					Access	17 / 2	LOS	50	104.1
							NLOS	200	144.4
	60	30.1	10.9	23.7	Backhaul	7 / 7	LOS	50	102.9
							NLOS	200	137.1
					Access	7 / 1.5	LOS	50	103.5
							NLOS	200	135.5

shadow fading factor = 10dB for the NLOS scenario for a 28GHz access channel with differently selected TX and RX antenna heights. The LOS path loss estimated by the proposed MiDDCM at 50m range shows good agreement with the CI measurement values, whereas a deviation is observed for the long range NLOS case. A similar trend is observed for the 73GHz mmWave channel characterization. The MiDDCM channel simulator yields lower NLOS path loss compared to the measurement values. We attribute this variation in NLOS path loss to multiple reasons, as stated below:

(i) The MiDDCM design considers spatial filtering of directional antennas which causes the elimination of higher order reflections, thereby reducing the angular spread of channel MPCs. This understanding is in agreement with the reduced diversity and the drop in the number of clusters stated in mmWave transmission [32]. For instance, the NYUSIM model is reported to yield only 1-2 strong clusters and several weaker clusters [36]. The mmWave directional channel characterization using MiDDCM generates three specular reflected paths of differing delays at d = 200m for the selected antenna HPBW of 10.9°. However, at d = 50m, a ground reflection and a single wall reflection contribute to the received signal strength in addition to the direct LOS component.

(ii) The path loss determined by the proposed deterministic model for a given d (as provided in Table 5.1) varies based on the exact 3D UE location (d_{3D}). In fact, the path loss value evaluated for a specified 2D separation distance d can change depending on the actual placement of the UE along the width of the street, i.e., depending on the value of d_{r_w}. The path loss provided in Table 5.1 is for a vertically polarized transmission with d_{r_w} = 4m; however, these values could increase if the RX placement is unaligned with TX. Specifically, the NLOS path loss for the 28GHz access link changed to 139dB on considering d_{r_w} = 10m. Also, a higher path loss of 147.4dB was obtained with d_{r_w} = 16m for 60GHz mmWave transmission. These increased values of directional path loss will reduce the deviation between the proposed deterministic ray tracing evaluation and the CI prediction. As it is clear, acquiring such detailed channel information for the existing channel models is challenging because of their non-dependency on SC deployment parameters. To provide a detailed insight on the path loss variations with varying 3D UE locations, we examine the channel path loss evaluated for varying UE placements across the street (i.e., with the same 2D distance d) in Figure 5.6. Precisely, we consider both vertical and horizontal polarizations at three different mmWave carrier frequencies. Regardless of the differences in FSPL and foliage losses at 60- and 73GHz

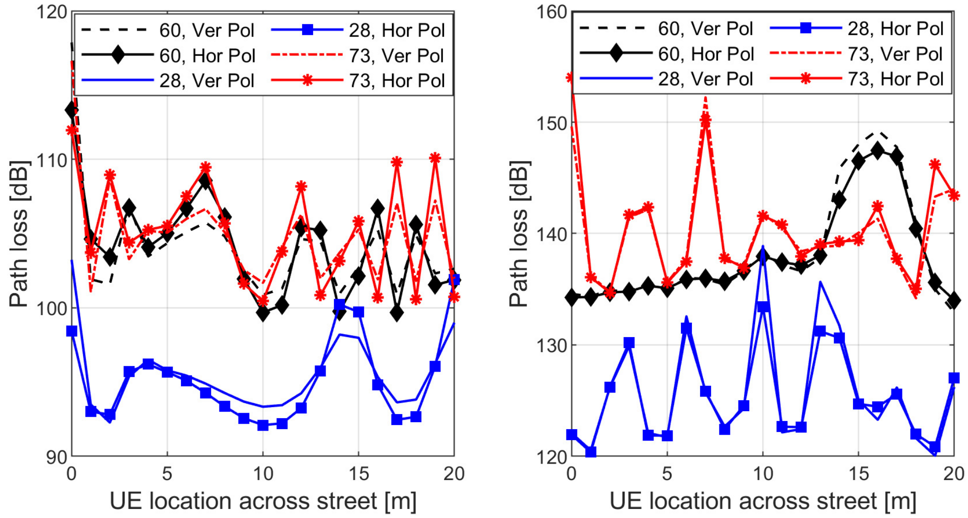

(a) (b)

Figure 5.6 Path loss evaluated for varying mmWave frequencies and polarizations at different UE locations along the street width for (a) LOS and (b) NLOS.

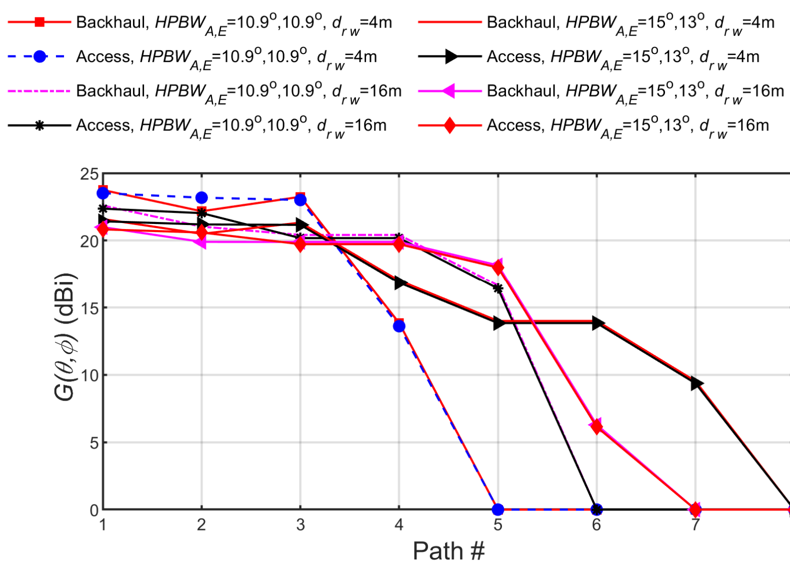

Figure 5.7 Horn antenna gains analysed for various scenarios to emphasize the need for magnifying each MPC by placing in the angle dependent antenna gains.

frequencies, their LOS path loss for UEs located closer to the transmitter (d = 50m) are comparable. We also observe minor NLOS path loss variations with changing polarization for all the analysed frequencies compared to LOS variations.

(iii) The variation in NLOS path loss could also be due to the modeling strategy of MiDDCM, wherein the channel path loss is evaluated by including directional antenna effects in the path loss slope. That is, we discreetly magnify every strong MPC by its corresponding direction dependent antenna gain $G_{g,i}(\phi, \theta)$ as a function of (ϕ, θ) as explained in Chapter 3. The approach is known to yield accurate estimations in directional channel analysis than including boresight antenna gains directly in the link budget as applied by most of the reported models [32], [36]. It highlights the antenna dependency of the directional channel response. Accordingly, we next analyse the horn antenna gains that magnify each participating MPC for varying scenarios of HPBWs and UE locations in Figure 5.7. Here, path # 1 and 2 refer to direct LOS and ground reflection paths. Path # 3 and 4 refer to the first order, 5 and 6 to the second order, and 7 and 8 to the third order for the near and far wall reflections, respectively. A unique feature of directional transmission is that the MPCs with larger delays are magnified by much smaller antenna gains than the antenna boresight gains. There is a need to explicitly take account of this in the directional channel modeling.

So far, we have validated MiDDCM against the statistical CI approach built on measurement values for the frequencies and scenarios available in the literature. The validation displayed comparable results with few discrepancies which were adequately reasoned out. In the next section, we aim at demonstrating the advantages of MiDDCM formulation. In specific, we present modeling scenarios that are impossible to investigate with statistical channel models and their usage in mmWave directional channel study.

5.2.4 COMPREHENSIVE SC CHANNEL CHARACTERIZATION FOR 60GHZ

To fully realize the capabilities of the low complexity MiDDCM that describes an outdoor SC scenario, we now characterize the channel specifically for the 60GHz frequency range. The 60GHz channel creates the worst-case path loss assessments due to its high atmospheric absorption compared to several other frequencies present in the mmWave band. An interesting insight from the previous section is that while using the transmit power and antenna HPBWs specified for 28GHz in [26], MiDDCM generates an EIRP of 53.8dBm exceeding the FCC limit of 40dBm. Furthermore, the high EIRP value limits the possibility of further increasing the antenna directionality

Table 5.2 Channel simulation parameters of MiDDCM for 60GHz.

Parameter	Value	Parameter	Value
TX/RX $HPBW_A$	15°	**Channel bandwidth**	1.5GHz
TX/RX $HPBW_E$	13°	**Oxygen absorption loss**	16dB/km
Antenna polarization	V-V	**Link margin**	5dB
Antenna gain	21.6dBi	**Target bit rate**	2Gbps
Max P_t	13.4dBm	**Noise figure**	3dB
Max EIRP	35dBm	**Min E_b/N_o**	12dB
Carrier frequency	60GHz	**Receiver sensitivity**	-66dBm

to enhance the link performance. Even though the 2013 FCC report allows an increase in the existing average EIRP range (raised to 40-82dBm), the amendment is just for a highly directional unlicensed 60GHz outdoor link and not for other mmWave frequencies. Hence, we reconsider the simulation parameters by assimilating mmWave directional link budget parameters from [27], [28], [68]. The new model parameters and link budget evaluation are as provided in Table 5.2. Note that the directional antenna HPBW considered is 15° for azimuth and 13° for elevation which increases the number of participating multipaths, consequently providing directional mmWave propagation even in the blocked LOS scenarios. Unlike with 10.9° HPBW (4 paths), MiDDCM now models 6 specular reflections (7 paths) at d_{max} = 200m. That is reflections from the ground, 1st order near and far walls, 2nd order walls, and 3rd order near-wall beginning to appear at 44.1m, 30.7m, 123m, 153.8m, and 184.6m, respectively.

We additionally observed that many existing works [27], [94] and references therein validated their simulations for $d \geq$ 30m accounting for the power controlled nature of the UEs positioned closer to the BS (in the near-field region). However, the mmWave antenna array systems will have small form factors within the range of 100-300mm at the BSs and less than 100mm at the UEs. Accordingly, the downlink far-field distance will typically begin at 1.9m for 28GHz and 4m for 60GHz. This motivates us to

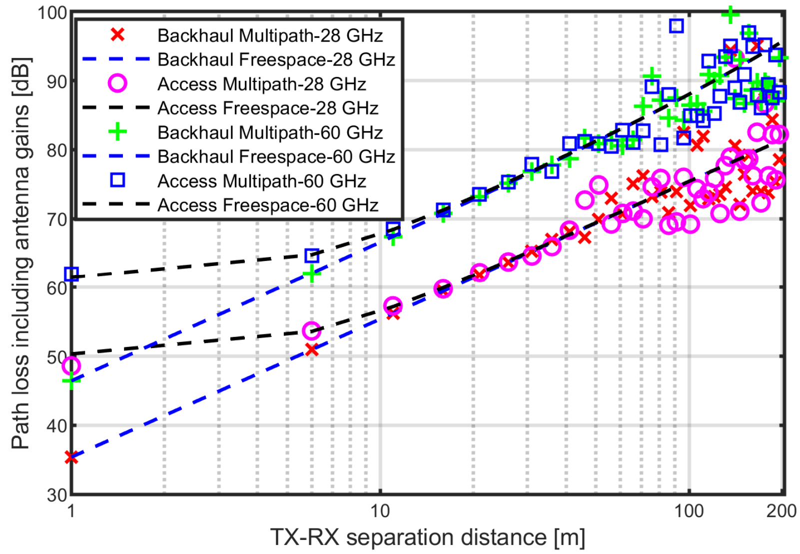

Figure 5.8 Path loss evaluated using MiDDCM at 28 GHz and 60 GHz for LOS UMi SC scenario.

assess the channel characteristics starting from 1m. Accordingly, Figure 5.8 provides the path loss as a function of d simulated for 28- and 60GHz backhaul and access channels for PG1 geometry with d_{r_w} fixed at 4m. As the goal is to study the fading relative to the free space benchmark, LOS transmission is assumed for the complete range. It is shown that the path loss variance relative to its free space value increases with distance. Also, the path loss at 60GHz demonstrates reduced variance compared to 28GHz due to the significantly attenuated 60GHz propagation.

Further, we capture and compare the directional path loss for two UE positions. That is, (i) on the same side of the street as the TX is placed (i.e., for UEs closer to near reflecting wall); (ii) across the street from where TX is located (i.e., for UEs closer to far reflecting wall). For this, we set the value of d_{r_w} as 4m and 16m, respectively. In Figure 5.9, we analyse the access channel path loss for both beam aligned and non-aligned cases under LOS transmission over the range [1m,60m] and NLOS transmission over [61m,200m], assuming that the LOS path is unavailable. The obtained path loss values are identical for both the UE placements if the beams are aligned. However, they vary for non-aligned antenna beams. The observation emphasizes the significance of dynamic beam steering in a 3D plane while

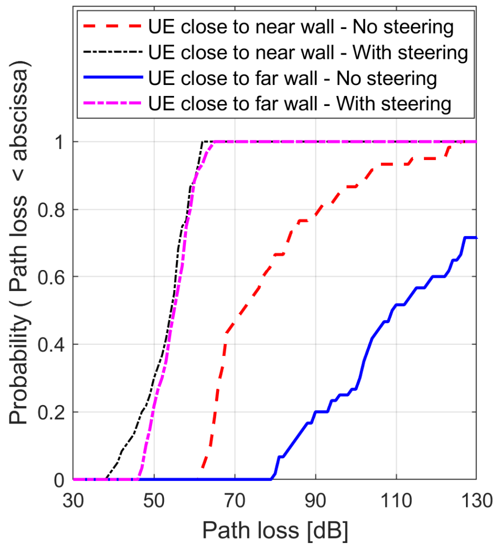

(a)

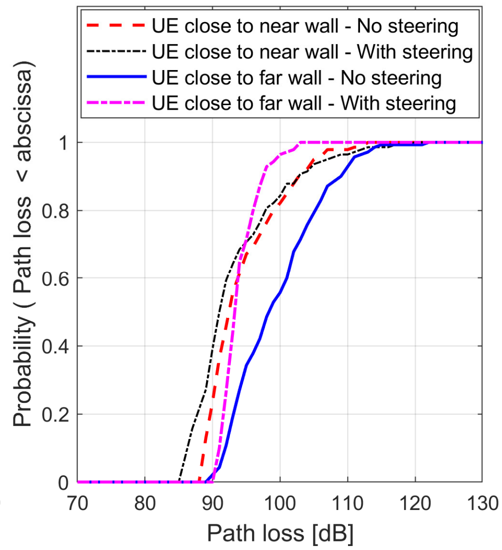

(b)

Figure 5.9 Path loss for two distinct locations of UE: close to the near reflecting wall and the far reflecting wall for both (a) LOS and (b) NLOS transmissions.

transmitting directional mmWave signals with strong and sparse MPCs. As such, the path loss values are higher for UEs positioned closer to the far wall for both LOS and NLOS conditions.

Next, we examine the access path loss obtained upon mounting the TX antenna on the lamp post (PG1) or on the building itself (PG2) for both LOS and NLOS conditions. We plot the CDF of the path loss for two different usage scenarios in Figure 5.10 upon varying the TX antenna h_t uniformly over the interval [5m,20m], keeping the position of UE fixed at h_r = 1.5m and d_{r_w} = 4m. We provide the following insights. Firstly, irrespective of the height of TX, its positioning has minimal impact on the NLOS path loss evaluated at d = 200m with or without beam steering. However, steering the beam in the direction of the blocked LOS rather than steering it in the boresight can reduce the maximum channel path loss to some extent. Secondly, we observe that when the antenna beam is corrected in the elevation plane alone and not in the azimuth plane, the choice of antenna placement is extremely critical in the LOS path loss evaluation. If beam steering in the 3D plane is enabled, then the LOS path loss (at d = 50m) is always less than 65dB for TX mounted on the building or the lamppost. On the other hand, antenna placement on the lamppost is beneficial for

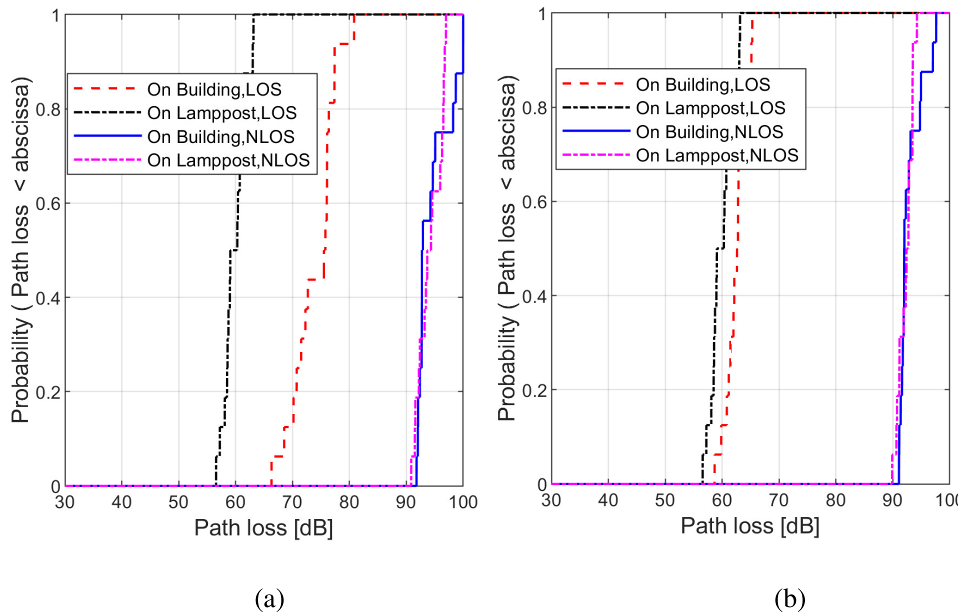

Figure 5.10 Path loss evaluated at two TX locations, on the lamp post (PG1) and on the reflecting building (PG2) for (a) PS1 with elevation steering for LOS and PS2 for NLOS (b) PS1 with elevation and azimuth steering for LOS and PS3 for NLOS.

mmWave directional systems employing 2D beam steering for elevation angle correction. In fact, the separation distance between TX and reflecting walls aid an increased number of contributing multiple paths.

In the previous analysis, we characterized the SC channel keeping either the x-coordinate or the y-coordinate as a fixed value. Next, we now provide a comprehensive characterization of LOS and NLOS path loss as a function of the TX coordinates for the entire SC layout. Here, x denotes d in the [0-200m] range, and y represents d_s in the [0-20m] range. From the simulation results in Figure 5.11, the following insights are derived. As anticipated, the PS1 simulation results show no signal fluctuations at small separation distances. As earlier explained, the channel here is non-fading with reflected rays falling outside the directional antenna beamwidth of the receiver. In all the cases, the signal fluctuations at large link ranges are due to the constructive and destructive interference of the reflected signal with the LOS signal. These fluctuations are observed to increase with increasing distance progressively. Furthermore, the LOS path loss in PG2 generates higher values compared to PG1 due to the reduced number of contributing reflections resulting from the proximity of TX to the reflecting wall. As inferred from the NLOS path loss, with

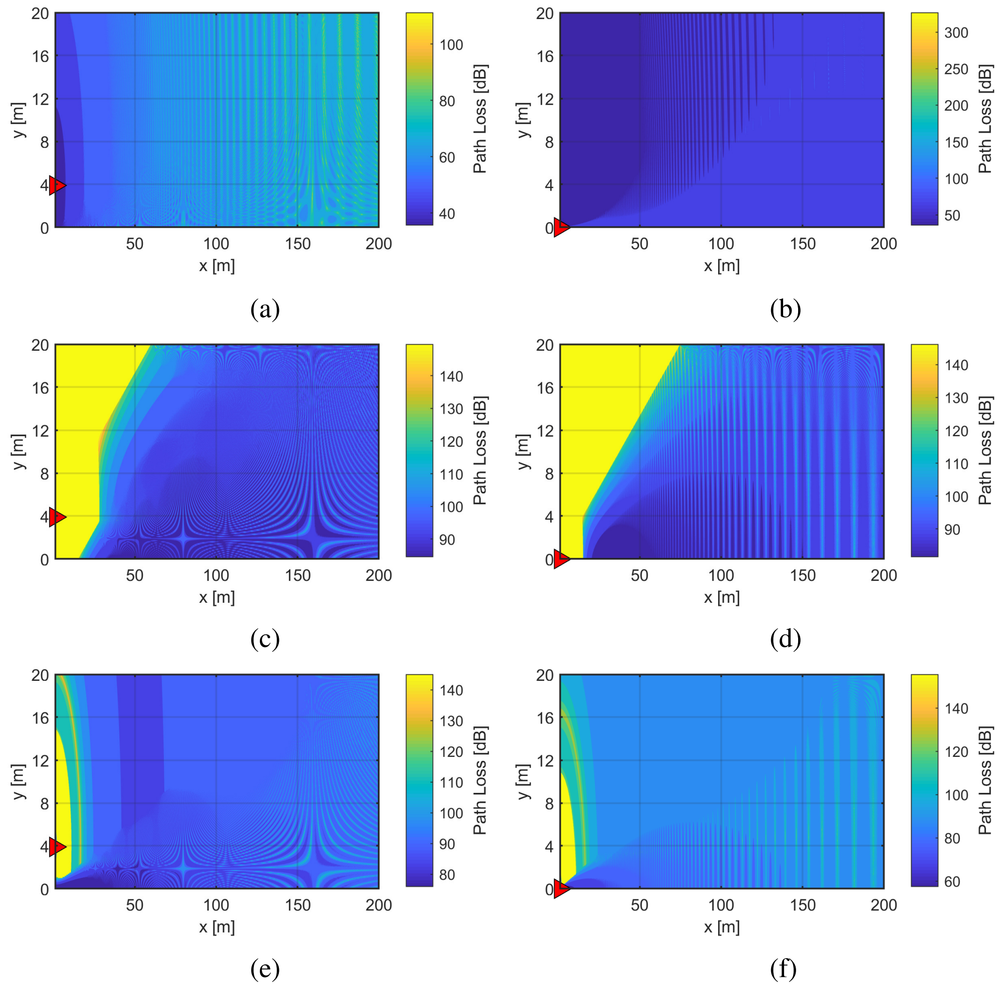

Figure 5.11 MiDDCM results with TX located on the lamppost (PG1) and the reflecting building (PG2) in different scenarios of LOS (PS1), NLOS with TX antenna oriented along boresight (PS2), and NLOS with TX antenna steered for maximum signal strength (PS3): (a) PG1, PS1 (b) PG2, PS1 (c) PG1, PS2 (d) PG2, PS2 (e) PG1, PS3 (f) PG2, PS3.

or without beam steering and for both PG1 and PG2 deployments, the absence of the LOS path manifests in higher path loss. Intuitively, steering the beam reduces signal attenuation in the near TX region for PG1 and PG2, the improvement being significant while steering in both azimuthal and elevation directions.

5.2.5 COMPARISON OF REFLECTED RAYS WITH 3GPP CLUSTER RAYS

In this section, the specular reflected rays and the LOS ray generated by MiDDCM are compared with the cluster rays generated by the 3GPP model specified in [68]. To

Table 5.3 Power delay profile of the received signal at cell edge for 28GHz LOS.

Path	**Backhaul** ***HPBW$_{A,E}$*** **(10.9°,10.9°)** ***d_{r_w}*** **= 4m**		**Access** ***HPBW$_{A,E}$*** **(10.9°,10.9°)** ***d_{r_w}*** **= 16m**		**Backhaul** ***HPBW$_{A,E}$*** **(15°,13°)** ***d_{r_w}*** **= 4m**		**Access** ***HPBW$_{A,E}$*** **(15°,13°)** ***d_{r_w}*** **= 16m**	
#	Delay [ns]	Power [dBm]	Delay [ns]	Power [dBm]	Delay [ns]	Power [dBm]	Delay [ns]	Power [dBm]
1	0	-29.85	0	-32.63	0	-34.15	0	-35.7
2	1.63	-36.42	0.34	-35.34	1.63	-39.77	0.35	-38.21
3	0.53	-31.16	2.13	-37.78	0.53	-34.99	2.13	-38.68
4	8.48	-50.97	2.13	-37.78	8.48	-44.62	2.13	-38.68
5	-	-	5.30	-45.63	13.20	-51.00	5.30	-42.48
6	-	-	-	-	13.20	-51.00	20.96	-67.27
7	-	-	-	-	18.93	-58.53	-	-
8	-	-	-	-	-	-	-	-

this end, we provide the power delay profile of the mmWave directional received signal evaluated by MiDDCM formulation for various input specifications in Table 5.3. Here, the simulation is run by setting the input parameters identical to the specifications in Table 5.1 for a 28GHz transmission, as specified by popular literature. The received power values are evaluated at d = 200m, assuming the LOS channel without any beam steering to compare with 3GPP clusters. Here, the path delays represent the reflected paths' delays normalized relative to the dominant LOS path. As the model deterministically determines the specular paths, the power delay profile of 60GHz transmission generates the same delay parameters with lower received power values. As apparent, the NLOS case yields lesser paths as well as reduced power. It may also be noted that increasing the HPBW increases the number of participating specular reflections, thereby dynamically adjusting the order of MiDDCM.

In Table 5.4, we provide the LOS and NLOS root mean square (RMS) delay spread (DS) values at a link range of 200m for 28GHz mmWave directional transmission. The delay spread generally describes the variance of the time delays of the MPCs.

Table 5.4 RMS delay spread for 28 GHz directional LOS and NLOS.

Parameter	Backhaul $HPBW_{A,E}$ (10.9°,10.9°) d_{r_w} = 4m	Access $HPBW_{A,E}$ (10.9°,10.9°) d_{r_w} = 16m	Backhaul $HPBW_{A,E}$ (15°,13°) d_{r_w} = 4m	Access $HPBW_{A,E}$ (15°,13°) d_{r_w} = 16m
RMS DS LOS [ns]	0.72	1.14	2.47	1.53
RMS DS NLOS [ns]	0.83	1.18	3.09	1.51

The lower RMS delay spreads in mmWave directional propagation environments attributes to two significant reasons: (i) the reduced specular reflections in directional links compared to omnidirectional transmissions and, (ii) severe multipath fading in highly attenuated mmWaves as compared to traditional sub-6GHz propagation. The channel employing large beam width directional antennas has a slightly larger delay spread which can be attributed to more reflected paths reaching the RX than channels using narrow beam antennas. From the MiDDCM simulation, we also observed the delay spreads of 60GHz identical to that of 28GHz with small variations of 0.2 - 0.5ns. From reference [125], the maximum value of modelled and measured RMS delay spread is 0.125ns for SC scenario operating at mmWave E-band channel which was modelled using a geometry-based single-bounce channel model and verified using channel measurements. Moreover, the LOS measurements on 28GHz and 73GHz in [26] reported the RMS delay spreads to be always less than 2ns.

We additionally simulated the 3GPP channel model by using the standard channel generation procedure as well as the large scale parameters provided in TR. 38.901. Accordingly, Table 5.5 provides a sample simulated cluster delay line (CDL) profile for LOS and NLOS UMi Scenario. In the 3GPP context, the term cluster refers to a group of MPCs with a unique AoD-AoA combination centered around a mean propagation delay. The 3GPP channel model design typically normalizes the cluster delay relative to the first cluster with the minimum absolute delay value. The model also removes the clusters having power values less than -25dB compared to the maximum power. This creates only 5 LOS clusters and 9 NLOS clusters in the sample simulation even though the 3GPP specification table defines a maximum of 12 and 19

Table 5.5 CDL table generated using the 3GPP model for UMi LOS and NLOS conditions.

Cluster	**LOS UMi**		**NLOS UMi**	
#	Delay [ns]	Power [dB]	Delay [ns]	Power [dB]
1	0	-13.2185	0	-19.63
2	16.0223	-29.1809	6.46	-21.73
3	41.6431	-35.0350	61.02	-18.08
4	57.4291	-33.5692	85.07	-10.57
5	96.5252	-37.7167	130.45	-1.15
6	-	-	149.36	-18.41
7	-	-	154.08	-11.26
8	-	-	179.85	-18.27
9	-	-	382.16	-24.19

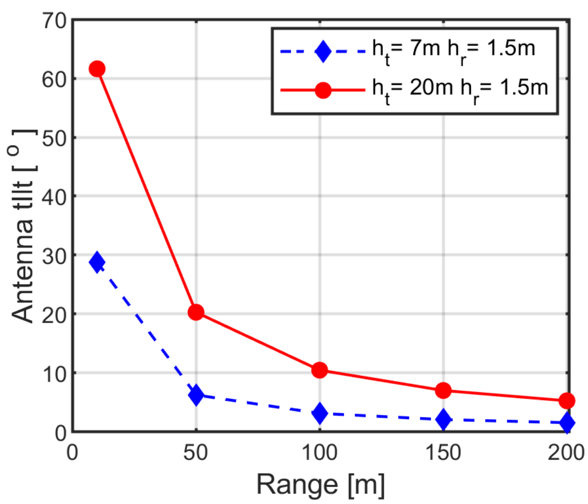

Figure 5.12 Antenna tilt angle required to maintain beam correction.

clusters for the LOS and NLOS UMi SC environments, respectively. The unrealistically large cluster number chosen by the 3GPP model can over-predict the diversity of mmWave directional channels [94].

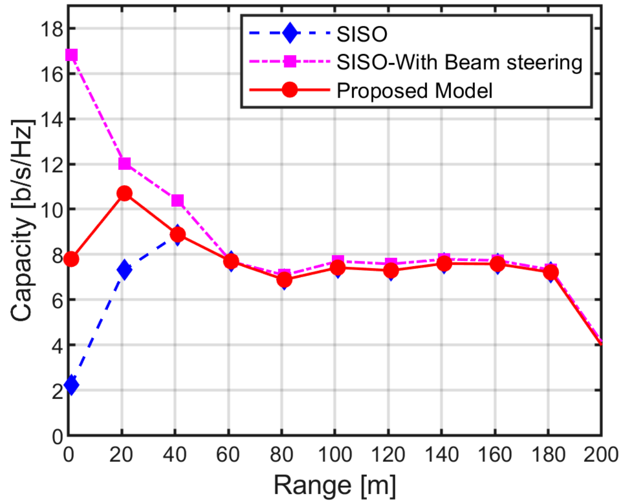

Figure 5.13 Capacity analysis of access channel for SISO and proposed model devoid of dynamic beam steering.

5.2.6 ANALYSIS OF SIMPLIFIED GEOMETRY DEVOID OF BEAM STEERING

In this section, we provide the simulated results for the suggested SC geometry without beam steering. Towards this, the tilt angles required to orient the beam in the direction of each other are calculated in Figure 5.12 for two different cases: with the proposed height of 7m and with the traditional BS height of 20m. As shown, an antenna tilt is primarily required in the UE serving area closer to the BS for mmWave channels with small cell size and low height antennas employed on lamp posts or like structures. Hence, the proposed geometry considers two separate antenna elements, i.e., a beam tilted by 15° with respect to the horizontal in addition to the antenna beam oriented along the boresight to provide a uniform signal strength at any UE location within the cell area of radius 200m. In Figure 5.13, we assess the capacity for an access channel that inherently requires beam steering and compare it with the capacity of the proposed model wherein the beams are oriented in two fixed directions. Though the proposed model geometry fails to acquire the peak data rates offered by a steerable antenna at low link ranges, it yields a moderately uniform capacity over the entire range for an unobstructed LOS channel.

5.2.7 ANALYSIS OF SPATIAL DIVERSITY

From the SISO MiDDCM simulation results presented earlier, the mmWave sparse directional channels were observed to have large signal fluctuations relative to FSPL and moreover, their distributions largely changed even for small variations in the deployment geometry in terms of antenna height, position along the street, or distance from the reflecting walls. Establishing spatial diversity by introducing multiple antennas with an antenna separation d_{sep} mitigates the issue to an extent. In this section, we assess the channel performance for a vertical diversity of 2x2 MIMO with uniform spacing between the antenna elements. To this end, in Figure 5.14, we present the received power at d = 200m for a MISO system (refer to Figure 3.10) with spatial matched filtering by considering d_{sep} ranging from 1 - 400mm. The strength of the received signal at $\lambda/2$ (2.5mm) is simulated as -66.8dBm, whereas the free space value is -60.64dBm. However, at 5λ and 15λ we obtained the best value of -53.24dBm, implying the need to provide a minimum separation of 5 or 15 times λ to obtain a better received signal. This trend was observed for various antenna height settings. Hence, we choose $d_{sep} = 5\lambda$ in all further analyses. As observed in the graph, received signal strength evaluated even at λ spacing is below the free space value. However, the value obtained in our previous work [103] was above the free space condition at λ and with different signal strength characteristics as we had considered the approximate phase differences between the two ground reflected paths stated in (3.35) in the analysis. The study also showed that the minimum antenna separation requirement reduced with increasing mmWave frequencies, reinforcing the theory of using an antenna separation of $\lambda/2$ for lower frequencies and multiples of λ for mmWave bands. The analysis can be refined if the channel model is approximated using higher ray tracing techniques in place of considering only direct and ground reflected rays as in this case.

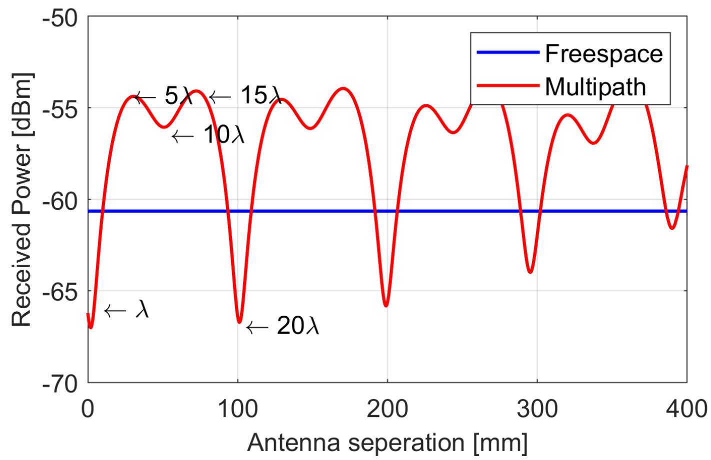

(a)

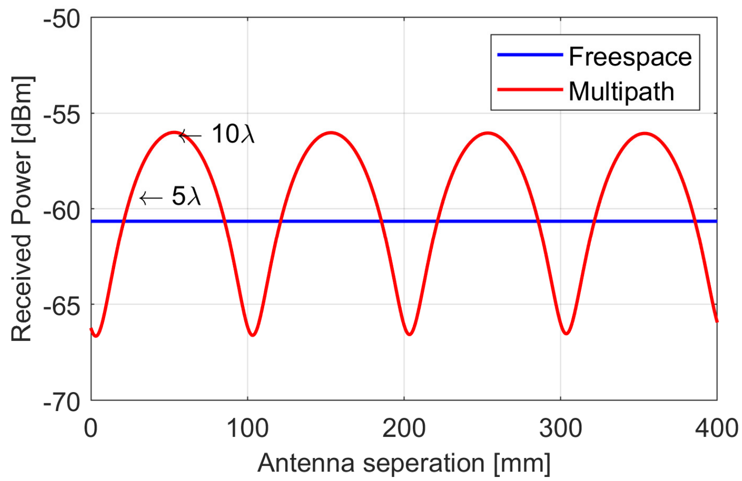

(b)

Figure 5.14 Signal variations introduced with spatial diversity for antenna separation varying up to 400mm with $h_t = h_r = 5$m. (a) at RX1 due to TX1 and TX2 (b) at RX2 due to TX1 and TX2.

Next in Figure 5.15, the variation in CDF on varying the link distance is compared for the SISO channel (both two ray and MiDDCM formulation) and multiple channel geometry with transmit diversity by keeping other parameters fixed. Note that the link range is varied between 30m and 200m as the link below 30m is non faded due to directionality. MISO demonstrates a higher signal power as expected, with a reduced fading probability of fading. The signal strength is always above the receiver

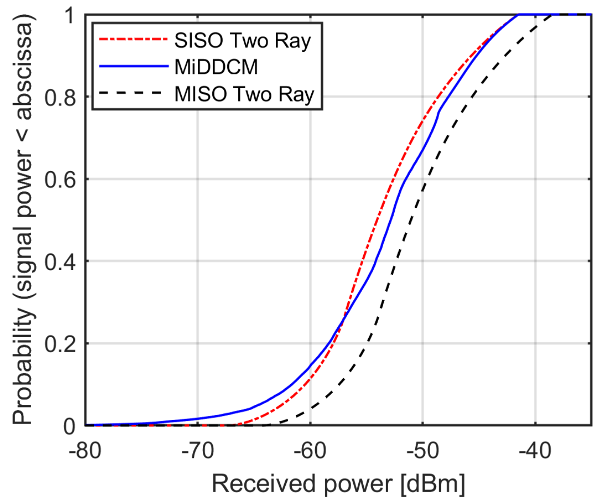

Figure 5.15 Comparison of received power for SISO and MISO mmWave link with h_t = h_r = 7m.

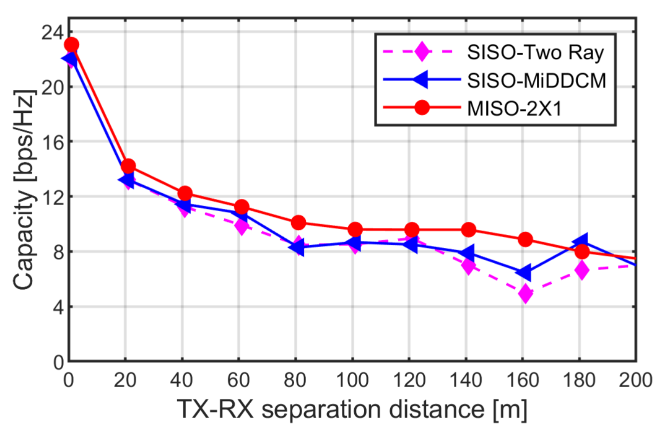

Figure 5.16 Capacity analysis for backhaul channel using SISO two ray, SISO MiDDCM, and multi antenna transmit diversity models.

sensitivity of -66dBm. Figure 5.16 provides the capacity analysis performed for the entire link range for the SISO and MISO systems. As illustrated, two ray and MiDDCM graphs are different for higher link ranges, where the higher order reflections start contributing to the received signal strength. Figure 5.17 illustrates the channel capacity as we vary antenna heights for the backhaul link, i.e., h_t = h_r = [5m,10m]. As observed, MIMO maximizes the channel capacity and exhibits reduced variations compared to MISO.

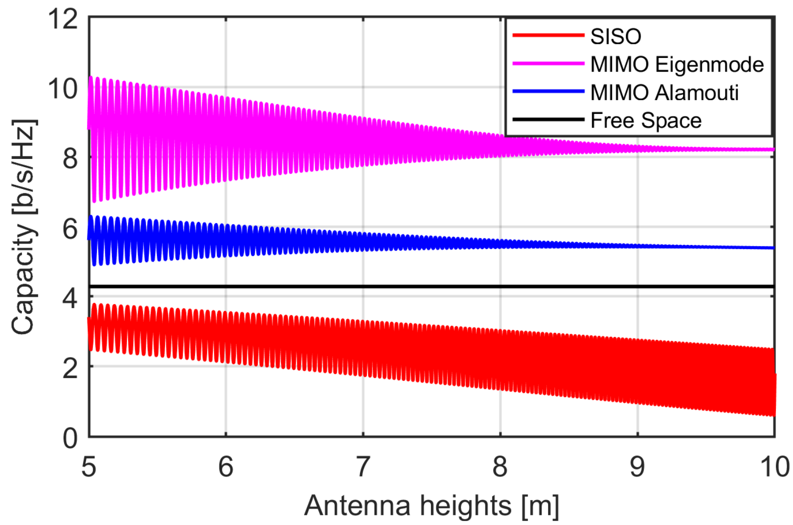

Figure 5.17 Channel capacity variations with the antenna height for the backhaul channel.

The eigenvalues of the backhaul MIMO are such that one of the singular values is extremely small. Hence, dominant eigenmode transmission schemes using only the largest singular value yield identical capacity as water filling that accumulates the channel capacity. However, for access link water filling yielded higher capacity values.

5.2.8 IMPACT OF CROSSROADS IN UMI SC

This section characterizes PG3 representing "System II" SC deployment wherein discontinuities in sidewalls are introduced in the form of crossroads. To investigate the effect of street-grid layout on the directional propagation characteristics of mmWaves, we assume three arbitrary locations for the crossroads, two along the street side of the near reflecting wall and one along the far reflecting wall side. That is, we assume d_{cTE} as d_{121} = 35m and d_{122} = 42m for the first crossroad, d_{221} = 80m and d_{222} = 92m for the second crossroad along the canyon side that is closer to the near reflecting wall while d_{111} = 60m and d_{112} = 67m for the crossroad along the other side of the canyon. The directional mmWave received power evaluated in discrete steps of d for the PG1 and PG3 deployment with TX positioned on the lamppost is depicted in Figure 5.18 for both backhaul and access cases. "System I"

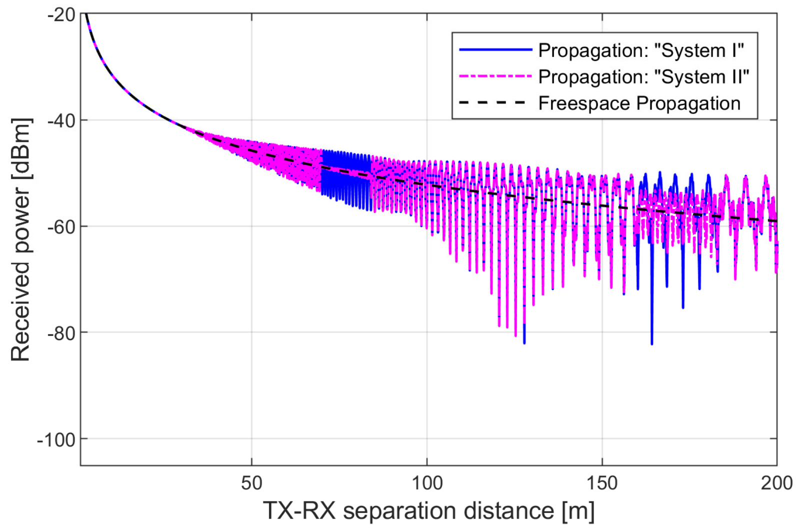

(a)

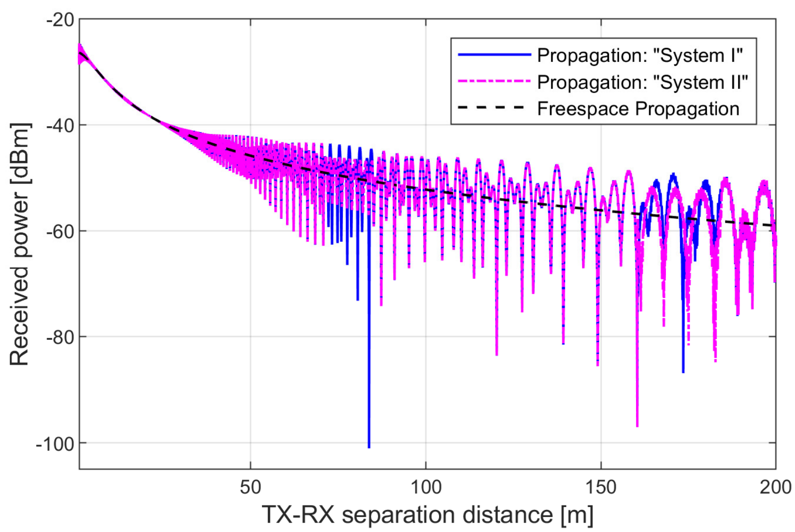

(b)

Figure 5.18 Received power evaluated for PG1 and PG3 scenarios for (a) backhaul with equal TX/RX heights and (b) access with different TX/RX heights.

with continuous sidewalls creates a larger number of reflected MPCs, eventually leading to increased fading. However, "System II" deployment leads to reduced fluctuations of the received power from its free space value because of the absence of reflecting walls in the crossroads positions. Intuitively, the lack of a reflecting wall prevents a transmitted signal from getting reflected to the RX, leading to fewer contributing multipaths in the channel and lesser fading. The variations appear less prominent at higher d values due to the larger number of participating reflections at

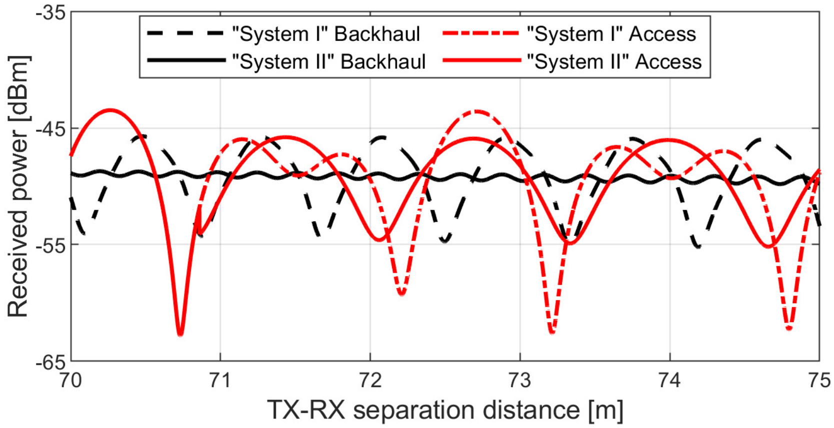

Figure 5.19 Path loss evaluated using MiDDCM at 28 GHz and 60 GHz for LOS UMi SC Scenario.

these values. In drawing these results, we considered LOS transmission with beam steering through beam tilting in both azimuth and elevation planes. Hence from the choice of deployment parameters as d_{t_w} = 16m, d_{r_w} = 4m, the reduced faded region bound can be obtained by multiplying the bound of crossroads with $d_{r\_w}/\big((d_s - d_{t\_w})/2\big) = 4/(20-16)/2) = 2$, as stated in (3.25). As illustrated in Figure 5.18, the received power of "System I" and "System II" varies at distances two times that of the crossroad distance bound at 70-84m, 120-134m, and 160-184m. Figure 5.19 provides an enlarged result graph illustrating the signal strength variations in the link range 70-75m for improved precision.

Further, the CDF of received power for "System I" and "System II" are compared in Figure 5.20, (a) for backhaul, and (b) for access channels. We vary the link range for LOS over a 1-60m range and NLOS over 61-200m, as stated in standard references [26], [36]. The variations are observed to be less significant in channels having a strong LOS path. Note that they perfectly align in the graph as the LOS range for MiDDCM is [1m,60m] while signal variations between the two systems are introduced beyond 60m (at 70m) for the choice of d_{cTE}. The NLOS scenario obviously illustrates larger fluctuations in the received power. Moreover, the signal fluctuations introduced by the crossroads are observed more in backhaul channels than in the access.

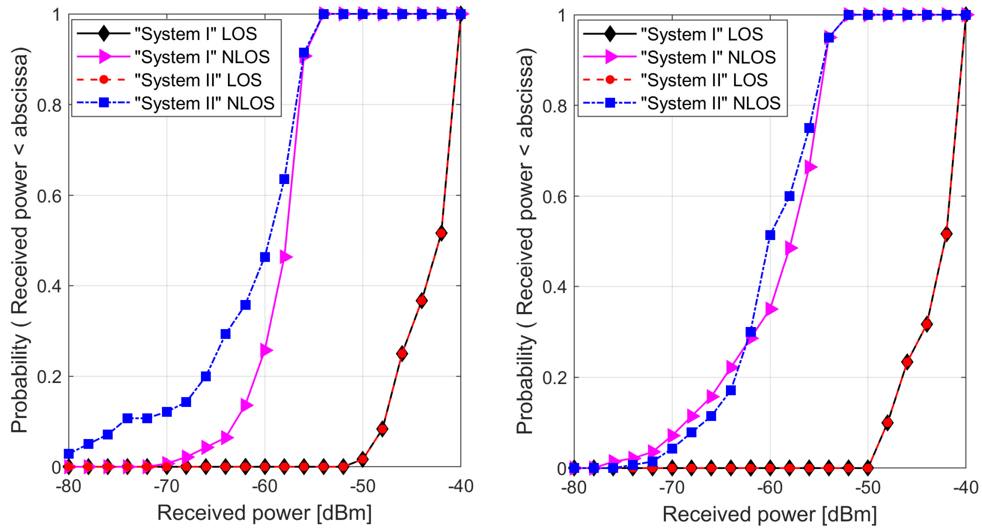

Figure 5.20 Received power CDF for "System I" and "System II" for both (a) backhaul channel and (b) access channel.

In Figure 5.21, we compare the LOS and NLOS path loss with beam steering for PG3 for the entire layout. The region with reduced channel fluctuations due to crossroads is found in both LOS and NLOS scenarios. However, this region is very clearly visible in the NLOS case due to the absence of the strong LOS path (refer to Figure 5.21 (b) and (c)). To analyse the effect of beam steering and to validate the analytical formulations proposed in (3.24) and (3.25), we consider beam steered NLOS transmission for two cases; (i) Case 1, i.e., NLOS with TX antenna steered in the 2D plane to provide elevation angle correction depicted in Figure 5.21 (b) and (ii) Case 2, i.e., NLOS with TX antenna steered in the 3D plane for both elevation and azimuthal angle correction (i.e., $\Delta\theta$ and $\Delta\phi$) depicted in Figure 5.21 (c). The NLOS path loss results demarcate two distinct regions with reduced signal fluctuations that illustrate the receiver locations with increased fading due to discontinuities on the near reflecting wall. Simulations show good agreement with the analytical formulations in (3.24) and (3.25).

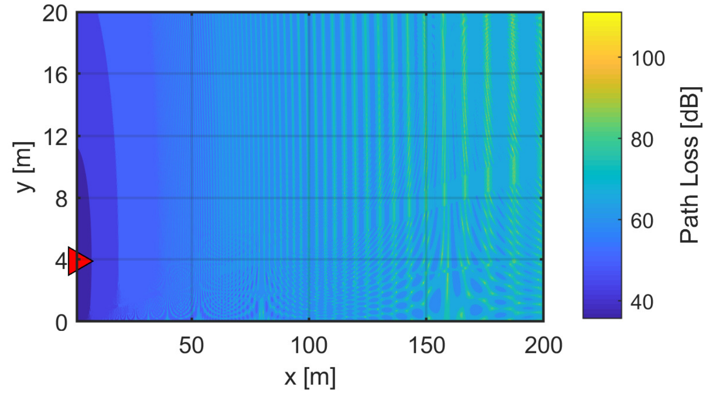

(a)

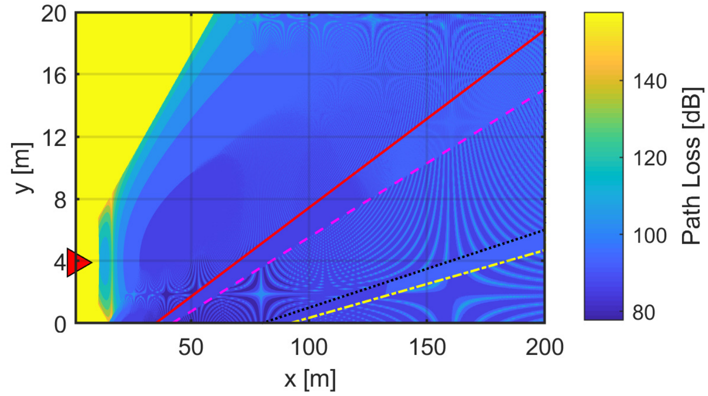

(b)

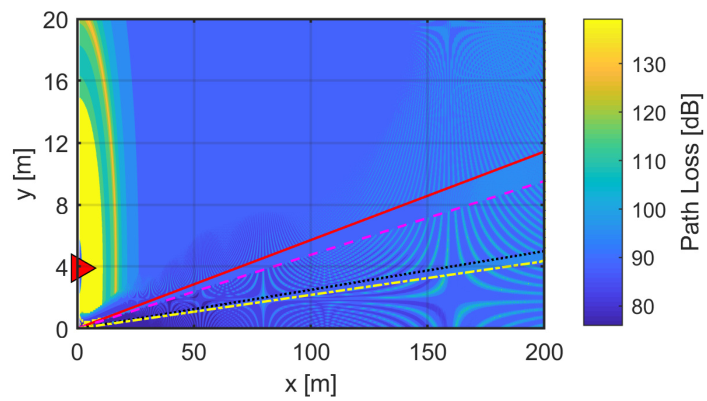

(c)

Figure 5.21 MiDDCM path loss for street-grid layout (a) LOS (b) NLOS with elevation angle correction (c) NLOS with elevation and azimuth angle correction.

5.3 STATISTICAL ANALYSIS OF DIRECTIONAL DETERMINISTIC PATH LOSS DATA

This section provides the significant results of statistical analysis performed on MiDDCM to understand the implications of antenna directionality on mmWave statistical model formulation.

5.3.1 ESTIMATION OF STATISTICAL PARAMETERS

In this section, we make use of the mmWave channel characteristics developed using MiDDCM to evaluate the statistics of the path loss distribution. In specific, we calculate the path loss slope and the path loss fluctuations relative to the free space benchmark which are analogous to the PLE and the fading factor, respectively, present in the standard power-law path loss closed-form expression. To this end, the statistical model parameter $\sigma_{\text{stat,dB}}$ of the proposed model for various input settings are obtained using the MLE technique, i.e., MLE [path loss fluctuations relative to free space benchmark] = MLE $\left[-F_d^{\text{det}}\right]$. Moreover, their path loss exponents n^{stat} are calculated through the MMSE fit on all of the deterministic path loss data, by computing $J(n) = \sum_{k=1}^{M}[{PL_d}^{\text{det}}(k) - {PL_d}^{\text{stat}}(k)]^2$ for M receiver locations and further solving for the mean squared error. Alternatively, n^{stat} and $\sigma_{\text{stat,dB}}$ can be evaluated as; $n^{\text{stat}} = \sum(A.B)/\sum B^2$ and $\sigma_{\text{stat,dB}} = \sqrt{[\sum(A - n^{\text{stat}}B)^2]/M}$, where $A = ({PL_d}^{\text{det}} - {FSPL_{d_0}}^{\text{stat}})$ and $B = 10\log_{10}\left(\frac{d}{d_0}\right)$. Accordingly, we next provide the resulting graph for 60GHz mmWave analysis of ${PL_d}^{\text{det}}$[dB] as a function of d and the relevant statistical parametrization. Note that we analyse a non-obstructed backhaul link up to 200m similar to Figure 5.8 along with the access link NLOS analysis for [61m,200m] range, both without any foliage. As observed, the absence of foliage in the current study eliminates the additional loss of 21.6dB, attributing to the reduced path loss compared to earlier analysis. Hence, $FSPL_{d_0}$ = 25.15dB instead of the 46.75dB path loss value at d_0 = 1m in Figure 5.8. As likely, Figure 5.22 shows that the estimated value of n^{stat} for NLOS is large compared to LOS and its value further increases as the TX to RX antenna height difference increases. The NLOS n^{stat} for access link with h_t = 7m increases from 2.26 to 3.29 when foliage is accounted.

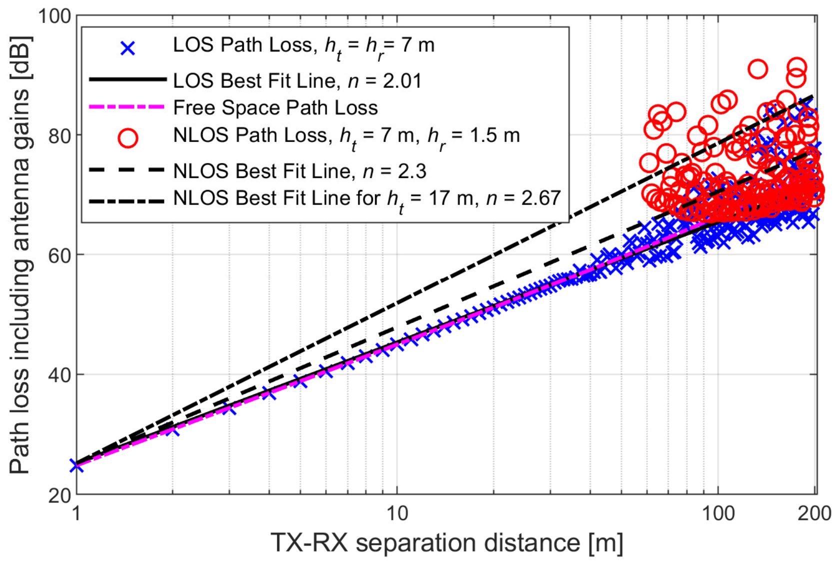

Figure 5.22 Path loss evaluated using MiDDCM at 60 GHz for LOS and NLOS UMi SC outdoor scenario.

The deterministic directional fading gain $F_d^{\mathrm{det}} = |h^r|^2$ that characterizes the fading phenomenon due to all resolvable specular reflections falling within the directional antenna beam area is further analysed for various input settings. Figure 5.23 shows the CDF of F_d^{det} for the entire range of the chosen input parameter, keeping the other parameters fixed. For instance, while simulating for varying d, the other parameters are set as $HPBW_E = 13^\circ$, $HPBW_A = 15^\circ$, $h_t = 7$m and $h_r = 1.5$m. Likewise, we considered the gains at 50m LOS and at 200m NLOS keeping a fixed h_t, $HPBW_A$, and $HPBW_E$ for the h_r varying instance. The results show that LOS directional transmission up to 60m is minimally impacted by variations in the UE locations and heights for all mmWave frequencies due to a strong LOS path and very few reflected paths interfering with them. However, this is not true for NLOS. As observed, almost 35% of the fading gains are above -1dB for 60- and 73GHz. However, the fading gain at 60GHz shows improved performance for their lower values due to the heavily attenuated higher order reflections. Regardless of the chosen ϕ_{HPBW}, F_d^{det} is always greater than 1dB at 60GHz compared to its distribution in the range of -5 to -1dB for 73GHz. Hence, we understand that the fading gains for various mmWave frequencies add differently to the total path loss besides the known increase of FSPL with frequency. This shows that the directional path loss varies as a function of channel

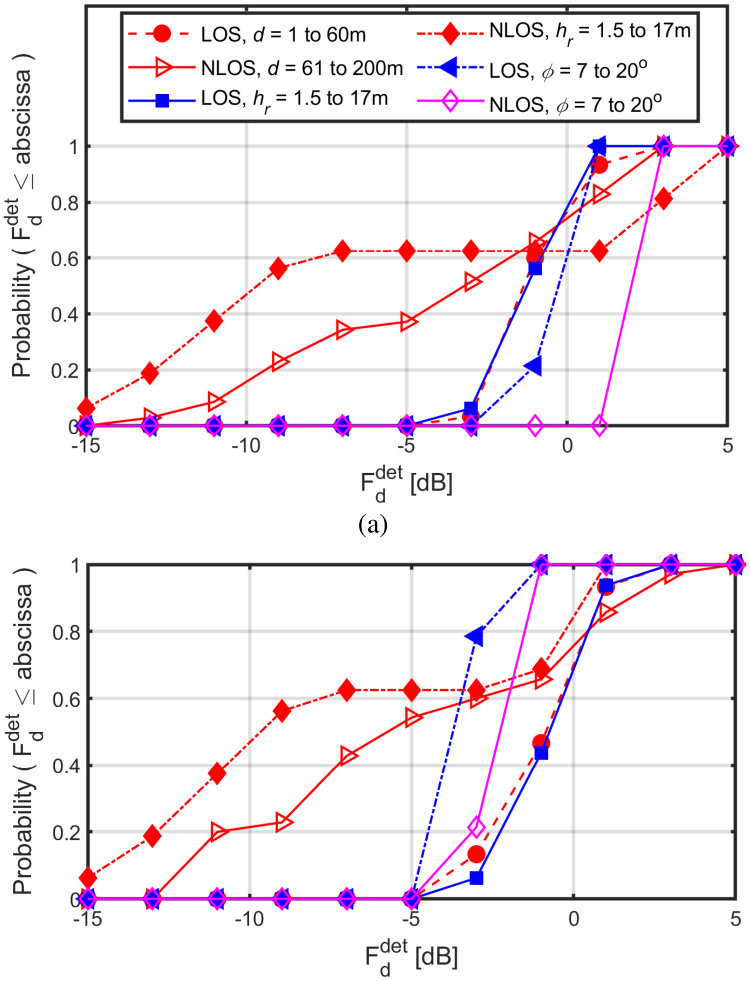

Figure 5.23 CDFs of directional fading gain of MiDDCM for various UE locations and heights as well as antenna beamwidths for (a) 60GHz and (b) 73GHz.

parameters even beyond their influence captured at d_0 as reported in CI and ABG models.

Table 5.6 outlines n^{stat} and $\sigma_{\text{stat,dB}}$ obtained from the statistical analysis of MiDDCM for different mmWave frequencies. The results indicate that though different mmWave frequencies have distinct path loss values, their path loss relative to FSPL is almost identical for a given input specification with fixed antenna settings, like $HPBW_E = 13^{\circ}$, $HPBW_A = 15^{\circ}$. The backhaul analysis assumes a clear LOS path and the simulation parameters as h_t = h_r = 7m, d_{t_w} = 16m and d_{r_w} = 4m. For the access analysis with h_r modified as 1.5m, we have considered two distinct propagation

Table 5.6 PLE and fading gain variance of MiDDCM for varying frequencies in directional mmWave UMi SC LOS and NLOS transmission.

***Freq.* (GHz)**	**Backhaul LOS $1\text{m} \leq d \leq 200\text{m}$**		**Access LOS $1\text{m} \leq d \leq 60\text{m}$**		**Access NLOS $61\text{m} \leq d \leq 200\text{m}$**	
	n^{stat}	$\sigma_{\text{stat,dB}}$	n^{stat}	$\sigma_{\text{stat,dB}}$	n^{stat}	$\sigma_{\text{stat,dB}}$
30	1.98	3.81	2.03	1.49	2.19	6.00
60	2.08	3.98	2.07	1.47	2.29	6.29
90	1.99	4.03	2.03	1.49	2.19	6.02
120	1.99	4.00	2.03	1.49	2.20	6.03

environments, LOS (PS1) and NLOS (PS2). Next, we tabulate in Table 5.7, the statistical parameters ($\mu_{\text{stat,dB}}, \sigma_{\text{stat,dB}}$) of the path loss difference distribution at all distances by using MLE for a 60GHz unobstructed link with no foliage. We provide the values for different antenna directivity with backhaul and access conditions for distinct antenna heights. Clearly, the mean value is not always zero. A positive value implies that the path loss values are larger than the FSPL for most of the RX locations due to the stronger specular reflections destructively interfering with the LOS path. The $\mu_{\text{stat,dB}}$ values typically improved for wider antennas as well as for other mmWave frequencies. Evidently, $\sigma_{\text{stat,dB}}$ increases with wider antennas owing to the rise in the number of specular reflections participating in signal transmission. Their values also agree with the standard deviation of the fading factor proposed in [27] for the UMi SC LOS scenario. Figure 5.24 shows a sample probability distribution best fitting the path loss difference for the backhaul condition in the table ($h_t = h_r = 7$m, $d_{r_w} = 4$m).

Table 5.7 Statistical parameters of backhaul and access directional path loss distribution.

Backhaul (h_t = 7m, h_r = 7m) d_{r_w} = 4m			
$\theta_{HPBW}{}^{\circ}$	$\phi_{HP}{}^{\circ}$	$\mu_{\text{stat,dB}}$	$\sigma_{\text{stat,dB}}$
13	15	-0.21	3.98
7	9	0.01	3.23
20	30	-0.82	4.56

Backhaul (h_t = 7m, h_r = 7m) d_{r_w} = 16m			
$\theta_{HPBW}{}^{\circ}$	$\phi_{HPBW}{}^{\circ}$	$\mu_{\text{stat,dB}}$	$\sigma_{\text{stat,dB}}$
13	15	0	2.2
7	9	0	0.6
20	30	-0.61	3.78

Access (h_t = 7m, h_r = 1.5m) d_{r_w} = 4m			
$\theta_{HPBW}{}^{\circ}$	$\phi_{HPBW}{}^{\circ}$	$\mu_{\text{stat,dB}}$	$\sigma_{\text{stat,dB}}$
13	15	-0.61	4.31
7	9	-0.32	3.99
20	30	-1.13	4.79

Access (h_t = 7m, h_r = 1.5m) d_{r_w} = 16m			
$\theta_{HPBW}{}^{\circ}$	$\phi_{HPBW}{}^{\circ}$	$\mu_{\text{stat,dB}}$	$\sigma_{\text{stat,dB}}$
13	15	-0.08	3.7
7	9	0.03	3.43
20	30	-0.82	4.25

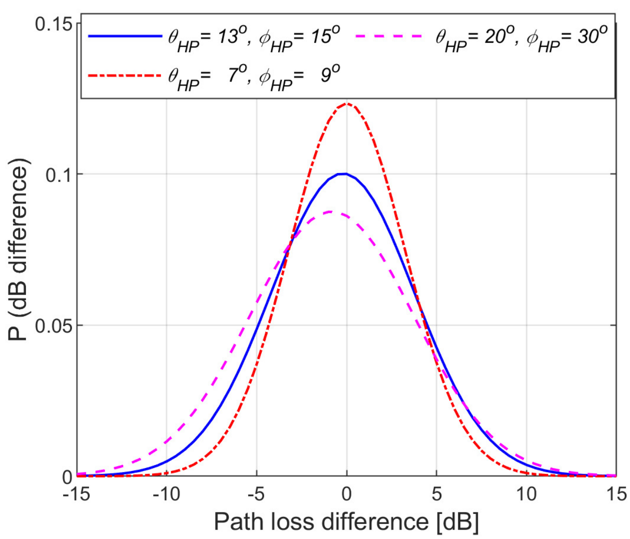

Figure 5.24 PDF of directional path loss difference with varying antenna beamwidths for backhaul channel with h_t = 7m, h_r = 7m and d_{r_w} = 4m.

Table 5.8 Statistical parameters of MiDDCM and other UMi SC outdoor path loss models.

Item	***Freq.* (GHz)**	**h_t (m)**	**h_r (m)**	***HPBW* (^{0})**	**Gain (dBi)**	**Env. Range (m)**	**Model Parameters**
Measureme-nt [26]	28	7/17	1.5	10.9	24.5	LOS $31 \le d \le 102$	$n^{\mathrm{CI}} = 1.9$, $SF^{\mathrm{CI}} = 1.1$dB
						NLOS $61 \le d \le 162$	$n^{\mathrm{CI}} = 4.5$, $SF^{\mathrm{CI}} = 10$dB
	73	17	2	7	27	LOS $48 \le d \le 54$	$n^{\mathrm{CI}} = 2.2$, $SF^{\mathrm{CI}} = 5.2$dB
						NLOS $59 \le d \le 181$	$n^{\mathrm{CI}} = 4.7$, $SF^{\mathrm{CI}} = 12.6$dB
3GPP [126]	6-100	10	1.5-22.5	Omni	1	LOS $10 \le d \le 5000$	$n^{\mathrm{CI}} = 2.1$, $SF^{\mathrm{CI}} = 4$dB
						NLOS $10 \le d \le 5000$	$n^{\mathrm{CI}} = 3.19$, $SF^{\mathrm{CI}} = 8.2$dB
MiWeba [64]	60	6.2	1.5	V = 14 H = 18	19.8	NLOS $25 \le d \le 50$	$\alpha^{\mathrm{ABG}} = 82.02$dB, $\beta^{\mathrm{ABG}} = 2.36$
This Work	28	7	7	V = 13 H = 15	21.6	LOS $1 \le d \le 30$	$n^{\mathrm{stat}} = 2.0$, $\sigma_{\mathrm{stat,dB}} = 0$dB
						LOS $31 \le d \le 60$	$n^{\mathrm{stat}} = 1.98$, $\sigma_{\mathrm{stat,dB}} = 1.2$dB
						NLOS $61 \le d \le 200$	$n^{\mathrm{stat}} = 2.15$, $\sigma_{\mathrm{stat,dB}} = 3.42$dB
	28	7	1.5	V = 13 H = 15	21.6	LOS $1 \le d \le 30$	$n^{\mathrm{stat}} = 2.0$, $\sigma_{\mathrm{stat,dB}} = 0$dB
						LOS $31 \le d \le 60$	$n^{\mathrm{stat}} = 2.0$, $\sigma_{\mathrm{stat,dB}} = 2.13$dB
						NLOS $61 \le d \le 200$	$n^{\mathrm{stat}} = 2.2$, $\sigma_{\mathrm{stat,dB}} = 6.05$dB

5.3.2 VERIFICATION AGAINST STANDARD PATH LOSS MODELS

In this section, we verify the n^{stat} and $\sigma_{\mathrm{stat,dB}}$ values of MiDDCM with the parameters predicted by other popular outdoor path loss models [64], [126], and measurement studies [26], for the input specifications, stated in the literature. The findings are provided in Table 5.9. Note that the backhaul parameters reported in [26] at 73GHz are almost identical to access and hence omitted. The path loss generated by MiDDCM is discretely analysed for three definite ranges and is fitted with an MMSE best fit n^{stat} separately for each window. Likewise, $\sigma_{\text{stat,dB}}$ values are also evaluated. The channel up to 30.7 m is non-fading, attributing to a slope of 2 and a zero variance. The n^{stat} values reduced on reducing the antenna HPBWs showing a path loss improvement. Also, it increased while including the gain factor in the path loss slope, as required in the directional channel analysis. Especially in the NLOS case, wherein the antenna gains $G_t(\phi,\theta)$ and $G_r(\phi,\theta)$ are different from their boresight values when the antenna major beams are misaligned. For example, a 7° HPBW has a boresight gain of 27dBi, yet it drops to 23dBi for a direct ray if the beams are not aligned. The major findings are presented here as well as in [121]. The NLOS PLE increased with frequency as the waves with shorter lengths are largely attenuated on reflection from the ground and side walls. This is also true for highly attenuated 60GHz transmissions. In general, all the model parameters are observed to increase with frequency. Also, the path loss variations in dB/decade of distance decreased with increasing beamwidths implying that the omnidirectional PLEs will be smaller than the directional PLEs. Moreover, increasing the TX height (in access links) or positioning the TX and RX on different sides of the street (in general) increased the model parameter. The existing path loss models however do not capture the channel dependence on antenna heights and gains.

Finally, the mmWave outdoor downlink is budgeted in Table 5.9 and compared with standard path loss models simulated using model parameters placed identical to the literature. The LOS path loss generated by MiDDCM is similar to the measurements, thus validating the model. The NLOS SNRs obtained from the measurement, and 3GPP models are extremely low. Hence, an increase in transmit power or a decrease in coverage distance or the channel bandwidth may be required for successful signal reception. We observe that NLOS path loss evaluated using MiDDCM is lower than that of the other models attributing to the fact that MiDDCM models fewer interfering multipaths owing to channel directionality. The lower path loss values are also due to the dependency of fading gain on antenna beamwidths. In general, the path loss values evaluated for NLOS are larger than the LOS, either value being higher for higher frequencies, well agreeing with the theoretical intuition. Note that the path loss

Table 5.9 UMi SC link budget analysis using different mmWave outdoor path loss models.

Link Budget	Measurement [26]				3GPP Model [126]		MiWeba [64]		This Work			
***Freq.* (GHz)**	28		73		28		60		28		73	
***BW* (MHz)**	800		800		100		250		800		800	
P_t (dBm)	30.1		14.6		35		15		30.1		14.6	
G_t (dBi)	24.5		27		1		15		24.5		27	
***EIRP* (dBm)**	54.6		41.6		36		30		54.6		41.6	
Env.	LOS	NLOS	LOS	NLOS	LOS	NLOS	LOS	NLOS	LOS	NLOS	LOS	NLOS
***d* (m)**	50	200	50	200	50	200	50	200	50	200	50	200
***PL* (dB)**	94.2	170.3	108.2	170	99.2	139.2	108.3	122.5	95	126	104.1	144.4
P_r (dBm)	-39.6	-115.7	-66.6	-128.4	-63.2	-103.2	-78.3	-92.5	-40.4	-71.4	-62.5	-102.8
G_r (dBi)	24.5		27		1		15		24.5		27	
P_r (dBm)	-15.1	-91.2	-39.6	-101.4	-62.2	-102.2	-63.3	-77.5	-15.9	-46.9	-35.5	-75.8
Noise (dBm)	-85		-85		-94		-90		-85		-85	
***F* (dB)**	7		7		9		10		7		7	
P_n (dBm)	-78		-78		-85		-80		-78		-78	
SNR (dB)	62.8	-13.2	38.4	-23.5	22.8	-17.2	16.7	2.5	62.1	31.1	42.5	2.2

values in Table 5.9, similar to Table 5.1, are evaluated by excluding the antenna gain terms from the path loss expression. This is to bring in similarity with the modeling strategy of including the antenna gain factors in the link budget followed by standard path loss models.

5.3.3 ANALYSIS OF TRADITIONAL AND MODIFIED POWER LAW EQUATIONS

This section provides the analysis of path loss evaluated by the MiDDCM formulation and that predicted by the popular CI statistical model which is based on the traditional

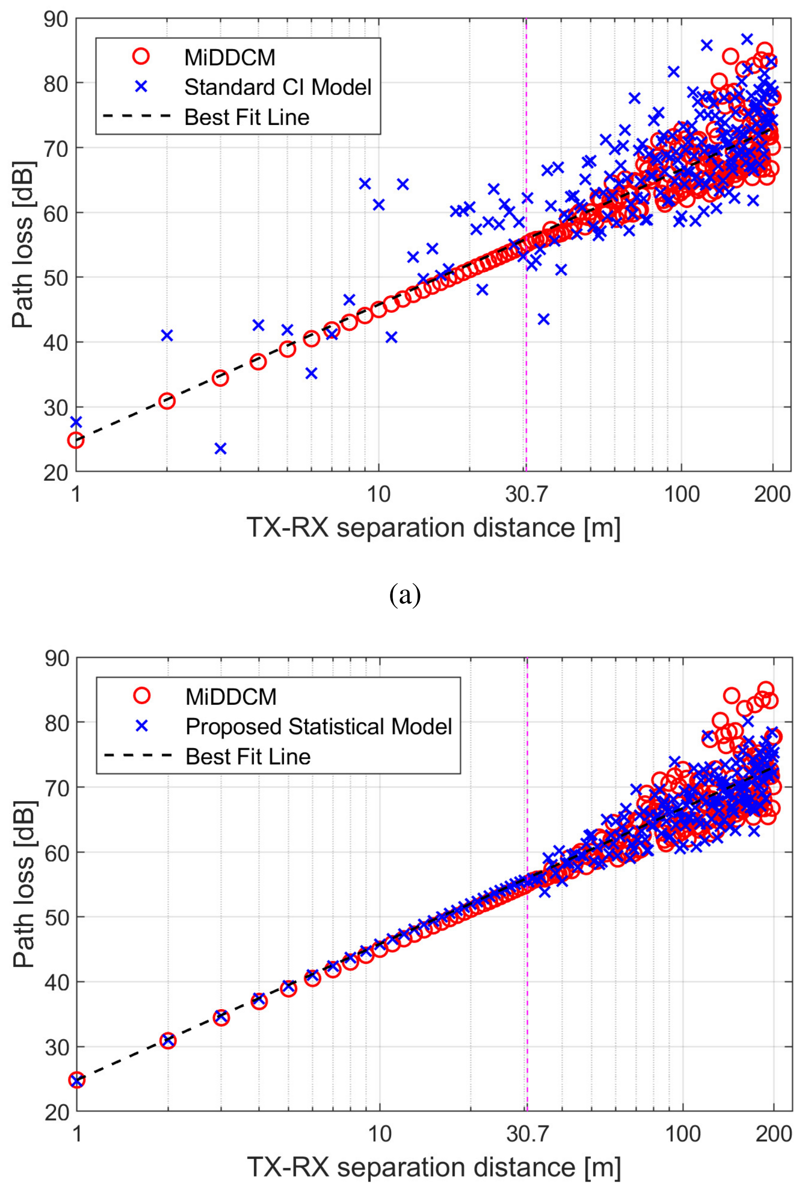

(b)

Figure 5.25 MiDDCM path loss over varying link distance compared with (a) standard statistical CI model and (b) proposed corrected statistical model.

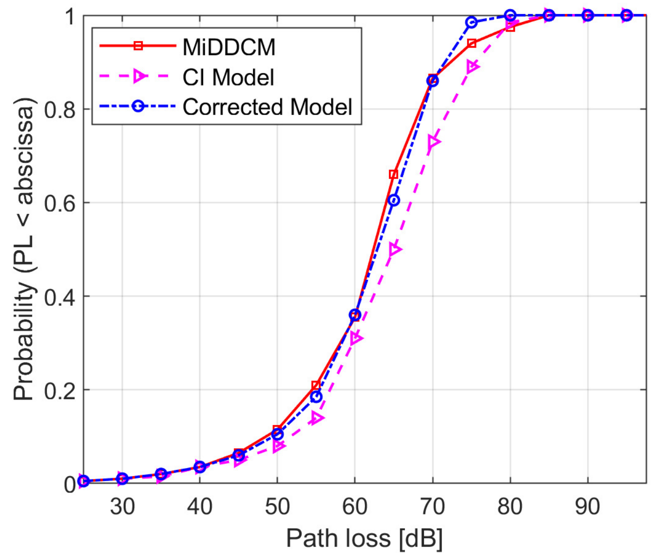

Figure 5.26 CDF of directional path loss compared among MiDDCM, standard CI model, and the proposed corrected statistical model.

power-law path loss equation. Accordingly, we emphasize the relevance of critical distance d_c in directional mmWave propagation as a function of antenna directivity and deployment parameters. Furthermore, the unique propagation characteristics of mmWave directional outdoor SC channel as modelled by MiDDCM (gradually increasing signal fluctuations with distance) is exploited to improve the prediction accuracy of traditional power-law equations. In specific, we highlight the need for a distance-dependent correction factor proposed in (4.14) to convert the uniform standard deviation $\sigma_{\mathrm{stat,dB}}$ to a non-uniform standard deviation $\sigma_{\mathrm{mod,dB}}$.

With this intend, we first compare the deterministic path loss evaluated by MiDDCM using (4.6) with the path loss predicted by the statistical CI model using (4.1) at every 1m TX-RX separation distance in Figure 5.25(a). The CI model parameters $\left(n^{\mathrm{CI}}, \sigma_{\mathrm{CI,dB}}\right)$ were set as (2.2, 5.2dB), whereas the MiDDCM model parameters were estimated as n^{stat} = 2.08 using MMSE and ($\mu_{\mathrm{stat,dB}}, \sigma_{\mathrm{stat,dB}}$) = (-0.11, 3.73dB) using MLE at 95% confidence level with the confidence bounds [-0.64, 0.41] and [3.4, 4.14], respectively. As observed, the dB difference of path loss (i.e., Path loss-FSPL) evaluated by MiDDCM for a directional mmWave channel has a funnel shape where the small distances yield a smaller variance in the path loss values than the large distances. This observation motivates us to modify $\sigma_{\mathrm{stat,dB}}$, a constant for the entire transmission range, by a distance-dependent correction factor. Accordingly, we evaluate $\sigma_{\text{mod,dB}}$ for every d based on (4.15) using the correction factor $\mathcal{C}_{\sigma}$. For the deployment parameters of $h_t = h_r = 7$m, $d_s = 20$m, $d_{t_w} = 16$m, $d_{r_w} = 4$m, $\theta_{HPBW} = 13°$, $\phi_{HPBW} = 15°$ chosen in this simulation, we obtained the critical distance as $d_c = \min(61.7, 30.7) = 30.7$. Accordingly, in Figure 5.25(b), we compare the MiDDCM path loss with the path loss predicted using the proposed modified statistical closed-form expression specified in (4.16). Note that the modified model with the corrected non-uniform standard deviation indicates a better consistency with the expected directional characteristics evaluated by the ray tracer. To quantify the results, we calculate the root mean square error (RMSE) between the deterministic MiDDCM path loss and those predicted by the standard CI model for every simulated observation as $e_{\text{CI}} = \sqrt{\frac{1}{O}\sum_k \left(PL_d{}^{\text{det}}(k) - PL_d{}^{\text{CI}}(k)\right)^2}$. Similarly, the RMSE between the deterministic MiDDCM path loss and those predicted by the corrected statistical model $e_{\text{mod}} = \sqrt{\frac{1}{O}\sum_k \left(PL_d{}^{\text{det}}(k) - PL_{d,\text{mod}}{}^{\text{stat}}(k)\right)^2}$. From the results yielded, $e_{\text{CI}} = 7.38$dB and $e_{\text{mod}} = 4.93$dB, it is found that the corrected model best fits the MiDDCM formulation in characterizing directional mmWave outdoor SC channels.

5.4 DEPLOYMENT GEOMETRY OPTIMIZATION

Summarizing the channel analysis using MiDDCM, we establish that the deterministic channel characteristics of directional mmWave SC outdoor layout are a strict function of the operating frequency, antenna directionality, SC geometry parameters h_t, h_r, d, d_s, d_{t_w}, d_{r_w}, and the transmission condition (LOS/NLOS). A small variation in these parameters creates significant fluctuations in the mmWave channel path loss due to a few strong contributing multipaths constituting the channel. Moreover, the extremely short wavelength of mmWaves causes even small spatial variations on the order of a few centimetres to create significant path loss variations. The path loss variations are illustrated in Figure 5.27, which plots the CDFs of the backhaul LOS path loss for $d = 200$m and $h_r = 7$m with d_{r_w} varying over the interval [0m, 20m]. While h_t is fixed either at 7m or at 7.01m, we analyse the path loss for two different cases, i.e., TX located at 4m from the near wall ($d_{t_w} = 16$m) and TX located 4m from the far wall ($d_{t_w} = 4$m) to show the path loss variations even with a 1cm drift in the antenna height. This is extremely concerning as the antenna

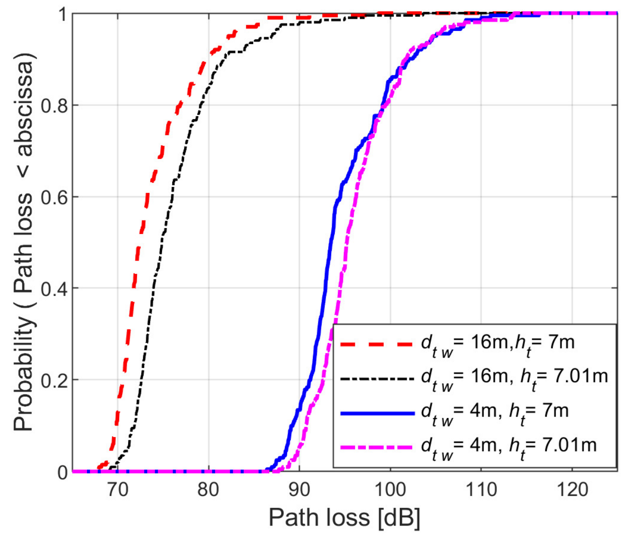

Figure 5.27 CDF of LOS path loss of 60GHz channel at the cell edge, illustrating path loss variations with small changes in TX antenna heights.

heights/positions can inevitably vary across various deployments even if their requirements in a typical network are pre-analysed and designed. Hence, we next apply the MiDDCM path loss results to optimize multiple deployment parameters aiming to minimize the channel path loss by using a metaheuristic PSO algorithm, and the significant results are presented in this section.

5.4.1 SIMULATION AND NUMERICAL RESULTS

In the simulation of the PSO algorithm, we set the acceleration coefficients, c_1 and c_2, to 1 and 1.5, respectively. Also, the inertia weight parameter ω is modelled as $\omega = \omega_{max} - ((\omega_{max} - \omega_{min}) iter/iter_{max})$, where we assume $\omega_{max} = 0.9$ and $\omega_{min} = 0.4$. $iter$ denotes the current iteration number and $iter_{max}$ the maximum iteration number.

The major results of the optimization problem are evaluated for sample input settings and are provided in Table 5.10 and Table 5.11. The findings are based on several trial runs. Table 5.10 tabulates the deployment parameters optimized for the LOS channel for d = 50m. Of the four cases analysed, the first two attempt to optimize the street width d_s and the distance between RX and the near reflecting wall d_{r_w} for a backhaul link with other parameters constant. The TX antenna is arbitrarily assumed at d_{t_w} =

Table 5.10 SC deployment parameters optimized for LOS for d = 50m.

	Cases	Parameter	Range (m)	Optimum Value (m)	Minimum PL (dB)	No: of iterations
1	h_t = 7m h_r = 7m d_{t_w} = 0m	d_s	5 - 20	5.066	53.544	10
		d_{r_w}	0 - d_s	0.034		
2	h_t = 7m h_r = 7m d_{t_w} = 2m	d_s	5 - 20	6.547	51.033	2
		d_{r_w}	0 - d_s	0.207		
3	d_s = 20m h_r = 7m d_{r_w} = 4m	h_t	5 - 17	14.126	55.596	5
		d_{t_w}	0 - 20	0.128		
4	d_s = 20m h_r = 1.5m d_{r_w} = 4m	h_t	5 - 17	6.533	55.725	9
		d_{t_w}	0 - 20	19.386		

0m and 2m. On extending the analysis to access links, the optimization model yielded d_s = 5.0463m, d_{r_w} = 0.0418m with a minimum path loss of 53.052dB for d_{t_w} = 0m, and d_s = 8.606m, d_{r_w} = 0.605m with PL = 51.006dB for d_{t_w} = 2m. In fact, a narrow SC geometry with RX located closer to the building on the near wall side yielded better signal reception for both backhaul and access conditions. The latter two cases considered d_s fixed as 20 m and d_{r_w} = 4m for both backhaul and access cases. The algorithm evaluated a higher antenna height of 14m as the best solution for the backhaul case. However, the optimal geometry for an access link is quite different. It is also observed that the TX and RX need not be geometrically aligned to yield minimum path loss because of the beam steering at both ends of the link.

Table 5.11 presents identical evaluations for NLOS at d = 200m. The results imply that both TX and RX should be aligned to achieve optimal path loss in NLOS without beam steering, unlike the LOS transmission with beam steering. For instance, the model generated optimum path loss when antennas are located on the sidewalk closer to the far wall, as in cases 1 and 2, or closer to the near wall as in cases 3 and 4. As expected, properly aligned TX and RX ensure constructive interference between

Table 5.11 SC deployment parameters optimized for NLOS for d = 200m.

	Cases	Parameter	Range (m)	Optimum Value (m)	Minimum PL (dB)	No: of iterations
1	h_t = 7m h_r = 7m d_{t_w} = 0m	d_s	5 - 20	5.166	81.844	7
		d_{r_w}	0 - d_s	5.018		
2	h_t = 7m h_r = 7m d_{t_w} = 2m	d_s	5 - 20	6.521	82.182	2
		d_{r_w}	0 - d_s	6.03		
3	d_s = 20m h_r = 7m d_{r_w} = 4m	h_t	5 - 17	7.005	85.334	3
		d_{t_w}	0 - 20	20		
4	d_s = 20m h_r = 1.5m d_{r_w} = 4m	h_t	5 - 17	5	85.239	4
		d_{t_w}	0 - 20	19.985		

different reflected paths. Another interesting observation is that a nominal antenna height of 5-7m is adequate to achieve significant signal strength at even a larger range of 200m. We have run the PSO algorithm with a population of 500 particle set and for a maximum iteration of 10. On reducing the population to 50, the algorithm converged to a higher path loss value, even with an increased iteration. Hence, increasing the maximum iteration may not improve the efficiency of the optimization problem, but a higher population can indeed provide a better optimal solution. The convergence characteristic of the best path loss solution of the proposed PSO problem is shown for a sample simulation case of an NLOS link (Case 1) in Figure 5.28.

The optimization model for deployment geometry is a novel contribution. Currently, no results are available for optimizing the deployment geometry by integrating the optimization algorithm with the mmWave directional channel model. Hence, it should be noted that the performance comparison of simulated results with any existing models is not provided at this time.

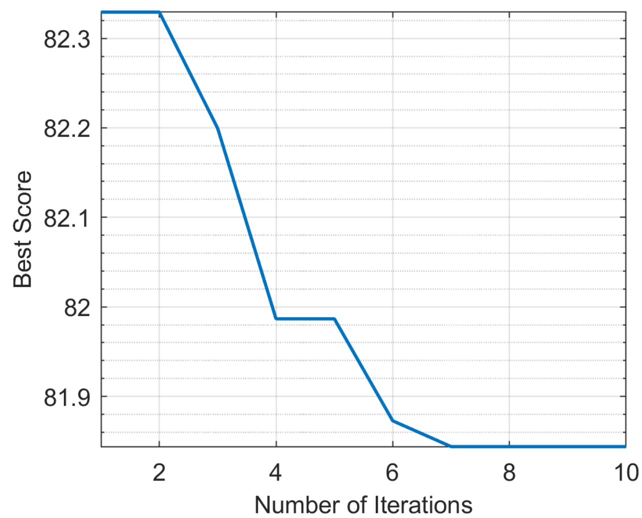

Figure 5.28 Convergence characteristic of the UMi SC deployment geometry NLOS system model for Case 1.

5.5 CHAPTER SUMMARY

In this chapter, we discussed the significant results of the proposed work highlighting several vital insights. Through simulation results, we established the effectiveness of deterministic channel models in modeling the sparse multipath structure of directional mmWave channels. As illustrated, the directional mmWave outdoor channel could be characterized realistically and with improved accuracy using the low complexity proposed model called MiDDCM which integrates antenna gain into the channel IR rather than considering them in the link budget. Several sample observations, including received power, path loss, and capacity performance varying with antenna HPBW, deployment parameters, and frequency, were provided. The model was shown to effectively characterize various transmission scenarios and use cases that cannot be assessed using traditional statistical channel models. The implication of mmWave channel directionality in UMi SC outdoor channels was examined and exploited in multiple ways using the custom ray tracing MiDDCM formulation. The statistical parameters of the directional channel model are estimated, and the link budget is performed. An accurate link budget helps to assess the link quality and thereby aids the optimal choice of modulation and coding scheme to enhance system throughput.

CHAPTER 6. CONCLUSIONS AND FUTURE WORK

6.1 CONCLUSIONS

The extended usage of smartphones and the penetration of new application scenarios to cellular networks have accelerated the research on mmWaves to address the current spectrum crunch. Channel study is a significant research area in the study of mmWaves. The statistical models are elicited from measurement campaigns conducted using channel sounding techniques and define channel model parameters by their statistical moments. However, deterministic models offer physical insights by modeling the interaction of rays with the surrounding environment. As MPCs are generated purely based on the environment geometry, the channel description using ray tracing is highly accurate and well suited for mmWave directional channel characterization.

We have developed a deterministic ray tracing model and have evaluated it as a prediction tool to examine the directional characteristics of an outdoor mmWave channel 3D for the UMi SC scenario. Our MiDDCM framework not only models the directional mmWave channel with reasonably well accuracy but also provides an excellent advantage through its capability to characterize different usage scenarios that are difficult to be modelled using statistical models. Our investigation shows that the directional channel is non-fading up to a critical distance beyond which the signal fluctuations increase as a function of distance. For optimal channel performance in channels with UE/AP positioned misaligned with TX/BS in either horizontal or vertical plane, it is shown that beam steering is desired. The channel validation with standard models and measurements displayed good agreement for LOS, yet the NLOS path loss varied due to the reduced specular reflections analysed by MiDDCM as well as its modeling strategy of including the directional antenna effects in the path loss slope itself. We have examined the power delay profile and delay spread for the channel for varying input specifications. Our investigations on spatial diversity also show that antenna separations of few multiples of mmWave wavelength are required to achieve significant signal strength.

Understanding that a detailed analysis of MPCs might not always be required, particularly in channel analysis which requires understanding the path loss distributions and not their instantaneous values, we devised a statistical approach identical to the standard CI model to define the directional path loss distribution by using curve fitting over the deterministic path loss data set. Through simulation results, we tried to establish the inadequacy of traditional power-law path loss models in capturing directionality. Accordingly, a novel correction expression as a function of model geometry, antenna beamwidth, and separation distance has been established and assessed through simulation. The obtained results using this corrected model indicate a good consistency with the expected directional characteristics evaluated by the ray tracer. Finally, the SC deployment geometry is attempted to optimize in terms of any two deployment parameters to yield minimum path loss and several interesting insights have been presented.

6.2 FUTURE RESEARCH DIRECTIONS

The model provides a good approximation of the UMi SC outdoor channel employing directional transmission, and the validation displays only low discrepancies compared to popular statistical models. However, the model considers only specular reflections and by considering diffraction and scattering effects, the precision can be further improved. The statistical learning of deterministic data is performed in this study for the SISO channel with unobstructed LOS transmission. The study can be further extended to analyse NLOS as well as the multi-antenna case for comprehensive characterization. In this work, we have used the optimization strategy PSO to typically optimize two free parameters. However, it is an interesting problem to consider more free parameters and jointly optimize them to enhance accuracy but with implementation complexity traded off.

REFERENCES

[1] A. Y. Ding and M. Janssen, "Opportunities for applications using 5G networks: Requirements, challenges, and outlook," ACM Int. Conf. Proceeding Ser., pp. 27–34, Oct. 2018, doi: 10.1145/3278161.3278166.

[2] M. Nekovee, "Opportunities and enabling technologies for 5G and beyond-5G spectrum sharing," in Handbook of Cognitive Radio, vol. 3–3, 2019, pp. 1971–1972.

[3] F. Khan, LTE for 4G mobile broadband: Air interface technologies and performance, vol. 9780521882. Cambridge: Cambridge University Press, 2009.

[4] GSMA, G. Intelligence, GSMA, and G. Intelligence, "Understanding 5G: Perspectives on future technological advancements in mobile," GSMA Intell. Underst. 5G, no. December, pp. 3–15, 2014, [Online]. Available: https://gsmaintelligence.com/research/?file=141208-5g.pdf&download.

[5] C. X. Wang et al., "Cellular architecture and key technologies for 5G wireless communication networks," IEEE Commun. Mag., vol. 52, no. 2, pp. 122–130, Feb. 2014, doi: 10.1109/MCOM.2014.6736752.

[6] J. G. Andrews et al., "What will 5G be?," IEEE J. Sel. Areas Commun., vol. 32, no. 6, pp. 1065–1082, 2014, doi: 10.1109/JSAC.2014.2328098.

[7] ITU-R M.2083, "IMT Vision – Framework and overall objectives of the future development of IMT for 2020 and beyond," 2015.

[8] M. Shafi et al., "5G: A tutorial overview of standards, trials, challenges, deployment, and practice," IEEE J. Sel. Areas Commun., vol. 35, no. 6, pp. 1201–1221, 2017, doi: 10.1109/JSAC.2017.2692307.

[9] F. Boccardi, R. Heath, A. Lozano, T. L. Marzetta, and P. Popovski, "Five disruptive technology directions for 5G," IEEE Commun. Mag., vol. 52, no. 2, pp. 74–80, 2014, doi: 10.1109/MCOM.2014.6736746.

[10] Ericcson, "Ericsson Mobility Report," 2020. [Online]. Available:

https://www.ericsson.com/49da93/assets/local/mobility-report/documents/2020/june2020-ericsson-mobility-report.pdf.

[11] Samsung Electronics, "5G Vision," 2015. [Online]. Available: http://www.samsung.com/.

[12] Z. Pi and F. Khan, "An introduction to millimeter-wave mobile broadband systems," IEEE Commun. Mag., vol. 49, no. 6, pp. 101–107, 2011, doi: 10.1109/MCOM.2011.5783993.

[13] T. S. Rappaport et al., "Millimeter wave mobile communications for 5G cellular: It will work!," IEEE Access, vol. 1, pp. 335–349, 2013, doi: 10.1109/ACCESS.2013.2260813.

[14] H. Zhao et al., "28 GHz millimeter wave cellular communication measurements for reflection and penetration loss in and around buildings in New York city," IEEE Int. Conf. Commun., no. Icc, pp. 5163–5167, 2013, doi: 10.1109/ICC.2013.6655403.

[15] J. Karjalainen, M. Nekovee, H. Benn, W. Kim, J. Park, and H. Sungsoo, "Challenges and opportunities of mm-wave communication in 5G networks," Proc. 2014 9th Int. Conf. Cogn. Radio Oriented Wirel. Networks Commun. CROWNCOM 2014, pp. 372–376, 2014, doi: 10.4108/icst.crowncom.2014.255604.

[16] Y. Niu, Y. Li, D. Jin, L. Su, and A. V. Vasilakos, "A survey of millimeter wave communications (mmWave) for 5G: opportunities and challenges," Wirel. Networks, vol. 21, no. 8, pp. 2657–2676, 2015, doi: 10.1007/s11276-015-0942-z.

[17] J. M. Kelif and O. Simon, "Impact of directional receiving antennas on the performance and quality of service of wireless networks," 2014, doi: 10.1109/VTCFall.2014.6966002.

[18] G. R. Maccartney, M. K. Samimi, and T. S. Rappaport, "Exploiting directionality for millimeter-wave wireless system improvement," IEEE Int. Conf. Commun., vol. 2015-Septe, no. June, pp. 2416–2422, 2015, doi:

10.1109/ICC.2015.7248687.

[19] M. Giordani, M. Polese, A. Roy, D. Castor, and M. Zorzi, "Standalone and non-standalone beam management for 3gpp nr at mmwaves," IEEE Commun. Mag., vol. 57, no. 4, pp. 123–129, 2019, doi: 10.1109/MCOM.2019.1800384.

[20] P. Zhou, X. Fang, X. Wang, Y. Long, R. He, and X. Han, "Deep learning-based beam management and interference coordination in dense mmWave networks," IEEE Trans. Veh. Technol., vol. 68, no. 1, pp. 592–603, 2019, doi: 10.1109/TVT.2018.2882635.

[21] Y. N. R. Li, B. Gao, X. Zhang, and K. Huang, "Beam Management in Millimeter-Wave Communications for 5G and beyond," IEEE Access, vol. 8, pp. 13282–13293, 2020, doi: 10.1109/ACCESS.2019.2963514.

[22] V. Degli-Esposti et al., "Ray-tracing-based mm-wave beamforming assessment," IEEE Access, vol. 2, pp. 1314–1325, 2014, doi: 10.1109/ACCESS.2014.2365991.

[23] R. J. Weiler et al., "Quasi-deterministic millimeter-wave channel models in MiWEBA," Eurasip J. Wirel. Commun. Netw., vol. 2016, no. 1, 2016, doi: 10.1186/s13638-016-0568-6.

[24] F. Fuschini, M. Zoli, E. M. Vitucci, M. Barbiroli, and V. Degli-Esposti, "A Study on Millimeter-Wave Multiuser Directional Beamforming Based on Measurements and Ray Tracing Simulations," IEEE Trans. Antennas Propag., 2019, doi: 10.1109/TAP.2019.2894271.

[25] D. Steinmetzer, J. Classen, and M. Hollick, "MmTrace: Modeling millimeter-wave indoor propagation with image-based ray-tracing," in Proceedings - IEEE INFOCOM, 2016, vol. 2016-Septe, pp. 429–434, doi: 10.1109/INFCOMW.2016.7562115.

[26] T. S. Rappaport, G. R. MacCartney, M. K. Samimi, and S. Sun, "Wideband millimeter-wave propagation measurements and channel models for future wireless communication system design," IEEE Trans. Commun., vol. 63, no. 9, pp. 3029–3056, 2015, doi: 10.1109/TCOMM.2015.2434384.

[27] A. I. Sulyman, A. Alwarafy, G. R. MacCartney, T. S. Rappaport, and A. Alsanie, "Directional Radio Propagation Path Loss Models for Millimeter-Wave Wireless Networks in the 28-, 60-, and 73-GHz Bands," IEEE Trans. Wirel. Commun., vol. 15, no. 10, pp. 6939–6947, 2016, doi: 10.1109/TWC.2016.2594067.

[28] H. Zhang, S. Venkateswaran, and U. Madhow, "Channel modeling and MIMO capacity for outdoor millimeter wave links," IEEE Wirel. Commun. Netw. Conf. WCNC, pp. 8–13, 2010, doi: 10.1109/WCNC.2010.5506714.

[29] J. Du et al., "Directional Measurements in Urban Street Canyons from Macro Rooftop Sites at 28 GHz for 90% Outdoor Coverage," arXiv, 2019, doi: 10.1109/tap.2020.3044398.

[30] M. Khatun, H. Mehrpouyan, D. Matolak, and I. Guvenc, "Millimeter wave systems for airports and short-range aviation communications: A survey of the current channel models at mmWave frequencies," in AIAA/IEEE Digital Avionics Systems Conference - Proceedings, 2017, vol. 2017-Septe, doi: 10.1109/DASC.2017.8102042.

[31] J. Yang, B. Ai, D. He, L. Wang, Z. Zhong, and A. Hrovat, "A Simplified Multipath Component Modeling Approach for High-Speed Train Channel Based on Ray Tracing," Wirel. Commun. Mob. Comput., vol. 2017, 2017, doi: 10.1155/2017/8517204.

[32] I. A. Hemadeh, K. Satyanarayana, M. El-Hajjar, and L. Hanzo, "Millimeter-Wave Communications: Physical Channel Models, Design Considerations, Antenna Constructions, and Link-Budget," IEEE Commun. Surv. Tutorials, vol. 20, no. 2, pp. 870–913, 2018, doi: 10.1109/COMST.2017.2783541.

[33] A. N. Uwaechia and N. M. Mahyuddin, "A comprehensive survey on millimeter wave communications for fifth-generation wireless networks: Feasibility and challenges," IEEE Access, vol. 8, pp. 62367–62414, 2020, doi: 10.1109/ACCESS.2020.2984204.

[34] M. S. Kumari and N. Kumar, "Channel model for simultaneous backhaul and

access for mmWave 5G outdoor street canyon channel," Wirel. Networks, vol. 26, 2020, doi: 10.1007/s11276-020-02421-0.

[35] K. Haneda et al., "5G 3GPP-like channel models for outdoor urban microcellular and macrocellular environments," in IEEE Vehicular Technology Conference, 2016, vol. 2016-July, doi: 10.1109/VTCSpring.2016.7503971.

[36] T. S. Rappaport, Y. Xing, G. R. MacCartney, A. F. Molisch, E. Mellios, and J. Zhang, "Overview of Millimeter Wave Communications for Fifth-Generation (5G) Wireless Networks-With a Focus on Propagation Models," IEEE Transactions on Antennas and Propagation, vol. 65, no. 12. pp. 6213–6230, 2017, doi: 10.1109/TAP.2017.2734243.

[37] Qualcomm Technologies, "Future of 5G," 2020. [Online]. Available: https://www.qualcomm.com/media/documents/files/making-5g-nr-a-commercial-reality.pdf.

[38] H. Singh, K. Saxena, V. Kumar, B. Bonev, and R. Prasad, "An Empirical Model for Prediction of Environmental Attenuation of Millimeter Waves," Wirel. Pers. Commun., vol. 115, no. 1, pp. 809–826, 2020, doi: 10.1007/s11277-020-07599-2.

[39] H. Singh, R. Prasad, and B. Bonev, "The Studies of Millimeter Waves at 60 GHz in Outdoor Environments for IMT Applications: A State of Art," Wirel. Pers. Commun., vol. 100, no. 2, pp. 463–474, 2018, doi: 10.1007/s11277-017-5090-6.

[40] G. Liu and D. Jiang, "5G: Vision and Requirements for Mobile Communication System towards Year 2020," Chinese J. Eng., vol. 2016, no. March 2016, 2016, doi: 10.1155/2016/5974586.

[41] G. Wunder et al., "5GNOW: Challenging the LTE design paradigms of orthogonality and synchronicity," IEEE Veh. Technol. Conf., 2013, doi: 10.1109/VTCSpring.2013.6691814.

[42] A. Morgado, K. M. S. Huq, S. Mumtaz, and J. Rodriguez, "A survey of 5G technologies: regulatory, standardization and industrial perspectives," Digit.

Commun. Networks, vol. 4, no. 2, pp. 87–97, 2018, doi: 10.1016/j.dcan.2017.09.010.

[43] O. Teyeb, G. Wikström, M. Stattin, T. Cheng, S. Faxér, and H. Do, "Evolving LTE to Fit the 5G Future," 2017. [Online]. Available: https://www.ericsson.com/en/reports-and-papers/ericsson-technology-review/articles/evolving-lte-to-fit-the-5g-future.

[44] Nidhi, A. Mihovska, and R. Prasad, "Overview of 5G New Radio and Carrier Aggregation: 5G and Beyond Networks," in 2020 23rd International Symposium on Wireless Personal Multimedia Communications (WPMC), Okayama, Japan, 2021, pp. 1–6, doi: 10.1109/wpmc50192.2020.9309496.

[45] S. E. Elayoubi et al., "5G service requirements and operational use cases: Analysis and METIS II vision," in EUCNC 2016 - European Conference on Networks and Communications, 2016, pp. 158–162, doi: 10.1109/EuCNC.2016.7561024.

[46] S. Rangan, T. S. Rappaport, and E. Erkip, "Millimeter-wave cellular wireless networks: Potentials and challenges," Proc. IEEE, vol. 102, no. 3, pp. 366–385, 2014, doi: 10.1109/JPROC.2014.2299397.

[47] E. Björnson, J. Hoydis, and L. Sanguinetti, "Massive MIMO Networks," IEEE Commun. Mag., vol. 1, no. 1, p. 4, 2017, doi: 10.1561/2000000093.Simulation.

[48] B. Wang, F. Gao, S. Jin, H. Lin, and G. Y. Li, "Spatial- and frequency-wideband effects in millimeter-wave massive MIMO systems," IEEE Trans. Signal Process., vol. 66, no. 13, pp. 3393–3406, 2018, doi: 10.1109/TSP.2018.2831628.

[49] A. N. Uwaechia, N. M. Mahyuddin, M. F. Ain, N. M. Abdul Latiff, and N. F. Za'bah, "On the Spectral-Efficiency of Low-Complexity and Resolution Hybrid Precoding and Combining Transceivers for mmWave MIMO Systems," IEEE Access, vol. 7, pp. 109259–109277, 2019, doi: 10.1109/access.2019.2933785.

[50] A. G. Gotsis, S. Stefanatos, and A. Alexiou, "UltraDense Networks: The New

Wireless Frontier for Enabling 5G Access," IEEE Veh. Technol. Mag., vol. 11, no. 2, pp. 71–78, 2016, doi: 10.1109/MVT.2015.2464831.

[51] L. Wei, R. Hu, Y. Qian, and G. Wu, "Key elements to enable millimeter wave communications for 5G wireless systems," IEEE Wirel. Commun., vol. 21, no. 6, pp. 136–143, 2014, doi: 10.1109/MWC.2014.7000981.

[52] T. M. Nguyen, W. Ajib, and C. Assi, "A novel cooperative Non-Orthogonal Multiple Access (NOMA) in wireless backhaul two-tier HetNets," IEEE Trans. Wirel. Commun., vol. 17, no. 7, pp. 4873–4887, 2018, doi: 10.1109/TWC.2018.2832625.

[53] P. Banelli, S. Buzzi, G. Colavolpe, A. Modenini, F. Rusek, and A. Ugolini, "Modulation formats and waveforms for 5G networks: Who will be the heir of OFDM?: An overview of alternative modulation schemes for improved spectral efficiency," IEEE Signal Process. Mag., vol. 31, no. 6, pp. 80–93, Nov. 2014, doi: 10.1109/MSP.2014.2337391.

[54] P. Zhang, C. Yi, and H. Wang, " 5G Wireless Testbeds ," Wiley 5G Ref, pp. 1–32, 2020, doi: 10.1002/9781119471509.w5gref063.

[55] J. Kalliovaara et al., "Designing a Testbed Infrastructure for Experimental Validation and Trialing of 5G Vertical Applications," in Lecture Notes of the Institute for Computer Sciences, Social-Informatics and Telecommunications Engineering, LNICST, vol. 228, 2018, pp. 247–263.

[56] M. Peuster, S. Schneider, D. Behnke, M. Muller, P. B. Bok, and H. Karl, "Prototyping and demonstrating 5g verticals: The smart manufacturing case," in Proceedings of the 2019 IEEE Conference on Network Softwarization: Unleashing the Power of Network Softwarization, NetSoft 2019, Jun. 2019, pp. 236–238, doi: 10.1109/NETSOFT.2019.8806685.

[57] M. Femminella, M. Pergolesi, and G. Reali, "Simplification of the design, deployment, and testing of 5G vertical services," in Proceedings of IEEE/IFIP Network Operations and Management Symposium 2020: Management in the Age of Softwarization and Artificial Intelligence, NOMS 2020, Apr. 2020, pp.

1–7, doi: 10.1109/NOMS47738.2020.9110401.

[58] Verizon, "What is 5G NR?," 2019. [Online]. Available: https://www.telit.com/blog/what-is-5g-nr/.

[59] 3GPP TS 38.101, "5G; NR; User Equipment (UE) radio transmission and reception," 2018. [Online]. Available: http://www.etsi.org/standards-search.

[60] Ericsson, "Developing mmWave mobile radio interface," 2017. [Online]. Available: https://www.ericsson.com/en/blog/2017/8/developing-mmwave-mobile-radio-interface.

[61] M. Xiao et al., "Millimeter Wave Communications for Future Mobile Networks," IEEE Journal on Selected Areas in Communications, vol. 35, no. 9. pp. 1909–1935, 2017, doi: 10.1109/JSAC.2017.2719924.

[62] H. Zhang and U. Madhow, "Statistical modeling of fading and diversity for outdoor 60 GHz channels," in Proceedings of the Annual International Conference on Mobile Computing and Networking, MOBICOM, Sep. 2010, pp. 45–49, doi: 10.1145/1859964.1859977.

[63] S. K. Saha, V. V. Vira, A. Garg, and D. Koutsonikolas, "60 GHz Multi-Gigabit Indoor WLANs: Dream or Reality?," 2015, [Online]. Available: http://arxiv.org/abs/1509.04274.

[64] MiWEBA, "WP5: Propagation, Antennas and Multi-Antenna Techniques D5.1: Channel Modeling and Characterization," 2014. [Online]. Available: https://www.miweba.eu/wp-content/uploads/2014/07/MiWEBA_D5.1_v1.01.pdf.

[65] B. Neekzad, K. Sayrafian-Pour, J. Perez, and J. S. Baras, "Comparison of ray tracing simulations and millimeter wave channel sounding measurements," IEEE Int. Symp. Pers. Indoor Mob. Radio Commun. PIMRC, pp. 1–5, 2007, doi: 10.1109/PIMRC.2007.4394537.

[66] ITU-R M.2376, "The technical feasibility of IMT in the bands above 6 GHz," 2015. [Online]. Available: https://www.itu.int/pub/R-REP-M.2376.

[67] T. S. Rappaport et al., "Wireless communications and applications above 100 GHz: Opportunities and challenges for 6g and beyond," IEEE Access, vol. 7, pp. 78729–78757, 2019, doi: 10.1109/ACCESS.2019.2921522.

[68] 3GPP TR 38.901, "TR 138 901 - V14.0.0 - 5G; Study on channel model for frequencies from 0.5 to 100 GHz (3GPP TR 38.901 version 14.0.0 Release 14)," 2017. [Online]. Available: http://www.etsi.org/standards-search.

[69] E. Torkildson, B. Ananthasubramaniam, U. Madhow, and M. Rodwell, "Millimeter-wave MIMO: Wireless links at optical speeds," in 44th Annual Allerton Conference on Communication, Control, and Computing 2006, 2006, vol. 1, pp. 235–243.

[70] T. S. Rappaport, F. Gutierrez, E. Ben-Dor, J. N. Murdock, Y. Qiao, and J. I. Tamir, "Broadband millimeter-wave propagation measurements and models using adaptive-beam antennas for outdoor Urban cellular communications," IEEE Trans. Antennas Propag., vol. 61, no. 4, pp. 1850–1859, 2013, doi: 10.1109/TAP.2012.2235056.

[71] S. G. Larew, T. A. Thomas, M. Cudak, and A. Ghosh, "Air interface design and ray tracing study for 5G millimeter wave communications," 2013 IEEE Globecom Work. GC Wkshps 2013, pp. 117–122, 2013, doi: 10.1109/GLOCOMW.2013.6824972.

[72] S. Buzzi, C. D'andrea, T. Foggi, A. Ugolini, and G. Colavolpe, "Single-carrier modulation versus OFDM for millimeter-wave wireless MIMO," IEEE Trans. Commun., vol. 66, no. 3, pp. 1335–1348, 2018, doi: 10.1109/TCOMM.2017.2771334.

[73] N. F. Abdullah, R. Nordin, A. Doufexi, and A. R. Nix, "Effect of Beamforming on mmWave Systems in Various Realistic Environments," 2017, doi: 10.1109/VTCSpring.2017.8108315.

[74] E. Ruggeri et al., "Fiber Wireless A-RoF/IFoF Uplink of 0.4Gb/s 16-QAM and 0.6Gb/s QPSK over a 32-Element 60GHz Phased Array Antenna for 5G Fronthaul Networks," Oct. 2019, doi: 10.1109/MWP.2019.8892146.

[75] M. Giordani, M. Mezzavilla, A. Dhananjay, S. Rangan, and M. Zorzi, “Channel dynamics and SNR tracking in millimeter wave cellular systems,” Eur. Wirel. Conf. 2016, EW 2016, pp. 306–313, 2016.

[76] E. Torkildson, H. Zhang, and U. Madhow, “Channel modeling for millimeter wave MIMO,” 2010 Inf. Theory Appl. Work. ITA 2010 - Conf. Proc., pp. 300–307, 2010, doi: 10.1109/ITA.2010.5454109.

[77] L. Zhang et al., “A Survey on 5G Millimeter Wave Communications for UAV-Assisted Wireless Networks,” IEEE Access, vol. 7, pp. 117460–117504, 2019, doi: 10.1109/access.2019.2929241.

[78] P. L. Mehta and R. Prasad, “Aerial-Heterogeneous Network: A Case Study Analysis on the Network Performance Under Heavy User Accumulations,” in Wireless Personal Communications, 2017, vol. 96, no. 3, pp. 3765–3784, doi: 10.1007/s11277-017-4283-3.

[79] E. Bjornson, L. Van Der Perre, S. Buzzi, and E. G. Larsson, “Massive MIMO in sub-6 GHz and mmWave: Physical, practical, and use-case differences,” IEEE Wirel. Commun., vol. 26, no. 2, pp. 100–108, 2019, doi: 10.1109/MWC.2018.1800140.

[80] P. Series, “Recommendation ITU-R, Attenuation by atmospheric gases,” 2016. [Online]. Available: http://www.itu.int/dms_pubrec/itu-r/rec/p/R-REC-P.676-11-201609-I!!PDF-E.pdf.

[81] H. J. Liebe, “MPM-An atmospheric millimeter-wave propagation model,” Int. J. Infrared Millimeter Waves, vol. 10, no. 6, pp. 631–650, 1989, doi: 10.1007/BF01009565.

[82] A. M. Al-Saman, M. Cheffena, M. Mohamed, M. H. Azmi, and Y. Ai, “Statistical Analysis of Rain at Millimeter Waves in Tropical Area,” IEEE Access, vol. 8, pp. 51044–51061, 2020, doi: 10.1109/ACCESS.2020.2979683.

[83] D. Nandi and A. Maitra, “Study of rain attenuation effects for 5G Mm-wave cellular communication in tropical location,” IET Microwaves, Antennas Propag., vol. 12, no. 9, pp. 1504–1507, 2018, doi: 10.1049/iet-map.2017.1029.

[84] J. Senic, C. Gentile, P. B. Papazian, K. A. Remley, and J. K. Choi, "Analysis of E-Band Path Loss and Propagation Mechanisms in the Indoor Environment," IEEE Trans. Antennas Propag., vol. 65, no. 12, pp. 6562–6573, Dec. 2017, doi: 10.1109/TAP.2017.2722876.

[85] K. Bechta, M. Rybakowski, F. Hsieh, and D. Chizhik, "Modeling of radio link budget with beamforming antennas for evaluation of 5G systems," IEEE 5G World Forum, 5GWF 2018 - Conf. Proc., no. November, pp. 427–432, 2018, doi: 10.1109/5GWF.2018.8516969.

[86] J. Lota, S. Sun, T. S. Rappaport, and A. Demosthenous, "5G Uniform Linear Arrays With Beamforming and Outdoor Urban Communication : A," IEEE Trans. Veh. Technol., vol. 66, no. 11, pp. 9972–9985, 2017.

[87] P. Zhou, X. Fang, and Y. Long, "Throughput and robustness guaranteed beam tracking for mmWave wireless networks," 2017 IEEE/CIC Int. Conf. Commun. China, ICCC 2017, vol. 2018-Janua, pp. 1–6, 2018, doi: 10.1109/ICCChina.2017.8330376.

[88] C. X. Wang, J. Bian, J. Sun, W. Zhang, and M. Zhang, "A survey of 5g channel measurements and models," IEEE Communications Surveys and Tutorials, vol. 20, no. 4. pp. 3142–3168, 2018, doi: 10.1109/COMST.2018.2862141.

[89] B. Antonescu, M. T. Moayyed, and S. Basagni, "Outdoor mmWave Channel Propagation Models using Clustering Algorithms," 2020 Int. Conf. Comput. Netw. Commun. ICNC 2020, pp. 860–865, 2020, doi: 10.1109/ICNC47757.2020.9049734.

[90] M. Lecci et al., "Simplified Ray Tracing for the Millimeter Wave Channel: A Performance Evaluation," in Information Theory and Applications Workshop (ITA), San Diego, US, 2020, 2020, no. February, [Online]. Available: http://arxiv.org/abs/2002.09179.

[91] Y. Liu, C. X. Wang, J. Huang, J. Sun, and W. Zhang, "Novel 3-D Nonstationary MmWave Massive MIMO Channel Models for 5G High-Speed Train Wireless Communications," IEEE Trans. Veh. Technol., vol. 68, no. 3,

pp. 2077–2086, Mar. 2019, doi: 10.1109/TVT.2018.2866414.

[92] S. Wu, C. X. Wang, E. H. M. Aggoune, M. M. Alwakeel, and X. You, "A General 3-D Non-Stationary 5G Wireless Channel Model," IEEE Trans. Commun., vol. 66, no. 7, pp. 3065–3078, 2018, doi: 10.1109/TCOMM.2017.2779128.

[93] Z. Hu, P. Zhang, H. Wang, Y. Zhou, X. An, and H. Wang, "Ray-Tracing Based Millimeter-Wave Large-Scale Channel Characteristics in Corridor Environment," 2019.

[94] T. S. Rappaport, S. Sun, and M. Shafi, "Investigation and comparison of 3GPP and NYUSIM channel models for 5G wireless communications," IEEE Veh. Technol. Conf., vol. 2017-Septe, pp. 1–5, 2018, doi: 10.1109/VTCFall.2017.8287877.

[95] M. Polese and M. Zorzi, "Impact of Channel Models on the End-to-End Performance of Mmwave Cellular Networks," in IEEE Workshop on Signal Processing Advances in Wireless Communications, SPAWC, Aug. 2018, vol. 2018-June, pp. 1–5, doi: 10.1109/SPAWC.2018.8445856.

[96] F. Fuschini et al., "Analysis of In-Room mm-Wave Propagation: Directional Channel Measurements and Ray Tracing Simulations," J. Infrared, Millimeter, Terahertz Waves, vol. 38, no. 6, pp. 727–744, 2017, doi: 10.1007/s10762-017-0366-1.

[97] P. Ferrand, M. Amara, S. Valentin, and M. Guillaud, "Trends and challenges in wireless channel modeling for evolving radio access," IEEE Commun. Mag., vol. 54, no. 7, pp. 93–99, 2016, doi: 10.1109/MCOM.2016.7509384.

[98] S. Jaeckel, L. Raschkowski, K. Borner, and L. Thiele, "QuaDRiGa: A 3-D multi-cell channel model with time evolution for enabling virtual field trials," IEEE Trans. Antennas Propag., vol. 62, no. 6, pp. 3242–3256, 2014, doi: 10.1109/TAP.2014.2310220.

[99] M. Peter, "Measurement results and final mmMAGIC channel models," 2017. [Online]. Available: https://bscw.5g-

mmmagic.eu/pub/bscw.cgi/d202656/mmMAGIC_D2-2.pdf.

[100] M. N. Kulkarni, E. Visotsky, and J. G. Andrews, “Correction factor for analysis of MIMO wireless networks with highly directional beamforming,” IEEE Wirel. Commun. Lett., vol. 7, no. 5, pp. 756–759, Oct. 2018, doi: 10.1109/LWC.2018.2818178.

[101] G. R. MacCartney and T. S. Rappaport, “Rural macrocell path loss models for millimeter wave wireless communications,” in IEEE Journal on Selected Areas in Communications, 2017, vol. 35, no. 7, doi: 10.1109/JSAC.2017.2699359.

[102] M. K. Samimi, T. S. Rappaport, and G. R. Maccartney, “Probabilistic Omnidirectional Path Loss Models for Millimeter-Wave Outdoor Communications,” IEEE Wirel. Commun. Lett., vol. 4, no. 4, pp. 357–360, 2015, doi: 10.1109/LWC.2015.2417559.

[103] M. Sheeba Kumari, S. A. Rao, and N. Kumar, “Characterization of mmWave link for outdoor communications in 5G networks,” in 2015 International Conference on Advances in Computing, Communications and Informatics, ICACCI 2015, Sep. 2015, pp. 44–49, doi: 10.1109/ICACCI.2015.7275582.

[104] M. Sheeba Kumari, N. Kumar, and R. Prasad, “Optimization of street canyon outdoor channel deployment geometry for mmWave 5G communication,” AEU - Int. J. Electron. Commun., vol. 125, 2020, doi: 10.1016/j.aeue.2020.153368.

[105] Y. Wang, M. Narasimha, and R. W. Heath, “MmWave Beam Prediction with Situational Awareness: A Machine Learning Approach,” in IEEE Workshop on Signal Processing Advances in Wireless Communications, SPAWC, 2018, vol. 2018-June, doi: 10.1109/SPAWC.2018.8445969.

[106] L. Bai et al., “Predicting Wireless MmWave Massive MIMO Channel Characteristics Using Machine Learning Algorithms,” Wirel. Commun. Mob. Comput., vol. 2018, 2018, doi: 10.1155/2018/9783863.

[107] C. Zhang, Y.-L. Ueng, C. Studer, and A. Burg, “Artificial Intelligence for 5G and Beyond 5G: Implementations, Algorithms, and Optimizations,” IEEE J.

Emerg. Sel. Top. Circuits Syst., vol. 10, no. 2, pp. 149–163, 2020, doi: 10.1109/jetcas.2020.3000103.

[108] O. Kanhere and T. S. Rappaport, “Position Locationing for Millimeter Wave Systems,” 2018, doi: 10.1109/GLOCOM.2018.8647983.

[109] H. Ganame, L. Yingzhuang, H. Ghazzai, and D. Kamissoko, “5G base station deployment perspectives in millimeter wave frequencies using meta-heuristic algorithms,” Electron., vol. 8, no. 11, 2019, doi: 10.3390/electronics8111318.

[110] S. Sun, G. R. Maccartney, M. K. Samimi, and T. S. Rappaport, “Synthesizing omnidirectional antenna patterns, received power and path loss from directional antennas for 5G millimeter-wave communications,” 2015, doi: 10.1109/GLOCOM.2014.7417335.

[111] U. Madhow, Introduction to Communication Systems. Cambridge University Press, 2014.

[112] F. Communications and Commission, “FCC report and order on ultra wideband technology,” 2002. [Online]. Available: http://www.jstor.org/stable/10.2307/724927.

[113] P. El-Sallabi, H. M., Vainikainen, H. M. El-Sallabi, and P. Vainikainen, “Modeling and simulation of wideband radio channel characterization for an urban line-of-sight microcell,” in IEEE Vehicular Technology Conference, 1999, vol. 4, pp. 2383–2387, doi: 10.1109/vetecf.1999.797365.

[114] M. Sheeba Kumari, S. A. Rao, and N. Kumar, “Outdoor millimeter-wave channel modeling for uniform coverage without beam steering,” in Lecture Notes of the Institute for Computer Sciences, Social-Informatics and Telecommunications Engineering, LNICST, 2018, vol. 218, pp. 233–244, doi: 10.1007/978-3-319-73423-1_21.

[115] M. Sheeba Kumari, N. Kumar, and R. Prasad, “Performance of mmWave Ray Tracing Outdoor Channel Model Exploiting Antenna Directionality,” in 2020 IEEE 3rd 5G World Forum, 5GWF 2020 - Conference Proceedings, 2020, pp. 607–612, doi: 10.1109/5GWF49715.2020.9221090.

[116] A. M. Al-Samman, T. A. Rahman, M. H. Azmi, A. Sharaf, Y. Yamada, and A. Alhammadi, “Path loss model in indoor environment at 40 GHz for 5G wireless network,” in Proceedings - 2018 IEEE 14th International Colloquium on Signal Processing and its Application, CSPA 2018, 2018, pp. 7–12, doi: 10.1109/CSPA.2018.8368676.

[117] S. Sun, G. R. MacCartney, and T. S. Rappaport, “Millimeter-wave distance-dependent large-scale propagation measurements and path loss models for outdoor and indoor 5G systems,” 2016, doi: 10.1109/EuCAP.2016.7481506.

[118] M. B. Majed, T. A. Rahman, O. A. Aziz, M. N. Hindia, and E. Hanafi, “Channel characterization and path loss modeling in indoor environment at 4.5, 28, and 38GHz for 5G cellular networks,” Int. J. Antennas Propag., vol. 2018, 2018, doi: 10.1155/2018/9142367.

[119] V. Raghavan, A. Partyka, L. Akhoondzadeh-Asl, M. A. Tassoudji, O. H. Koymen, and J. Sanelli, “Millimeter Wave Channel Measurements and Implications for PHY Layer Design,” IEEE Trans. Antennas Propag., vol. 65, no. 12, pp. 6521–6533, 2017, doi: 10.1109/TAP.2017.2758198.

[120] K. Guan et al., “Measurements and Analysis of Large-Scale Fading Characteristics in Curved Subway Tunnels at 920 MHz, 2400 MHz, and 5705 MHz,” IEEE Trans. Intell. Transp. Syst., vol. 16, no. 5, pp. 2393–2405, 2015, doi: 10.1109/TITS.2015.2404851.

[121] S. Kumari, S. A. Rao, and N. Kumar, “Modeling and Link Budget Estimation of Directional mmWave Outdoor Environment for 5G,” in 2019 European Conference on Networks and Communications, EuCNC 2019, Aug. 2019, pp. 106–111, doi: 10.1109/EuCNC.2019.8802001.

[122] J. Medbo et al., “Channel modelling for the fifth generation mobile communications,” 8th Eur. Conf. Antennas Propagation, EuCAP 2014, pp. 219–223, 2014, doi: 10.1109/EuCAP.2014.6901730.

[123] M. K. Samimi and T. S. Rappaport, “Statistical channel model with multi-frequency and arbitrary antenna beamwidth for millimeter-wave outdoor

communications," 2015 IEEE Globecom Work. GC Wkshps 2015 - Proc., pp. 1–7, 2015, doi: 10.1109/GLOCOMW.2015.7414164.

[124] Y. Zhang, S. Wang, and G. Ji, "A Comprehensive Survey on Particle Swarm Optimization Algorithm and Its Applications," Mathematical Problems in Engineering, vol. 2015. Hindawi Limited, 2015, doi: 10.1155/2015/931256.

[125] M. Kyrö, V. M. Kolmonen, and P. Vainikainen, "Experimental propagation channel characterization of mm-wave radio links in urban scenarios," IEEE Antennas Wirel. Propag. Lett., vol. 11, pp. 865–868, 2012, doi: 10.1109/LAWP.2012.2210532.

[126] 3GPP TR 38.803, "TSG RAN TR 38.803 v14.1.0 Study on new radio access technology: Radio Frequency (RF) and co-existence aspects," 2017. [Online]. Available: http://www.etsi.org/deliver/etsi_tr/138900_138999/138912/14.01.00_60/tr_138912v140100p.pdf.

CO-AUTHORSHIP STATEMENTS

The co-authorship statements for all the co-authored scientific publications are attached in the following pages.

Serial #	Co-authorship Statements	
A	**Journal Publications**	**Page**
A.1	Sheeba Kumari M., N. Kumar, R. Prasad, "Path Loss Model for nonuniform Variance in Directional mmWave Outdoor Channel," IEEE Transactions on Wireless Communications, 2021 (submitted).	169
A.2	Sheeba Kumari M., N. Kumar, R. Prasad, "Optimization of Street Canyon Outdoor Channel Deployment Geometry for mmWave 5G Communication," AEÜ – International Journal of Electronics and Communications, Vol 125, Oct 2020, doi: 10.1016/j.aeue.2020.153368.	170
A.3	Sheeba Kumari M., N. Kumar, "Channel Model for Simultaneous Backhaul and Access for mmWave 5G Outdoor Street Canyon Channel," Springer Wireless Networks, The Journal of Mobile Communication, Computation and Information, July 2020, doi: 10.1007/s11276-020-02421-0.	171
B	**Book Chapters**	**Page**
B.1	Sheeba Kumari M., S. A. Rao, N. Kumar, "Outdoor Millimeter-Wave Channel Modeling for Uniform Coverage Without Beam Steering," Ubiquitous Communications and Network Computing. UBICNET 2017. Lecture Notes of the Institute for Computer Sciences, Social Informatics and Telecommunications Engineering, vol 218. Springer, 2017, doi: 10.1007/978-3-319-73423-1_21.	172
C	**Conference Publications**	**Page**
C.1	Sheeba Kumari M., N. Kumar, R. Prasad, "Simplified Approach for Directional Multipath Component Modeling for mmWaves using Ray Tracing," Wireless World Research Forum 45 (WWRF45) Hyperconnectivity: Beyond 5G, Opportunities & Challenges, Malaysia, Jan 2021.	173

C.2	Sheeba Kumari M., N. Kumar, R. Prasad, "Performance of mmWave Ray Tracing Outdoor Channel Model Exploiting Antenna Directionality," 2020 IEEE 5G World Forum (5GWF), Bangalore, India, pp. 607-612, 2020, doi: 10.1109/5GWF49715.2020.9221090.	174
C.3	R. Makkar, V. Kotha, M. Sheeba Kumari, D. Rawal, V. K. Chakka and N. Kumar, "Performance of Downlink SISO NR System using MMSE-IRC Receiver," 2020 IEEE 3rd 5G World Forum (5GWF), Bangalore, India, 2020, pp. 619-624, doi: 10.1109/5GWF49715.2020.9221267.	175
C.4	Sheeba Kumari M., S. A. Rao, N. Kumar, "Deterministic Modeling for mmWave Outdoor Street Canyon Channel," 2019 IEEE PhD Colloquium on Ethically Driven Innovation and Technology (PhD EDITS), Bangalore, India, August 2019, doi: 10.1109/PhDEDITS47523.2019.8986945.	176
C.5	Sheeba Kumari M., S. A. Rao, N. Kumar, "Modeling and Link Budget Estimation of Directional mmWave Outdoor Environment for 5G," 2019 European Conference on Networks and Communications (EuCNC), Valencia, Spain, pp.106-111, June 2019, doi: 10.1109/EuCNC.2019.8802001.	177
C.6	Sheeba Kumari M., S. A. Rao, N. Kumar, "Characterization of mmWave Link for Outdoor Communications in 5G Networks," IEEE International Conference on Advances in Computing, Communications and Informatics (ICACCI), Kochi, India, pp. 44-49, Sept. 2015, doi: 10.1109/ICACCI.2015.7275582	178

AARHUS BSS SCHOOL OF BUSINESS AND SOCIAL SCIENCES AARHUS UNIVERSITY

Declaration of co-authorship*

Full name of the PhD student: Sheeba Kumari M

This declaration concerns the following article/manuscript:

Title:	Path Loss Model for nonuniform Variance in Directional mmWave Outdoor Channel
Authors:	Sheeba Kumari M, Navin Kumar, Ramjee Prasad

The article/manuscript is: Published ☐ Accepted ☐ Submitted ☒ In preparation ☐

If published, state full reference:

If accepted or submitted, state journal: IEEE Transactions on Wireless Communications

Has the article/manuscript previously been used in other PhD or doctoral dissertations?

No ☒ Yes ☐ If yes, give details:

The PhD student has contributed to the elements of this article/manuscript as follows:

A. Has essentially done all the work
B. Major contribution
C. Equal contribution
D. Minor contribution
E. Not relevant

Element	Extent (A-E)
1. Formulation/identification of the scientific problem	B
2. Planning of the experiments/methodology design and development	B
3. Involvement in the experimental work/clinical studies/data collection	A
4. Interpretation of the results	A
5. Writing of the first draft of the manuscript	A
6. Finalization of the manuscript and submission	B

Signatures of the co-authors

Date	Name	Signature
16/02/2021	Navin Kumar	
16/02/2021	Ramjee Prasad	

In case of further co-authors please attach appendix

Date: 16/02/2021

Signature of the PhD student

*As per policy the co-author statement will be published with the dissertation.

AARHUS BSS SCHOOL OF BUSINESS AND SOCIAL SCIENCES
AARHUS UNIVERSITY

Declaration of co-authorship*

Full name of the PhD student: Sheeba Kumari M

This declaration concerns the following article/manuscript:

Title:	Optimization of Street Canyon Outdoor Channel Deployment Geometry for mmWave 5G Communication
Authors:	Sheeba Kumari M, Navin Kumar, Ramjee Prasad

The article/manuscript is: Published ☒ Accepted ☐ Submitted ☐ In preparation ☐

If published, state full reference: Elsevier AEÜ - International Journal of Electronics and Communications, Vol 125, Oct 2020, doi: 10.1016/j.aeue.2020.153368

If accepted or submitted, state journal:

Has the article/manuscript previously been used in other PhD or doctoral dissertations?

No ☒ Yes ☐ If yes, give details:

The PhD student has contributed to the elements of this article/manuscript as follows:

A. Has essentially done all the work
B. Major contribution
C. Equal contribution
D. Minor contribution
E. Not relevant

Element	Extent (A-E)
1. Formulation/identification of the scientific problem	B
2. Planning of the experiments/methodology design and development	B
3. Involvement in the experimental work/clinical studies/data collection	A
4. Interpretation of the results	A
5. Writing of the first draft of the manuscript	A
6. Finalization of the manuscript and submission	B

Signatures of the co-authors

Date	Name	Signature
16/02/2021	Navin Kumar	
16/02/2021	Ramjee Prasad	

In case of further co-authors please attach appendix

Date: 16/02/2021

Signature of the PhD student

*As per policy the co-author statement will be published with the dissertation.

AARHUS BSS SCHOOL OF BUSINESS AND SOCIAL SCIENCES AARHUS UNIVERSITY

Declaration of co-authorship*

Full name of the PhD student: Sheeba Kumari M

This declaration concerns the following article/manuscript:

Title:	Channel Model for Simultaneous Backhaul and Access for mmWave 5G Outdoor Street Canyon Channel
Authors:	Sheeba Kumari M, Navin Kumar

The article/manuscript is: Published ☒ Accepted ☐ Submitted ☐ In preparation ☐

If published, state full reference: Springer Wireless Networks, The Journal of Mobile Communication, Computation and Information, July 2020, doi: 10.1007/s11276-020-02421-0

If accepted or submitted, state journal:

Has the article/manuscript previously been used in other PhD or doctoral dissertations?

No ☒ Yes ☐ If yes, give details:

The PhD student has contributed to the elements of this article/manuscript as follows:

A. Has essentially done all the work
B. Major contribution
C. Equal contribution
D. Minor contribution
E. Not relevant

Element	Extent (A-E)
1. Formulation/identification of the scientific problem	B
2. Planning of the experiments/methodology design and development	B
3. Involvement in the experimental work/clinical studies/data collection	A
4. Interpretation of the results	A
5. Writing of the first draft of the manuscript	A
6. Finalization of the manuscript and submission	B

Signatures of the co-authors

Date	Name	Signature
16/02/2021	Navin Kumar	

In case of further co-authors please attach appendix

Date: 16/02/2021

Signature of the PhD student

*As per policy the co-author statement will be published with the dissertation.

AARHUS BSS SCHOOL OF BUSINESS AND SOCIAL SCIENCES
AARHUS UNIVERSITY

Declaration of co-authorship*

Full name of the PhD student: Sheeba Kumari M

This declaration concerns the following article/manuscript:

Title:	Outdoor Millimeter-Wave Channel Modeling for Uniform Coverage Without Beam Steering
Authors:	Sheeba Kumari M, Sudarshan A Rao, Navin Kumar

The article/manuscript is: Published ☒ Accepted ☐ Submitted ☐ In preparation ☐

If published, state full reference: Ubiquitous Communications and Network Computing. UBICNET 2017. Lecture Notes of the Institute for Computer Sciences, Social Informatics and Telecommunications Engineering, vol 218. Springer, 2017, doi: 10.1007/978-3-319-73423-1_21

If accepted or submitted, state journal:

Has the article/manuscript previously been used in other PhD or doctoral dissertations?

No ☒ Yes ☐ If yes, give details:

The PhD student has contributed to the elements of this article/manuscript as follows:

A. Has essentially done all the work
B. Major contribution
C. Equal contribution
D. Minor contribution
E. Not relevant

Element	Extent (A-E)
1. Formulation/identification of the scientific problem	B
2. Planning of the experiments/methodology design and development	B
3. Involvement in the experimental work/clinical studies/data collection	A
4. Interpretation of the results	B
5. Writing of the first draft of the manuscript	A
6. Finalization of the manuscript and submission	A

Signatures of the co-authors

Date	Name	Signature
16/02/2021	Navin Kumar	
16/02/2021	Late Sudarshan A Rao	Deceased on 26 May 2018

In case of further co-authors please attach appendix

Date: 16/02/2021

Signature of the PhD student

*As per policy the co-author statement will be published with the dissertation.

AARHUS BSS SCHOOL OF BUSINESS AND SOCIAL SCIENCES AARHUS UNIVERSITY

Declaration of co-authorship*

Full name of the PhD student: Sheeba Kumari M

This declaration concerns the following article/manuscript:

Title:	Simplified Approach for Directional Multipath Component Modeling for mmWaves using Ray Tracing
Authors:	Sheeba Kumari M, Navin Kumar, Ramjee Prasad

The article/manuscript is: Published ☒ Accepted ☐ Submitted ☐ In preparation ☐

If published, state full reference: Wireless World Research Forum 45 (WWRF45) Hyperconnectivity: Beyond 5G, Opportunities & Challenges, Malaysia, Jan 2021

If accepted or submitted, state journal:

Has the article/manuscript previously been used in other PhD or doctoral dissertations?

No ☒ Yes ☐ If yes, give details:

The PhD student has contributed to the elements of this article/manuscript as follows:

- A. Has essentially done all the work
- B. Major contribution
- C. Equal contribution
- D. Minor contribution
- E. Not relevant

Element	Extent (A-E)
1. Formulation/identification of the scientific problem	B
2. Planning of the experiments/methodology design and development	B
3. Involvement in the experimental work/clinical studies/data collection	A
4. Interpretation of the results	A
5. Writing of the first draft of the manuscript	A
6. Finalization of the manuscript and submission	A

Signatures of the co-authors

Date	Name	Signature
16/02/2021	Navin Kumar	
16/02/2021	Ramjee Prasad	

In case of further co-authors please attach appendix

Date: 16/02/2021

Signature of the PhD student

*As per policy the co-author statement will be published with the dissertation.

AARHUS BSS SCHOOL OF BUSINESS AND SOCIAL SCIENCES AARHUS UNIVERSITY

Declaration of co-authorship*

Full name of the PhD student: Sheeba Kumari M

This declaration concerns the following article/manuscript:

Title:	Performance of mmWave Ray Tracing Outdoor Channel Model Exploiting Antenna Directionality
Authors:	Sheeba Kumari M, Navin Kumar, Ramjee Prasad

The article/manuscript is: Published ☒ Accepted ☐ Submitted ☐ In preparation ☐

If published, state full reference: 2020 IEEE 5G World Forum (5GWF), Bangalore, India, pp. 607-612, 2020, doi: 10.1109/5GWF49715.2020.9221090

If accepted or submitted, state journal:

Has the article/manuscript previously been used in other PhD or doctoral dissertations?

No ☒ Yes ☐ If yes, give details:

The PhD student has contributed to the elements of this article/manuscript as follows:

A. Has essentially done all the work
B. Major contribution
C. Equal contribution
D. Minor contribution
E. Not relevant

Element	Extent (A-E)
1. Formulation/identification of the scientific problem	B
2. Planning of the experiments/methodology design and development	B
3. Involvement in the experimental work/clinical studies/data collection	A
4. Interpretation of the results	A
5. Writing of the first draft of the manuscript	A
6. Finalization of the manuscript and submission	B

Signatures of the co-authors

Date	Name	Signature
16/02/2021	Navin Kumar	
16/02/2021	Ramjee Prasad	

In case of further co-authors please attach appendix

Date: 16/02/2021

Signature of the PhD student

*As per policy the co-author statement will be published with the dissertation.

AARHUS BSS SCHOOL OF BUSINESS AND SOCIAL SCIENCES AARHUS UNIVERSITY

Declaration of co-authorship*

Full name of the PhD student: Sheeba Kumari M

This declaration concerns the following article/manuscript:

Title:	Performance of Downlink SISO NR System using MMSE-IRC Receiver
Authors:	Rahul Makkar, Venugopalachary Kotha, Sheeba Kumari M, Divyang Rawal, Vijay Kumar Chakka, Navin Kumar

The article/manuscript is: Published ☒ Accepted ☐ Submitted ☐ In preparation ☐

If published, state full reference: 2020 IEEE 5G World Forum (5GWF), Bangalore, India, pp. 619-624, doi: 10.1109/5GWF49715.2020.9221267

If accepted or submitted, state journal:

Has the article/manuscript previously been used in other PhD or doctoral dissertations?

No ☒ Yes ☐ If yes, give details:

The PhD student has contributed to the elements of this article/manuscript as follows:

A. Has essentially done all the work
B. Major contribution
C. Equal contribution
D. Minor contribution
E. Not relevant

Element	Extent (A-E)
1. Formulation/identification of the scientific problem	C
2. Planning of the experiments/methodology design and development	C
3. Involvement in the experimental work/clinical studies/data collection	B
4. Interpretation of the results	B
5. Writing of the first draft of the manuscript	C
6. Finalization of the manuscript and submission	C

Signatures of the co-authors

Date	Name	Signature
16/02/2021	Rahul Makkar	Rahul
16/02/2021	Venugopalachary Kotha	
16/02/2021	Divyang Rawal	D. R. Rawal
16/02/2021	Vijay Kumar Chakka	C. Vijay Kumar
16/02/2021	Navin Kumar	

In case of further co-authors please attach appendix

Date: 16/02/2021

Signature of the PhD student

*As per policy the co-author statement will be published with the dissertation.

AARHUS BSS SCHOOL OF BUSINESS AND SOCIAL SCIENCES AARHUS UNIVERSITY

Declaration of co-authorship*

Full name of the PhD student: Sheeba Kumari M

This declaration concerns the following article/manuscript:

Title:	Deterministic Modeling for mmWave Outdoor Street Canyon Channel
Authors:	Sheeba Kumari M, Sudarshan A Rao, Navin Kumar

The article/manuscript is: Published ☒ Accepted ☐ Submitted ☐ In preparation ☐

If published, state full reference: IEEE PhD Colloquium on Ethically Driven Innovation and Technology (PhD EDITS), Bangalore, India, August 2019, doi: 10.1109/PhDEDITS47523.2019.8986945

If accepted or submitted, state journal:

Has the article/manuscript previously been used in other PhD or doctoral dissertations?

No ☒ Yes ☐ If yes, give details:

The PhD student has contributed to the elements of this article/manuscript as follows:

A. Has essentially done all the work
B. Major contribution
C. Equal contribution
D. Minor contribution
E. Not relevant

Element	Extent (A-E)
1. Formulation/identification of the scientific problem	B
2. Planning of the experiments/methodology design and development	B
3. Involvement in the experimental work/clinical studies/data collection	A
4. Interpretation of the results	A
5. Writing of the first draft of the manuscript	A
6. Finalization of the manuscript and submission	A

Signatures of the co-authors

Date	Name	Signature
16/02/2021	Navin Kumar	
16/02/2021	Late Sudarshan A Rao	Deceased on 26 May 2018

In case of further co-authors please attach appendix

Date: 16/02/2021

Signature of the PhD student

*As per policy the co-author statement will be published with the dissertation.

AARHUS BSS SCHOOL OF BUSINESS AND SOCIAL SCIENCES AARHUS UNIVERSITY

Declaration of co-authorship*

Full name of the PhD student: Sheeba Kumari M

This declaration concerns the following article/manuscript:

Title:	Modeling and Link Budget Estimation of Directional mmWave Outdoor Environment for 5G
Authors:	Sheeba Kumari M, Sudarshan A Rao, Navin Kumar

The article/manuscript is: Published ☒ Accepted ☐ Submitted ☐ In preparation ☐

If published, state full reference: 2019 European Conference on Networks and Communications (EuCNC), Valencia, Spain, pp.106-111, June 2019, doi: 10.1109/EuCNC.2019.8802001

If accepted or submitted, state journal:

Has the article/manuscript previously been used in other PhD or doctoral dissertations?

No ☒ Yes ☐ If yes, give details:

The PhD student has contributed to the elements of this article/manuscript as follows:

A. Has essentially done all the work
B. Major contribution
C. Equal contribution
D. Minor contribution
E. Not relevant

Element	Extent (A-E)
1. Formulation/identification of the scientific problem	B
2. Planning of the experiments/methodology design and development	B
3. Involvement in the experimental work/clinical studies/data collection	A
4. Interpretation of the results	A
5. Writing of the first draft of the manuscript	A
6. Finalization of the manuscript and submission	B

Signatures of the co-authors

Date	Name	Signature
16/02/2021	Navin Kumar	
16/02/2021	Late Sudarshan A Rao	Deceased on 26 May 2018

In case of further co-authors please attach appendix

Date: 16/02/2021

Signature of the PhD student

*As per policy the co-author statement will be published with the dissertation.

AARHUS BSS SCHOOL OF BUSINESS AND SOCIAL SCIENCES AARHUS UNIVERSITY

Declaration of co-authorship*

Full name of the PhD student: Sheeba Kumari M

This declaration concerns the following article/manuscript:

Title:	Characterization of mmWave Link for Outdoor Communications in 5G Networks
Authors:	Sheeba Kumari M, Sudarshan A Rao, Navin Kumar

The article/manuscript is: Published ☒ Accepted ☐ Submitted ☐ In preparation ☐

If published, state full reference: IEEE International Conference on Advances in Computing, Communications and Informatics (ICACCI), Kochi, India, pp. 44-49, Sept. 2015, doi: 10.1109/ICACCI.2015.7275582

If accepted or submitted, state journal:

Has the article/manuscript previously been used in other PhD or doctoral dissertations?

No ☒ Yes ☐ If yes, give details:

The PhD student has contributed to the elements of this article/manuscript as follows:

A. Has essentially done all the work
B. Major contribution
C. Equal contribution
D. Minor contribution
E. Not relevant

Element	Extent (A-E)
1. Formulation/identification of the scientific problem	B
2. Planning of the experiments/methodology design and development	B
3. Involvement in the experimental work/clinical studies/data collection	A
4. Interpretation of the results	B
5. Writing of the first draft of the manuscript	A
6. Finalization of the manuscript and submission	B

Signatures of the co-authors

Date	Name	Signature
16/02/2021	Navin Kumar	
16/02/2021	Late Sudarshan A Rao	Deceased on 26 May 2018

In case of further co-authors please attach appendix

Date: 16/02/2021

Signature of the PhD student

*As per policy the co-author statement will be published with the dissertation.